

CONCEPTUAL PROJECT ON USING THE PUMPING SCHEME TO ELIMINATE ACID MINE DRAINAGE

Report to the
Water Research Commission

by

**Craig Sheridan^{1,2}, Ricky Bonner^{1,2}, Lenke Bruyns^{1,3}, Deanne Drake^{1,3}, Kevin
Harding^{1,2}, Jon Paul Janet^{1,2}, Karl Rumbold^{1,4} & Nabeela Saber^{1,2}**

¹ Industrial and Mining Water Research Unit

² School of Chemical and Metallurgical Engineering

³ School of Animal, Plant and Environmental Science

⁴ School of Molecular and Cell Biology

University of the Witwatersrand, Johannesburg

**WRC Report No. KV 337/14
ISBN 978-1-4312-0622-3**

January 2015

Obtainable from

Water Research Commission
Private Bag X03
Gezina 0031
South Africa

orders@wrc.org.za or download from www.wrc.org.za

The publication of this report emanates from a project entitled *Concept project on using the pumping scheme to eliminate AMD* (WRC Project No. K8/1034)

DISCLAIMER

This report has been reviewed by the Water Research Commission (WRC) and approved for publication. Approval does not signify that the contents necessarily reflect the views and policies of the WRC, nor does mention of trade names or commercial products constitute endorsement or recommendation for use.

EXECUTIVE SUMMARY

Acid mine drainage (AMD) poses a serious threat to water quality in the Witwatersrand region, owing to extensive, abandoned mine voids that have subsequently flooded. The formation of AMD requires a sulphide mineral (primarily pyrite), water and oxygen to regenerate ferric iron in order to produce net acidity. In response to the severity of the current situation, the South African government has undertaken construction and expansion of facilities to lower the water table to a safe level (e.g. where no AMD decants from the mine into the surrounding groundwater or surface water) in the worst affected portion of the basins through pumping and effluent treatment.

We propose using the same infrastructure that is currently being installed to manage the problem more effectively and sustainably by pumping from a greater depth. It is hypothesised that the anoxic conditions at this depth (ca. 2 km) will effectively preclude the generation of acid mine drainage and hence reduce the need for effluent treatment while maintaining the desired water level.

In this report, the increase in energy required by pumping from a depth of 2 km was calculated relative to the current depth of just below the environmentally critical level. It was determined that the expected energy increase would be in the region of 10%, suggesting that it is feasible to use the existing/planned pumping infrastructure at this depth.

In the second part of this study, we attempted to quantify how pH, temperature and initial availability of oxygen in reaction water affected the formation rate of AMD from Witwatersrand coal waste rock.

We observed no statistically significant effects of initial oxygen availability, pH or incubation temperature on the production of SO_4 from coal mine waste rock. In particular, decreased availability of O_2 in incubation water did not inhibit production of SO_4 . We did however note that dissolved oxygen in many of the low DO treatment replicates increased over the experiment, even though the incubation vessels were sealed, suggesting contamination.

In part three of the study, we studied how the aquifer would change by pumping from depth. In all cases, where we added oxygenated or low dissolved oxygen water to the column and pumped from the bottom of the column, we saw improved water quality with time (pH, EC, Fe and SO_4^{2-}). Additional experiments were conducted to determine if this effect was as a result of dilution without any formation of AMD or if it is as a result of dilution and no generation due to all insufficient sulphide present to cause ongoing reaction. These additional experiments confirmed that sulphide was not depleted, that the rate of water movement was slower than the rate of reaction and we therefore conclude that at laboratory-scale, we were able to prevent the formation of AMD.

ACKNOWLEDGEMENTS

The project team wishes to thank the following people for their contributions to the project.

Reference Group	Affiliation
Ms. Kerry Slatter	Kalao Solutions
Dr. Giles Searby	Anglo American
Dr. Frank Crundwell	CM Solutions
Mr. Phil Hobbs	CSIR
Dr. Jo Burgess	WRC
Others	
Mr. Rhod McCrae-Samuel	University of the Witwatersrand Bernard Price Institute

The financial support of the Water Research Commission, South Africa, as well as the University Research Council (URC) of the University of the Witwatersrand, Johannesburg, is gratefully acknowledged.

CONTENTS

EXECUTIVE SUMMARY	i
ACKNOWLEDGEMENTS	ii
CONTENTS	iii
LIST OF TABLES	v
LIST OF FIGURES	vi
ACRONYMS & ABBREVIATIONS	viii
CHAPTER 1: BACKGROUND	1
1.1 INTRODUCTION	1
1.2 PROJECT AIMS	1
1.3 SCOPE AND LIMITATIONS	1
CHAPTER 2: Increasing Pumping Depth as a Solution in the Long-Term Management of AMD	2
2.1 CHAPTER ABSTRACT.....	2
2.2 INTRODUCTION	2
2.3 LITERATURE REVIEW	2
2.3.1 Acid Mine Drainage.....	2
2.3.2 Prevalence and Severity of AMD in the Witwatersrand Basin	3
2.3.3 Mechanisms of AMD generation.....	4
2.3.4 Current Management Strategies.....	4
2.4 PROPOSED METHOD	5
2.5 COMPARISON OF PUMPING DUTY.....	6
2.5.1 Calculation of Pumping Duty.....	6
2.5.2 Theory	6
2.5.3 Assumptions and Important parameters.....	7
2.5.3.1 Environmentally Critical Level and Pumping Suction Depth	7
2.5.3.2 Flow rate, Pipe Dimensions and Properties	8
2.5.4 Fluid Properties	8
2.5.5 Calculation Results	8
2.6 EXPERIMENTAL APPROACH.....	10
2.7 CONCLUSIONS.....	10
CHAPTER 3: A benchtop study quantifying the role of pH, dissolved oxygen and temperature in formation of AMD from coal mine waste rock	12
3.1 INTRODUCTION	12
3.2 METHODS AND MATERIALS.....	13
3.2.1 Experimental Design.....	13
3.2.2 Laboratory Methods	13
3.3 RESULTS	13
3.4 DISCUSSION.....	16
CHAPTER 4: Column Experiments	18
4.1 INTRODUCTION	18
4.2 METHODS AND MATERIALS.....	19
4.2.1 Experimental Design.....	19
4.2.1.1 Proposed Method for Remediation in the Witwatersrand Basins.....	19
4.2.1.2 Reactor Theory	19
4.2.1.3 Residence-Time Distribution (RTD) Function.....	19
4.2.1.4 Mean Residence Time.....	20
4.2.1.5 Variance.....	20
4.2.1.6 Skewness	20
4.2.1.7 Tanks-in-Series (T-I-S) Model	21
4.2.1.8 The Peclet Number and Dispersion Coefficient	21
4.2.2 Experimental Design.....	21

4.2.2.1	Proposed Experimental Program	21
4.2.3	Experimental Set-up	22
4.2.4	Materials and Equipment required for Experimental Set-up	23
4.2.4.1	Experiment 1: Residence Time Distribution (RTD) Study	23
4.2.4.2	Experiment 5: Attempted Acid Regeneration using Column 3	26
4.2.4.3	Experiment 6: Attempted Acid Regeneration using Column 1	26
4.2.5	Methodology.....	26
4.2.5.1	Experiment 1: Residence Time Distribution (RTD) Study	26
4.2.5.2	Upon Start-up of Columns for Experiments 2, 3 and 4	28
4.2.5.3	Preparation of Equipment to be used in Experiments 2, 3 and 4.....	29
4.2.5.4	Commencement of Experiments 2, 3 and 4	30
4.2.5.5	Upon Replacement of Feed Water for Columns 2 and 3	30
4.2.5.6	Sample Collection during Experiments 2, 3 and 4	30
4.2.5.7	Testing of Iron and Sulphate Content.....	30
4.2.5.8	Testing of pH, dissolved oxygen content and electrical conductivity using Consort portable handheld probe	33
4.2.5.9	Usage of the Hydras Multiprobe for Experiments 2 and 4 (Columns 1 and 3).....	34
4.2.5.10	Experiment 5: Attempted Acid Regeneration using Column 3	35
4.2.5.11	Experiment 6: Attempted Acid Regeneration Using Column 1	35
4.3	SAFETY/ HAZOP CONSIDERATIONS	35
4.4	RESULTS	36
4.4.1	Experiment 1: Residence Time Distribution Study	36
4.4.1.1	Mean Residence Time.....	37
4.4.1.2	Variance and Skewness.....	38
4.4.1.3	Tanks-in-Series Model.....	39
4.4.1.4	The Peclet number, Dispersion Coefficient and Dispersion Number	39
4.4.1.5	Scaling of Residence Time obtained in RTD Study to Residence Time used in Experiments 2-4	40
4.4.2	Experiments 2, 3 and 4	41
4.4.2.1	Summary of experimental parameters	41
4.4.2.2	Comparison of Column 1 (oxygenated feed water), Column 2 (low deoxygenated feed water) and Column 3 (low deoxygenated feed water with multiple feed points).....	42
4.4.2.3	Comparison of Column 1 (oxygenated feed water) and Column 3 (low deoxygenated feed water with multiple feed points) using the Multiprobe.....	45
4.4.2.4	Comparison of pH with Iron and Sulphate Concentration and Electrical Conductivity (EC) for Column 1, Column 2 and Column 3.....	46
4.4.2.5	Comparison of Electrical Conductivity with Temperature for Column 1 (oxygenated feed water), Column 2 (low deoxygenated feed water) and Column 3 (low deoxygenated feed water with multiple feed points)	51
4.4.3	Experiment 5: Attempted Acid Regeneration using Column 3	52
4.4.4	Experiment 6: Attempted Acid Regeneration Using Column 1	56
4.5	CHAPTER CONCLUSIONS	57
	CHAPTER 5: The way forward.....	58
	CHAPTER 6: References.....	59
	Appendix A: Current Scenario	60
	Appendix B: Proposed Scenario.....	61

LIST OF TABLES

Table 2.1: Environmentally Critical Levels (ECLs) for various basins	5
Table 2.2: Summary of specified parameters used in pump calculations	8
Table 3.1: Sulphate formation during the first incubation – progressing quickly in the initial hours and days and reaching relative equilibrium by ~31 days.	15
Table 3.2: Sulphate formation during the second incubation progressed quickly and reached equilibrium by about day 3. Due to time limitations only one replicate per treatment was measured after 3-5 hours, and error estimates are not available.	15
Table 3.3: Dissolved oxygen concentrations in treatments on days 17 and 31 of the second incubation.	16
Table 3.4: Mean SO ₄ production in 3ℓ of incubation water from 400 g waste rock over 105 days. Standard deviations were estimated from the average coefficient of variation in the two incubations. There were no significant differences in total SO ₄ production between treatments.	16
Table 4.1: Summary of physical parameters for RTD study.....	36
Table 4.2: Comparison between mean residence time determined experimentally and the ideal residence time determined analytically	38
Table 4.3: Summary of parameters calculated from the RTD function and mean residence time.....	38
Table 4.4: Summary of parameters used in Reynolds number calculation as well as result of calculation	40
Table 4.5: Typical packed bed Reynolds number boundaries	40
Table 4.6: Base case parameters of potable water feed.....	41
Table A1: Calculation data for low estimate parameters, current scenario	60
Table A2: Calculation data for midrange estimate parameters, current scenario	60
Table A3: Calculation data for high estimate parameters, current scenario	61
Table B1: Calculation data for low estimate parameters, proposed scenario	61
Table B2: Calculation data for midrange estimate parameters, proposed scenario	62
Table B3: Calculation data for high estimate parameters, proposed scenario.....	62

LIST OF FIGURES

Figure 2.1: Western, central and eastern basins in relation to Johannesburg, South Africa (Council for Geoscience, 2010)	3
Figure 2.2: Schematic comparison of current short term management plan (left) and the proposed strategy of pumping from depth (right)	6
Figure 2.3: Comparison of percentage increase in pumping energy required using the method proposed	9
Figure 2.4: Sensitivity analysis for the proposed method using midrange estimates and a volumetric flow rate of 10 000 m ³ /day per pipe	9
Figure 2.5: Sensitivity analysis for the proposed method using midrange estimates and a volumetric flow rate of 10 000 m ³ /day per pipe	10
Figure 3.1. SO ₄ production in all treatments at pH 8 (top panels, A first incubation, and B, second incubation) and pH 3 (bottom panels, C, first incubation and D, second incubation). Error bars are standard deviations. In all treatments, a majority of SO ₄ formation occurred, and relative equilibrium concentrations were reached within in the first 3 days.....	14
Figure 3.2. Mean SO ₄ concentrations in mg/l at ~5 hours in the first incubation. The high DO/low pH treatment produced at least double the concentration of SO ₄ than the other treatments (P = 0.03) over this short time. Four of the six samples in the high DO/low pH category were over-range, and values shown (510 mg/l) are underestimates. Samples for SO ₄ analysis were drawn prior to placement in incubators, so replicates are not separated by temperature, and n = 6 for each treatment.	14
Figure 4.1: Schematic of RTD experiment	19
Figure 4.2: Experimental logic flow diagram	22
Figure 4.3: Experimental Set-up.....	23
Figure 4.4: Watson Marlow double head peristaltic pump	27
Figure 4.5: The three PVC columns loaded with coal waste rock containing pyrite	28
Figure 4.6: Merck iron and sulphate test kits.....	31
Figure 4.7: Hydras Multiprobe used to collect online data	34
Figure 4.8: Results of RTD study in relation to the rest of the experimental work	36
Figure 4.9: Concentration of tracer at exit pipe versus time.....	37
Figure 4.10: Residence-time distribution function	37
Figure 4.11: Distribution of residence times	37
Figure 4.12: Ideal flow of water through packed ore	38
Figure 4.13: Flow of water through packed ore with dispersion effects	38
Figure 4.14: Residence time distribution function for different numbers of tanks in series, from Fogler, 2012	39
Figure 4.15: Graphical interpretation of the magnitude of the dispersion number, from Fogler, 2012	39
Figure 4.16: Results of Experiments 2-4 in relation to the rest of the experimental work.....	41
Figure 4.17: pH in Column 1, Column 2 and Column 3 with increasing time as assessed at the end of each week.....	42
Figure 4.18: Electrical conductivity in Column 1, Column 2 and Column 3 with increasing time as assessed at the end of each week	43
Figure 4.19: Iron concentration in Column 1, Column 2 and Column 3 with increasing time as assessed at the end of each week.....	44

Figure 4.20: Sulphate concentration in Column 1, Column 2 and Column 3 with increasing time as assessed at the end of each week	45
Figure 4.21: pH, EC and temperature profiles within Column 1	46
Figure 4.22: pH, EC and temperature profiles within Column 3	46
Figure 4.23: pH and iron concentration profiles within Column 1	47
Figure 4.24: pH and iron concentration profiles within Column 2	47
Figure 4.25: pH and iron concentration profiles within Column 3	47
Figure 4.26: pH and sulphate concentration profiles within Column 1	48
Figure 4.27: pH and sulphate concentration profiles within Column 2	48
Figure 4.28: pH and sulphate concentration profiles within Column 3	49
Figure 4.29: pH and electrical conductivity profiles within Column 1	49
Figure 4.30: pH and electrical conductivity profiles within Column 2	50
Figure 4.31: pH and electrical conductivity profiles within Column 3	50
Figure 4.32: EC and temperature profiles within Column 1	51
Figure 4.33: EC and temperature profiles within Column 2	51
Figure 4.34: EC and temperature profiles within Column 3	52
Figure 4.35: Results and discussion of attempted acid regeneration experiments in relation to the rest of the experimental work	53
Figure 4.36: Variation of pH with depth inside column 3. Black line indicates 8 September and grey line indicates 15 September. The dashed line indicates the pH of tap water	54
Figure 4.37: Variation of conductivity of water with depth inside column 3. Black line indicates 8 September and grey line indicates 15 September	54
Figure 4.38: Extent of oxygen penetration and subsequent AMD formation	55
Figure 4.39: Variation of iron concentration with column depth. Black line indicates 8 September and grey line indicates 15 September	55
Figure 4.40: Variation of sulphate concentration with column depth. Black line indicates 8 September and grey line indicates 15 September	55
Figure 4.41: Variation of pH of water with time. The initial pH value was taken as the pH of the tap water used to fill the column	56
Figure 4.42: Variation of sulphate concentration in the water with time. The initial sulphate concentration was taken as the sulphate concentration of the tap water used to fill the column	56

ACRONYMS & ABBREVIATIONS

AMD	Acid Mine Drainage
DO	Dissolved Oxygen
EC	Electrical Conductivity
ECL	Environmentally Critical Level
HDSP	High Density Sludge Process
TCTA	Trans Caledon Tunnel Authority

CHAPTER 1: BACKGROUND

1.1 INTRODUCTION

This project arose from careful consideration of the short-term solution, as it is to be implemented for treating decant of AMD within the Witwatersrand Basins. Considering that the short-term solution being implemented was to pump from the aquifer, holding the ECL constant, and treating the pumped effluent using the HDSP, it was hypothesised that if we pumped from a lower level, whilst holding the same ECL, that acid might not be generated following removal of the initial acid present in the void as opposed to pumping from the ECL where acid would continuously be generated. This hypothesis is based on the premise that at depth, oxygen is very limited in water. This effect can be observed in marine environments, where corrosion of pier structures (due to oxidation) occurs in the surf zone which is highly oxygenated, whereas metallic wrecks remain uncorroded for centuries at the ocean floor. The phenomenon is also well observed in deep lakes where the deep levels in the lake are anaerobic. What we mean by depth is not defined, thus we ran the pumping scenario analysis for deep pumping – i.e. 2 km underground. The exact depth at which groundwater would become anaerobic is an unknown and would need to be addressed in future. In this project, we sought to simulate anaerobic, subsurface conditions with a view to testing our hypothesis.

As far as possible, we have attempted to write the chapters as scientific papers for peer-review dissemination. With this in mind, we request the readers' indulgence for any repetition which may occur across chapters.

1.2 PROJECT AIMS

In this project we wish to determine if the hypotheses posited are correct; namely:

- Pumping from the anaerobic region will not generate AMD ; and
- Pumping from a deep point within the aquifer will require similar energy costs.

It is important to clarify the first aim: we hypothesise that as the void fills with groundwater, that the water filling the void will be acidic. However, as water migrates to the well suction point it will gradually be replaced, not by acid, but by fresher and fresher water, until such time as the water is no longer acidic; i.e. as water is pumped from the anaerobic region, additional acid is not generated. Ultimately, a perched layer of acid will occur at the ECL.

1.3 SCOPE AND LIMITATIONS

This experiment is laboratory-scale and the results should be interpreted as such. Any data provided is presented in good faith.

Where possible, students have conducted the research under the guidance of qualified academic staff.

CHAPTER 2: INCREASING PUMPING DEPTH AS A SOLUTION IN THE LONG-TERM MANAGEMENT OF AMD

2.1 CHAPTER ABSTRACT

Acid mine drainage (AMD) poses a serious threat to water quality in the Witwatersrand region, owing to extensive, abandoned mine voids that have subsequently flooded. The formation of AMD requires a sulphide mineral (primarily pyrite), water and oxygen to regenerate ferric iron in order to produce net acidity. In response to the severity of the current situation, the South African government has undertaken construction and expansion of facilities to lower the water table to a safe level (e.g. where no AMD decants from the mine into the surrounding groundwater or surface water) in the worst affected portion of the basins through pumping and effluent treatment.

We propose using the same infrastructure that is currently being installed to manage the problem more effectively and sustainably by pumping from a greater depth. It is hypothesised that the anoxic conditions at this depth (ca. 2 km) will effectively preclude the generation of acid mine drainage and hence reduce the need for effluent treatment while maintaining the desired water level.

In this paper, the increase in energy required by pumping from a depth of 2 km is calculated relative to a current depth of just below the environmentally critical level. It is determined that the expected energy increase is in the region of 10%, suggesting that it is feasible to use the existing/planned pumping infrastructure at this depth. If pumping from lower depth is successful in extracting clean water, the ~10% increase in energy requirement should be at least partially offset by reduced cost of and energy demand for treatment.

2.2 INTRODUCTION

Extensive gold mining activity around the Witwatersrand Basin has resulted in the proliferation of acid mine drainage (AMD) and practical, cost effective solutions are urgently required to prevent and mitigate damage to freshwater resources and ecosystems. The potential AMD decant is in excess of 200 M³/day, and contains high levels of sulphate and dissolved toxic metals (McCarthy, 2011; Expert Team of the Inter-Ministerial Committee, 2010).

The South African government has awarded tenders to various industrial partners to mitigate the problem by pumping the water table down to below environmentally critical levels (ECLs) and treating the resulting effluent using the high density sludge process (HDSP) (Odendaal, 2013). This process is energy intensive as it requires transport of large quantities of lime to and from the treatment site and pumping between tanks and treatment ponds. Pumping and treatment can only, however, be a temporary solution to the problem, as fresh acid mine drainage will continue to be generated in the mine voids for an indefinite length of time and hence will continue to require treatment. This note proposes a modification to the intended pumping scheme which may potentially reduce the treatment required by altering the depth of the suction line.

2.3 LITERATURE REVIEW

2.3.1 Acid Mine Drainage

Acid mine drainage is generated in mine voids, primarily where pyrite-containing minerals are exposed to oxygenated water. The result is acidic (or alkaline, depending on the site) water that is rich in sulphates and toxic dissolved metals; this frequently includes uranium (Cukrowska et al., 2008). AMD poses a particular danger to the local environment of the Witwatersrand owing to the number of abandoned mines and characteristics of the water table in this semi-arid region (Durand, 2012). Decant of acid mine drainage (AMD) is a serious threat to the safety of communities and the environment of the Witwatersrand (Expert Team of the Inter-Ministerial Committee, 2010).

2.3.2 Prevalence and Severity of AMD in the Witwatersrand Basin

The immediate geological region of the Witwatersrand is named the Witwatersrand Supergroup, and consists of sedimentary rock approximately 7500 m thick (Durand, 2012). The Witwatersrand groundwater table is mainly supplied by karst aquifers located in the adjacent Transvaal Supergroup. Water flows from these dolomite-rich aquifers into the Witwatersrand Supergroup, and many of the gold mines in the area are located below the water level of karst aquifers. Hence, millions of litres of water were pumped out daily during peak mining activity periods. Mining activity depressed the water table by as much as 3 km (Durand, 2012). Following cessation of mining activities and associated pumping, groundwater has ingressed into pyrite-rich mine voids left behind, and is currently discharging into rivers in the provinces of Gauteng and the North West.

Mine voids in the Witwatersrand region are classified into the western basin, central basin and eastern basin (Figure 1). The western basin alone has an estimated void volume of at least 45 Gl. The condition of the water in the western basin is the worst of the three, containing the highest concentrations of metals and sulphides, with the lowest pH (Expert Team of the Inter-Ministerial Committee, 2010). Durand (2012) reports that decant of approximately 36 Mℓ of AMD per day was released from this basin into the Tweelopiespruit river in Krugersdorp in 2010, although pumping undertaken at Rand Uranium has reduced the decant considerably as of 2013 (Odendaal, 2013).

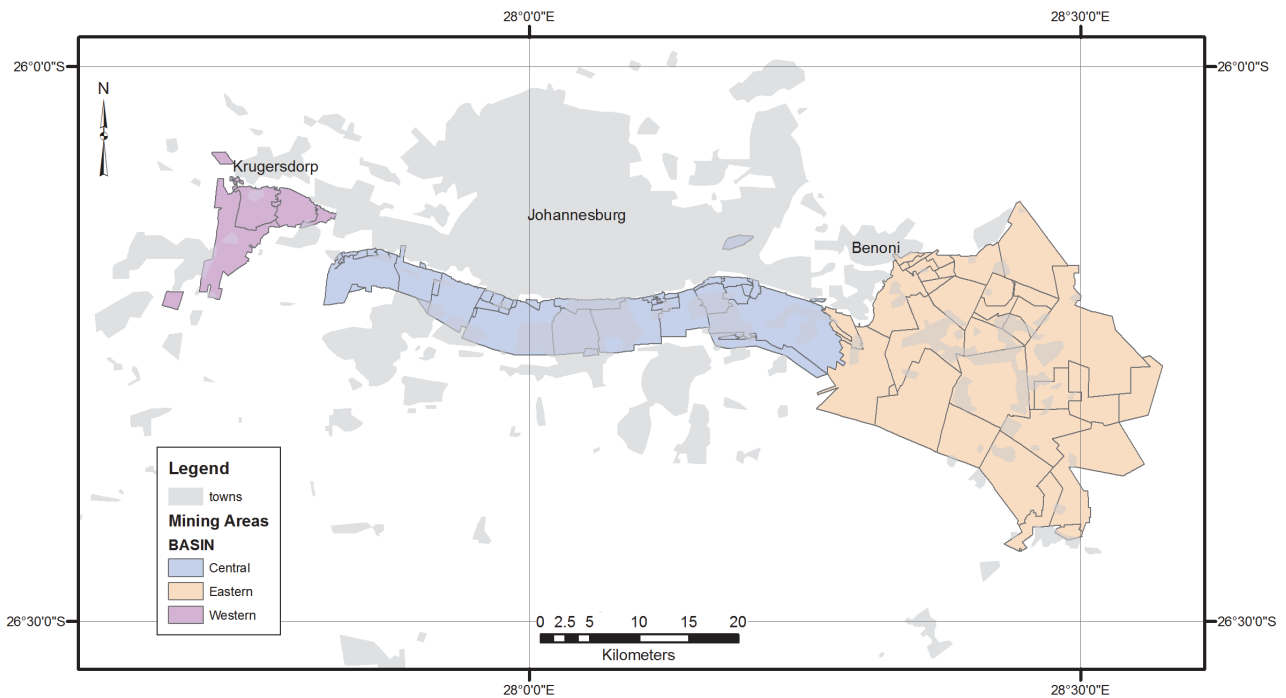


Figure 2.1: Western, central and eastern basins in relation to Johannesburg, South Africa (Council for Geoscience, 2010)

The water level in the central basin is still below the surface but is rising at a rate of 0.59 m/day, and is expected to reach the surface level over the course of 2013 (Expert Team of the Inter-Ministerial Committee, 2010). The situation in the eastern basin was assisted by pumping and treatment of mine water at the Grootvlei mine (Expert Team of the Inter-Ministerial Committee, 2010), but the level is currently at 423 m below grade, with decant to the surface expected by November 2014 (Odendaal, 2013).

The potential decant from the Witwatersrand Goldfield is estimated to be 350 Mℓ per day. This effluent not only poses serious ecological risks, but also threatens to contaminate drinking water supplies and undermine the dolomitic regions of the Gauteng and the North West, causing sinkholes (Durand, 2012).

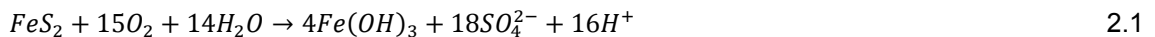
The severity of the AMD decant varies substantially with location. A study conducted by Cukrowska et al. (2008) on water quality in the Witwatersrand Basin indicated that the water quality nearest mining operations was most severely affected, with some samples having pH < 2 and sulphate concentrations exceeding

7000 mg/l in the worst cases. Also reported were high concentrations of iron (up to 1010 mg/l), as well as other metals including copper, nickel, cobalt and uranium.

In some cases, there are sufficient concentrations of uranium and other radioactive elements in mine decant and water bodies to pose serious risk to human health. For example, samples from some lakes near mining operations have been found to contain 14.8 mg/l of uranium, more than 1000 × the safe limit for irrigation water of 10 µg/l (Durand, 2012).

2.3.3 Mechanisms of AMD generation

The mechanisms of AMD generation are extensively reported in literature and are well-studied. The principal process involved occurs when pyrite-containing rocks (FeS₂) are contacted by oxygenated water, where the overall reaction (Equation 2.1) occurs (Hallberg and Johnson, 2005):



The above reaction occurs in multiple stages, and the primary oxidant is ferric iron instead of molecular oxygen – the attack of the ferric iron on the pyrite mineral occurs first, then the resulting ferrous iron is converted back to ferric iron by re-oxidation using oxygen dissolved in the mine water. Oxygenated water is therefore, essential for continuation of the cycle that produces acidity (Hallberg and Johnson, 2005).

While this is a naturally occurring reaction, the large surface areas exposed by mine voids and the subsequent flooding of the same, greatly increase the rate at which this process occurs.

The reaction can occur in the absence of bacterial activity, but micro-organisms such as *Acidithiobacillus ferrooxidans* can substantially increase the rate of generation by oxidising ferrous iron into ferric iron and breaking down sulphide minerals (Akcil and Koldas, 2006). The importance of biological activity is a strong function of pH, for example *A. ferrooxidans* is only active in water with a pH of 3.2 or less (Akcil and Koldas, 2006), and below pH 4, biological processes dominate (Hallberg and Johnson, 2005).

Due to the low pH of the mine water, leaching of various metals occurs, which results in contamination over and above the acidity and high sulphate content of the water. In the Witwatersrand, the primary metals of concern are manganese, aluminium, iron, nickel, zinc, cobalt, copper, lead, radium, thorium and uranium (Durand, 2012).

2.3.4 Current Management Strategies

According to a report prepared for the South African Government on management of AMD by the Expert Team of the Inter-Ministerial Committee (2010), the situation in the Witwatersrand requires action in three priority areas.

Firstly, in order to prevent ecological disaster, it is necessary to prevent uncontrolled decant of AMD into waterways. This is to be accomplished by pumping out of the three main basins in order to keep the water table below the environmentally critical level (ECL). The environmentally critical level is defined as the highest level within the mine void where no AMD decants from the mine into the surrounding groundwater or surface water systems (Expert Team of the Inter-Ministerial Committee, 2010). The area requiring the most urgent action is the Western Basin, where the level of the mine water is already at the surface. The ECLs for the three basins are provided in Table 2.1.

Secondly, limit the ingress of water into the mineshafts by sealing as many large openings as possible, which serves to reduce the volume of water entering the voids and therefore lowers the rate of decant as well as the pumping requirements.

Finally, the water that is pumped out of the void will still be acidic and contain dissolved heavy metals, and hence requires treatment before it can be released into the environment (Expert Team of the Inter-Ministerial Committee, 2010). There are many possible methods for neutralisation, including neutralisation with lime, passive remediation in limestone beds, bioremediation using aerobic wetlands, bioreactors and more

(Hallberg and Johnson, 2005). In-situ and passive methods are currently regarded as unfeasible for the Witwatersrand Basin because of the size and complexity of the voids as well the large decant rates expected. The expected cost of active treatment of the discharge is ZAR11 /m³ (Expert Team of the Inter-Ministerial Committee, 2010) or approximately USD1.1 /m³.

Table 2.1: Environmentally Critical Levels (ECLs) for various basins

Basin	ECL [elevation above sea level, m] (Expert Team of the Inter-Ministerial Committee, 2010)	ECL [m below grade] (Odendaal, 2013)
Western	1530	165
Central	1503	186
Eastern	1150	290

In response to the problem of AMD decant, the above strategies are currently being implemented. The state-owned Trans-Caledon Tunnel Authority (TCTA) awarded a R319 million contract to Group Five Engineering in December 2012 (Odendaal, 2013). The contract includes construction of pumping stations and high-density sludge treatment facilities to pump down the ECL in the central basin. In the western basin, upgrades are being carried out on the existing pumping and treatment facilities at Rand Uranium in order to expand capacity. Due to cost constraints, construction of pumping systems in the eastern basin has been postponed (Odendaal, 2013).

2.4 PROPOSED METHOD

The proposed method entails using the same pumping systems as currently intended, but instead of drawing water from just below the ECL (approximately 300 m below grade); the suction point of the system would be located 2-3 kilometres underground. The intention is to draw water up from an area sufficiently deep to contain no dissolved oxygen, at a rate that will essentially immobilise existing AMD in mine voids. It is hoped that drawing water from this depth will cause horizontal/lateral inflow of anoxic groundwater from neighbouring aquifers, and that existing AMD will be effectively perched, preventing formation of new AMD. Because the drawn volume being pumped out will equal recharge from the surface, the level of acidic groundwater can be maintained at the ECL, as in the current scheme.

Based on the understanding of AMD formation described above, it is believed that the lack of oxygen in the water at this depth will inhibit the reactions required to generate acid, *i.e.* the absence of a primary reactant for the creation of acid is missing. Therefore, it is expected that the water at this depth should be free of acid. Initially the water in the pipe may contain high sulphate concentrations and a low pH, but if the suction port is appropriately sealed, there should be no way for surface or upper level acid to enter the system. If there is no production of acid at this depth, after the initial phase, no treatment would be required for the water and it could be safely discharged or used for another purpose. This could provide sizeable economic and environmental advantages if additional water treatment is not required. It is further hypothesised that the proposed new suction depth will not result in a significant increase in pumping duty over the current project, and this is explored in more detail below.

If our hypothesis is correct, sealing the mine openings will be required to eliminate “short-circuiting” of oxygenated surface water into the excavations. This has already been recommended as a compliment to the current short-term solution. The proposed scheme is represented in Figure 2.2.

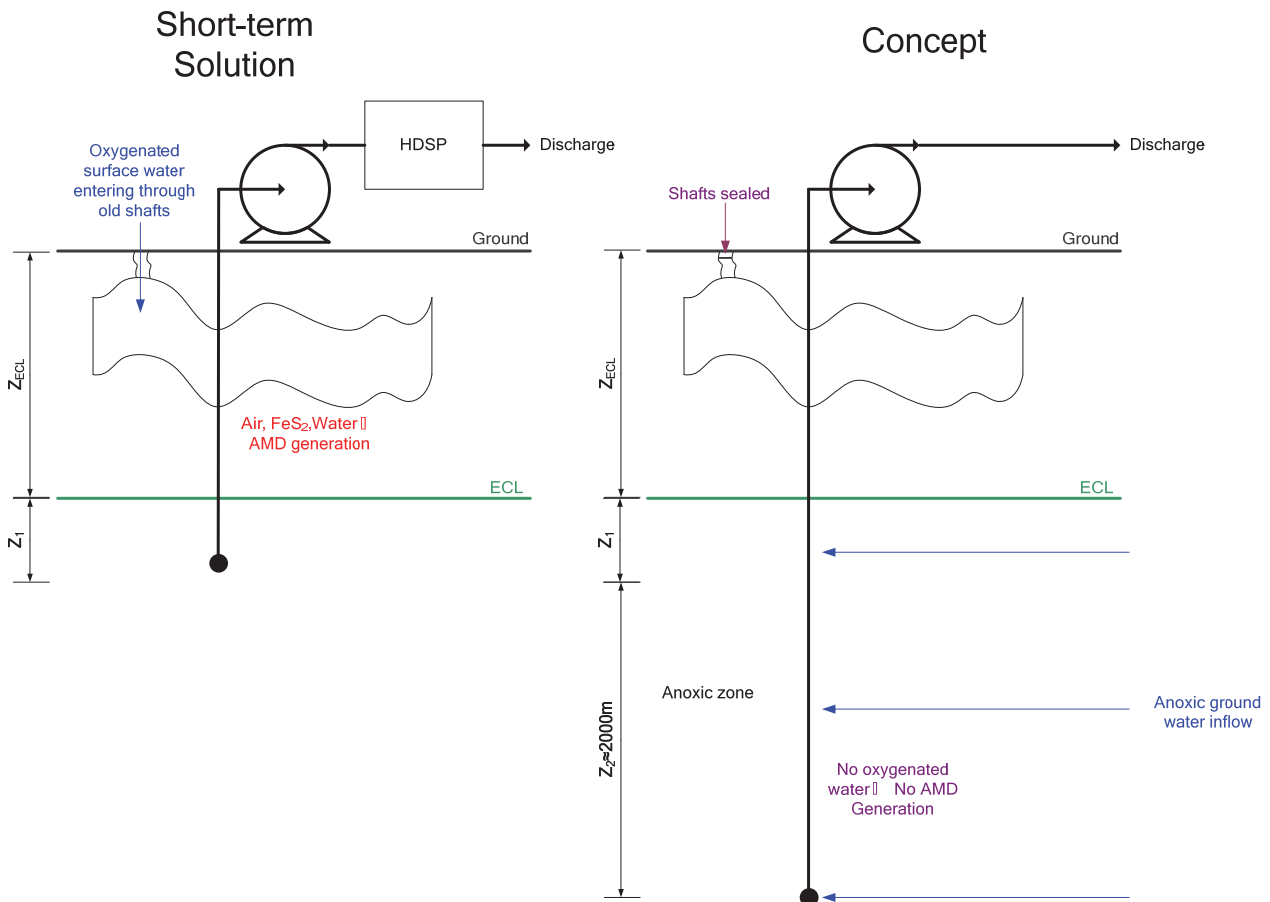


Figure 2.2: Schematic comparison of current short term management plan (left) and the proposed strategy of pumping from depth (right)

2.5 COMPARISON OF PUMPING DUTY

2.5.1 Calculation of Pumping Duty

The pumping calculations presented here follow the general layout and nomenclature indicated in Fig 2.2. For both systems, it is assumed that pumping is used to maintain a constant ECL using a pump situated at ground level.

2.5.2 Theory

In general, contributions to the head requirement of a pumping system can be divided into two components; a head difference between the source and the destination and losses due to friction (Rorrer et al., 2008). As will be shown, assuming a hydrostatic continuum, the head difference is independent of the depth of the pump suction inlet. Therefore, the difference between the energy requirements between the current pumping scheme and the proposed system stems only from different losses to friction due to different pipe lengths.

Assuming an incompressible fluid, the head addition by the pump, h_A , is given by Rorrer *et al.* (2008) as:

$$\left(\frac{1}{2g} u_i^2 + Z_i + \frac{P_i}{g\rho} \right) + h_A - h_L - h_R = \left(\frac{1}{2g} u_f^2 + Z_f + \frac{P_f}{g\rho} \right) \quad 2.2$$

In the above equation, the subscripts i and f are used for the conditions at the suction and delivery ends of the pipe respectively. Assuming no work extracted from the fluid ($h_R = 0$), and that the diameter of the pipe is constant ($u_i = u_f$), Equation 2. can be rewritten as:

$$h_A = \left[(Z_f - Z_i) + \frac{(P_f - P_i)}{g\rho} \right] + h_L \quad 2.3$$

From Fig 2.2 the depth of suction for the current solution scheme is some small distance below the ECL, therefore $Z_i = Z_{ECL} + Z_1$. The pressure at the suction depth is higher than the pressure at the ECL due to the mass of the fluid, and is given by $P_i = P_{ECL} + Z_1\rho g$. Applying the above to Equation 2. yields:

$$\begin{aligned} h_{A,Current} &= \left[Z_f - (Z_{ECL} + Z_1) + \frac{P_f - (P_{ECL} + Z_1\rho g)}{\rho g} \right] + h_{L,Current} \\ &= \left[Z_f - Z_{ECL} + \frac{P_f - P_{ECL}}{\rho g} \right] + h_{L,Current} \end{aligned} \quad 2.4$$

For the proposed method, the suction depth is Z_2 meters greater and is given as $Z_i = Z_{ECL} + Z_1 + Z_2$. The pressure at this depth is proportionally higher, with $P_i = P_{ECL} + Z_1\rho g + Z_2\rho g$. Applying these to Equation 2.3 yields:

$$\begin{aligned} h_{A,Proposal} &= \left[Z_f - (Z_{ECL} + Z_1 + Z_2) + \frac{P_f - (P_{ECL} + Z_1\rho g + Z_2\rho g)}{\rho g} \right] + h_{L,Proposal} \\ &= \left[Z_f - Z_{ECL} + \frac{P_f - P_{ECL}}{\rho g} \right] + h_{L,Proposal} \end{aligned} \quad 2.5$$

A comparison of Equations 2.4 and 2. reveals that the required pump head only differs in the losses incurred, as expected.

The frictional losses, h_L , are assumed to result only from friction along the length of the pipe. The losses may be related to the Fanning friction factor as follows (Rorrer et al., 2008):

$$h_L = 2f_f \frac{L u^2}{D g} \quad 2.6$$

Because there is a direct relationship between length and frictional losses, the proposed solution will require a greater pump head to compensate for a longer line. The line length of current solution is given as $L_{Current} = Z_{ECL} + Z_1$ and the length of the proposed line is given as $L_{Current} = Z_{ECL} + Z_1 + Z_2$.

The Fanning friction factor is a function of Reynolds number, but converges to a constant value, related to the material of construction and roughness of the pipe, at high Reynolds numbers/highly turbulent conditions. Haaland provides an expression for the Fanning friction factor on the interval $Re \in [4 \times 10^4; 10^8]$, $\frac{e}{D} \in [0; 0.05]$ to ± 1.5 % accuracy as (Haaland, 1983):

$$\frac{1}{\sqrt{f_f}} = -3.6 \log_{10} \left[\frac{6.9}{Re} + \left(\frac{e}{3.7D} \right)^{\frac{10}{9}} \right] \quad 2.7$$

It is observed that as the Reynolds number approaches infinity, the expression inside the logarithm converges to $\left(\frac{e}{3.7D} \right)^{\frac{10}{9}}$.

2.5.3 Assumptions and Important parameters

In determining the parameters required in the above calculations, an attempt has been made to be conservative; but considerable uncertainty remains in numerous parameters. Therefore low, midrange and high estimates of the required pumping duty are provided.

2.5.3.1 Environmentally Critical Level and Pumping Suction Depth

The ECL is an important parameter as it indicates the direct altitude difference between the pump inlet and discharge. As discussed in Section 2, the ECL in the Witwatersrand basin varies considerably, but 300 m was selected for all cases as a maximum. The depth of pumping for the current solution must be lower than

the ECL and was chosen, in the absence of other information, as 500 m below grade. For the proposed method, the pumping depth was conservatively set to 2500 m below grade. The pumps are assumed to be at ground level. It is assumed that the pressure at the ECL level is atmospheric, meaning $P_f - P_{ECL} = 0$ in Equations 2. and 2. .

2.5.3.2 Flow rate, Pipe Dimensions and Properties

A flow rate of 50 Ml/day was selected for pipe sizing for both scenarios. Assuming four parallel pipes, a 30 cm-diameter pipe provides an acceptable linear velocity ($u \approx 2 \text{ m.s}^{-1}$). A pipe diameter of 35 cm was selected for the low estimate, 30 cm for the midrange estimate and 25 cm for the high estimate. The pipes are assumed to be plastic and the absolute roughness for the low, midrange and high estimates are chosen as 7 μm , 15 μm and 20 μm respectively (Backhurst et al., 1999).

2.5.4 Fluid Properties

Fluid density and viscosity are important parameters affecting the pumping duty. Little information is available about the physical properties of the water in the Witwatersrand Basin at depths below 2 km. It is noted that temperature increases rapidly with depth, and the temperature at a depth of 3.8 km is reported to be 55°C (Owens, 2013). At this temperature, the viscosity of water is $0.55 \times 10^{-3} \text{ Pa.s}$, approximately 55% of the value at room temperature (Backhurst et al., 1999). However, because lower viscosity results in lower pipe friction, a value of $1 \times 10^{-3} \text{ Pa.s}$ was chosen to produce a conservative estimate. The density of fluid was chosen as 1000 kg/m^3 , 1050 kg/m^3 and 1100 kg/m^3 for the low, midrange and high estimates respectively. A summary of the various parameters are presented in Table 2.2.

Table 2.2: Summary of specified parameters used in pump calculations

Parameter		Estimate*	Current Scenario	Proposed scenario
Elevations Relative to pump	Pump Elevation [m]	-	0	0
	ECL [m]	-	-300	-300
	Suction Depth [m]	-	-500	-2500
Pipe Dimensions and Properties	Diameter [m]	Low	0.35	0.35
		Mid	0.3	0.3
		High	0.25	0.25
	Absolute Roughness [μm]	Low	7	7
		Mid	15	15
		High	20	20
Fluid Properties	Viscosity, Dynamic [Pa.s]	-	0.01	0.01
	Density [kg/m^3]	Low	1 000	1 000
		Mid	1 050	1 050
		High	1 100	1 100

Low, Midrange or High Estimate*

2.5.5 Calculation Results

The pumping energy requirement increases (exponentially) with increasing volumetric flow rates (*i.e.* the volume of water pumped per unit time through a pipe) (Figure 2.3). The energy difference between the conservative, midrange and high estimates is greater for higher flow rates, as the losses due to friction are proportional to the square of linear velocity. The maximum difference observed, for the high-range estimates and highest flow rates, is in the order of a 50% increase. Also indicated on Figure 2.3 are the regions where the linear velocity is within the normally accepted bounds of 1-2 m/s (Sinnott, 2005). By maintaining a maximum velocity of 2 m/s, none of the cases require more than 10% extra pumping energy to accomplish pumping from the greater depth.

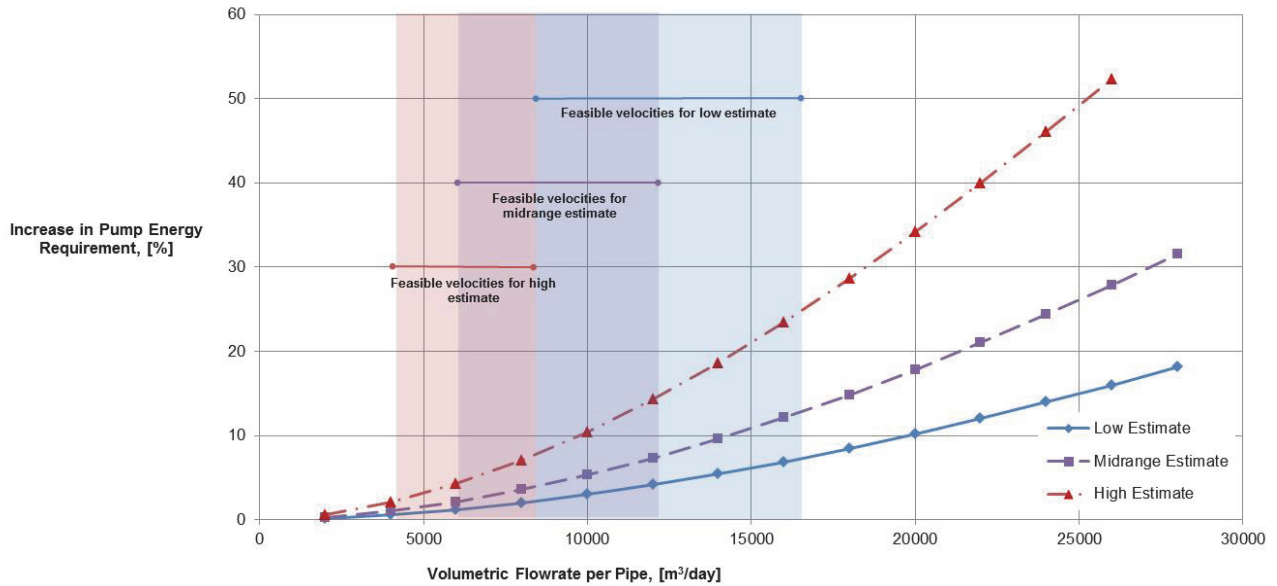


Figure 2.3: Comparison of percentage increase in pumping energy required using the method proposed

A sensitivity analysis was conducted in the linear velocity, pipe roughness and pipe length (Figure 2.4). The most important factor controlling the increase in energy requirement is to limit the linear velocity, or equivalently, ensuring a sufficient pipe diameter and number of parallel pipes to ensure the velocity is in the appropriate region. Pipe roughness has a very minor impact on pumping energy requirement, as even tripling the roughness of the pipe only increases the head losses by less than 2%. For comparison, a 100% increase in linearly velocity results in 346% increase in the head loss to friction. Pipe length is also varied as it is not known with certainty what piping depth is required to ensure withdrawal of consistently anoxic water, and this has a directly proportional effect on the head loss to friction.

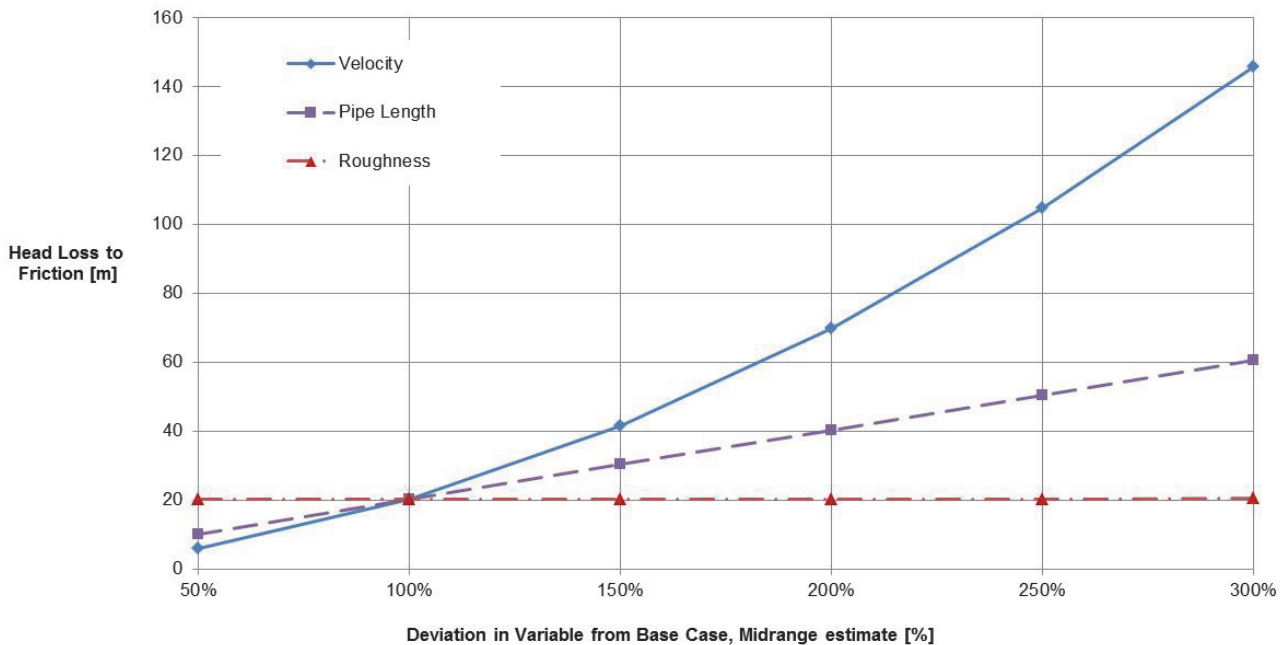


Figure 2.4: Sensitivity analysis for the proposed method using midrange estimates and a volumetric flow rate of 10 000 m³/day per pipe

2.6 EXPERIMENTAL APPROACH

The success of the proposed scheme relies on the validity of the assumption that AMD generation cannot occur in anoxic water. In order to test this, an experiment was designed and run at the University of Witwatersrand, School of Chemical and Metallurgical Engineering, starting in August 2013.

The experiment quantified generation of AMD in three packed columns, comparing the chemistry of oxygenated tap water and deoxygenated tap water that has passed through AMD-forming slimes. The columns were made from plastic, had heights of 12 m and measured approximately 30 cm in diameter. They were filled with pyrite-rich rock from a local mine. A small plastic casing ran down the middle of the column containing the pump suction line. A multi-channel peristaltic pump drew water from the bottom on the column for analysis and feed an equal flow rate of fresh water into the top of the column (Figure 5). For all units, the residence time was held constant at 4 weeks. The column effluent was analysed daily for pH, sulphate content and dissolved oxygen.

In the first column, the fresh water feed consisted of municipal potable water. In the second column, the fresh water was drawn from a tank containing potable water that had been sparged with nitrogen until it contained <1% dissolved oxygen, as indicated by a dissolved oxygen meter. This allowed testing of the hypothesis that no AMD is formed under anoxic conditions. For the final column, the feed was drawn from the same tank as the second, but the feed water was added at 3 m intervals down the column instead of at the top, in order to simulate ingress of deoxygenised water from aquifers at different levels as hypothesised.

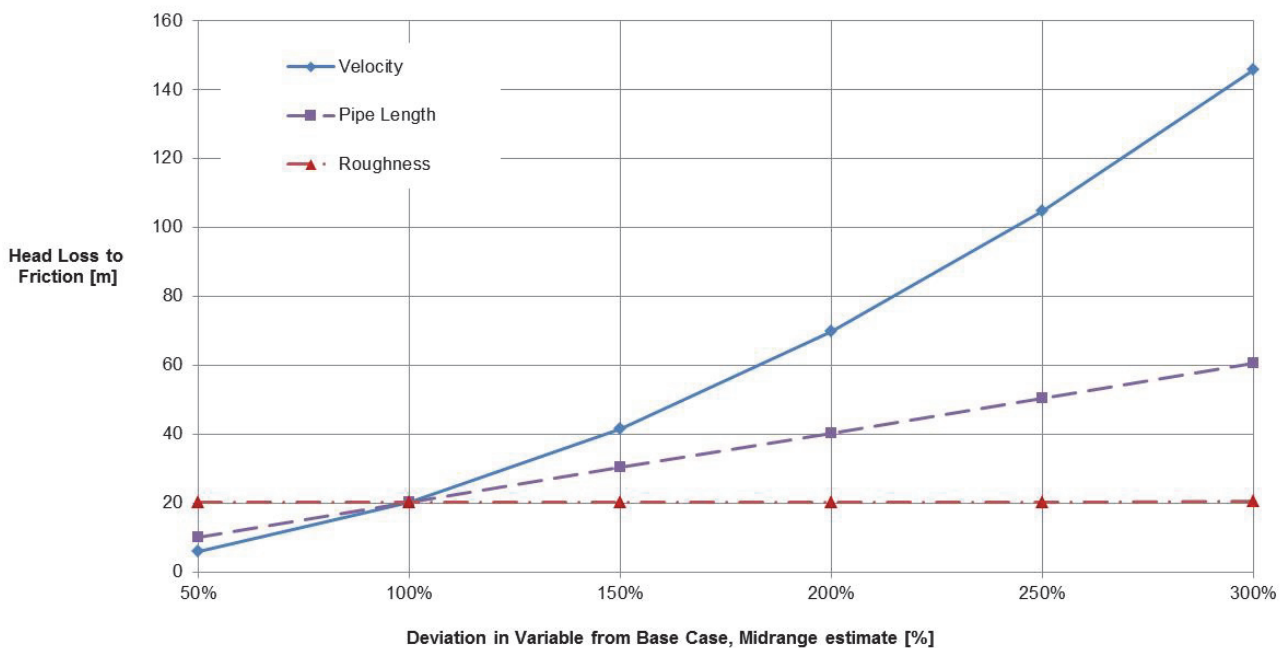


Figure 2.5: Sensitivity analysis for the proposed method using midrange estimates and a volumetric flow rate of 10 000 m³/day per pipe

2.7 CONCLUSIONS

This chapter provides a summary outline of a novel proposal for managing AMD on the Witwatersrand and elsewhere, with the potential advantage of eliminating the long-term requirement of water treatment. Given that AMD is already at the surface level in the western basin, and will soon reach the same level in other regions, urgent construction of pumping operations to keep the AMD level below the ECL is currently underway.

The method described here involves modifying the pumping scheme that is currently being implemented to draw water from a greater depth, theoretically containing no dissolved oxygen. The hypothesis is that since oxygen is a required component for the generation of AMD, the water at this level will be free of AMD and

therefore safe for discharge. This is in contrast to the current scheme, where the suction line is near the AMD generating zone and hence requires treatment before release. The hypothesis is supported by observations in literature about the process of AMD generation.

It is further hypothesised that the currently implemented/planned pumping infrastructure could be adapted to fit the proposal with minimal effort. Calculations indicate that the pumping energy requirement is less than 10% greater than at the current depth, as long as appropriate line velocities are maintained. This suggests that it would be possible to use the current pumps and maintain a suitable flow rate in order to maintain constant water level.

Additionally, an experiment designed to test the oxygen hypothesis is outlined, and will be conducted at the School of Chemical and Metallurgical Engineering at the University of the Witwatersrand, Johannesburg. The experiment will allow the effect of dissolved oxygen content on the process of AMD generation to be confirmed and a lab-scale demonstration of the proposed system will be conducted.

CHAPTER 3: A BENCHTOP STUDY QUANTIFYING THE ROLE OF pH, DISSOLVED OXYGEN AND TEMPERATURE IN FORMATION OF AMD FROM COAL MINE WASTE ROCK

3.1 INTRODUCTION

Mining activities over the last 120 years in the Witwatersrand Basin have exposed an enormous surface area of metal-sulphide rich minerals to oxygen and water, accelerating natural oxidation processes in mine voids and tailings piles. While the mines operated, water tables were kept artificially low through groundwater pumping, but as mines have closed, pumping has ceased and groundwater levels rise (Sheridan 2013). Most mines in the central Witwatersrand Basin have now been closed; in the pyrite-rich Witwatersrand alone there are approximately 6 000 closed mines and 270 tailings dams (Kolver 2013) either generating or with the potential to generate mine drainage. Rising water tables in mine voids are dissolving acidic salts that have formed on the exposed walls of the void (Johnson and Hallberg 2005) and as the water rises, exposed sulphide can react to acidic form (Name and Sheridan, 2014). Oxidation and dissolution of these minerals in water results in AMD formation (e.g. Sebestova *et al.* 1996, McCarthy 2011).

Although the characteristics of mine drainage vary with parent material, AMD is generally characterized by low pH (< 5.5), high electrical conductivity (>3000 $\mu\text{S}/\text{cm}$) and high iron, sulphate and other metal concentrations. Pollution of water by AMD has profound consequences for both humans and ecosystems. Mitigation of AMD is extremely expensive. Currently, the South African government is attempting to control the rate and location of AMD decant near Johannesburg by pumping groundwater to maintain the water table below the environmentally critical level (ECL – approximately 500 m) in and around abandoned mine voids. The pumped water contains AMD, and is to be treated at the surface using the high density sludge process (HDSP) (Odendaal, 2013). This requires additional pumping between tanks and treatment ponds, and also requires transport of large quantities of lime and metal-laden sludge to and from treatment sites. In addition, the cost while uncertain is prohibitive (Sheridan 2013). Although a number of AMD treatment methods are available (see Johnson and Hallberg, 2005), all of them, including pumping and HDSP, are energy-intensive either through direct energy demands, requirements for transport (e.g. of lime), or construction of treatment systems. The expense of AMD treatment results in it often being left untreated (e.g. Diz, 1997).

Pumping and HDSP treatment is clearly not viable over the long run because AMD will continue to be generated in mine voids and tailings piles for an indefinite length of time. We have proposed pumping water from well below the ECL (Janet *et al.* in review) in the hopes that this will yield water that does not require treatment after existing salts have been depleted, and given the hypothesis that acid can only be generated when oxygen is present. Our calculations show that pumping from 2 000 m as opposed to 500 m will require approximately 10% more energy, but if the resulting effluent (water pumped) is free of AMD, it will eliminate the need for pH neutralisation or sulphate/heavy metal removal.

A next logical test of the feasibility of pumping from greater depth is whether AMD formation occurs under conditions at 2000 m, where groundwater is almost certainly hypoxic or anoxic and temperatures and pressures are elevated. Of particular interest is whether AMD formation is retarded or slowed under low dissolved O_2 availability. As the void filled, it was almost certainly able to produce acid. If this water were removed, whilst being acidic initially, with time we have hypothesized that the acid generating capacity is reduced or potentially eliminated due to the absence of oxygen and it is for this reason that we anticipate that by pumping from this depth that the water quality would gradually increase.

This chapter details rates of AMD formation from coal mine waste rock (indicated by sulphate concentration) under conditions representing the ECL at depths of less than 500 m, including mine voids and at depth (~2000 m) where we expect very low DO and high temperature. Additionally, the pH of water moving through groundwater systems strongly affects both AMD generation (Akciil and Koldas 2006) and the chemistry of AMD after decant (Rose and Elliot 2005). The combined wet and dry acid deposition in the Johannesburg area is about 50 meq m^2/y , with some parts of northern Gauteng and areas near Johannesburg exceeding acid critical loads determined from soil buffering capacity (Josipovic *et al.* 2011).

Thus the pH of precipitation is decreasing with increasing industrial emissions in the Johannesburg area, and pH is also a factor of interest for AMD formation in the area, particularly in mine waste dumps.

The aim of this study was to quantify how pH, temperature and initial availability of oxygen in reaction water (i.e. the water in which coal mine waste rock is incubated) affect the formation rate of AMD from Witwatersrand coal waste rock. These are three of the main determinants of acid formation rates in AMD (Akcil and Koldas 2006).

3.2 METHODS AND MATERIALS

3.2.1 Experimental Design

High-sulphide mine waste rock, discarded during the coal mining process, was collected in Midrand, Gauteng, South Africa. A replicated, factorial-design experiment was used to examine the relative effects of pH and dissolved oxygen (DO) in reaction water, and incubation temperature on SO_4 production from this material. The waste rock was incubated in water for a total of 105 days, and the water was changed at day 76 to determine whether the salts on rock surfaces were becoming depleted (i.e. if SO_4 production decreased) and to examine potential limit on the production of AMD.

3.2.2 Laboratory Methods

Waste rock was lightly rinsed with tap water to minimise dust and O_2 adhering to rock surfaces, before the incubations were initiated. 400 g of waste rock was placed in each of twenty-four, 1.5 l sealable clear glass jars ($n = 3$ in each treatment). Two replicates of each of the treatments containing no coal were incubated as controls. Rock particles from 0.5-10.0 cm (maximum dimension) were used and we attempted to maintain consistent size distributions among all jars (visually estimated).

Starting conditions of reaction water were pH 3 or 8, DO of either $< 0.1 \text{ mg/l}$ or $> 3.45 \text{ mg/l}$, and incubation temperatures of either room temperature ($\sim 22^\circ\text{C}$) or 40°C . All incubations proceeded under dark conditions except during set-up and monitoring. Tap water was used for high pH treatments (pH 7.8-8.1) while HCl was added to bring pH to ~ 3 for the low pH treatments. Tap water with an initial DO of $\sim 3.5 \text{ mg/l}$ was used for the high DO treatments and low DO treatment water (0.1 mg/l) was produced by boiling tap water. Low DO treatments were sealed with parafilm and a sealable lid (removed only for measurements), while high DO treatments were left open to the atmosphere. DO and pH treatments (low, high) refer to water quality as the incubations were *initiated*, and we did not attempt maintain those conditions throughout the incubation. Both pH and DO changed considerably in all treatments over the incubations.

Sulphate quantification required removal of 10 ml from each jar at each sampling time. This volume was replaced with deionised water to maintain full jars and to ensure contact of water surface with the parafilm and limit diffusion of oxygen into the low DO treatments. Samples were stored frozen until spectrophotometric analysis. Solutions for a standard curve were made using sodium sulphate (analytical reagent grade). Sulphate concentrations were then determined using the turbidimetric method with barium chloride (Patnaik, 2010).

pH, temperature and SO_4 concentrations were measured 3-5 hours after the incubations were established, 3 days after initiation, and then at two-week intervals for a total of 74 days. Incubation water was then replaced with the same type of treatment water (initial low/high pH, low/high DO) and the incubations proceeded for an additional 31 days. pH was measured using a Hanna HI 9210N ATC pH meter. Dissolved oxygen was measured using a Thermo Scientific Orion 3 Star DO portable meter with Orion 083010 dissolved oxygen probe.

3.3 RESULTS

Overall, SO_4 formation proceeded at similar rates in all treatments with a majority of production occurring within hours to days of initiation (Figure 3.1, Table 3.1). Few significant differences in SO_4 formation were detected between treatments and incubations. In the first ~ 5 hours of incubation, however, waste rock exposed to high DO and low pH produced approximately twice as much SO_4 as the other treatments (Figure

2; two-way ANOVA $P = 0.03$). This difference was not seen in the second incubation. By day 3, however, SO_4 concentrations in the high DO/low pH treatment were statistically equal to other treatments (Table 3.1). By day three SO_4 concentrations in all treatments had increased to 300-730 mg/l (a majority of change seen), and within 31 days the treatments had generally reached relatively stable concentrations between 450-680 mg/l, not changing significantly over the following month. SO_4 production during the second incubation showed similar patterns, with almost all change occurring in the first three days of the incubation (Figure 3.2, Table 3.2).

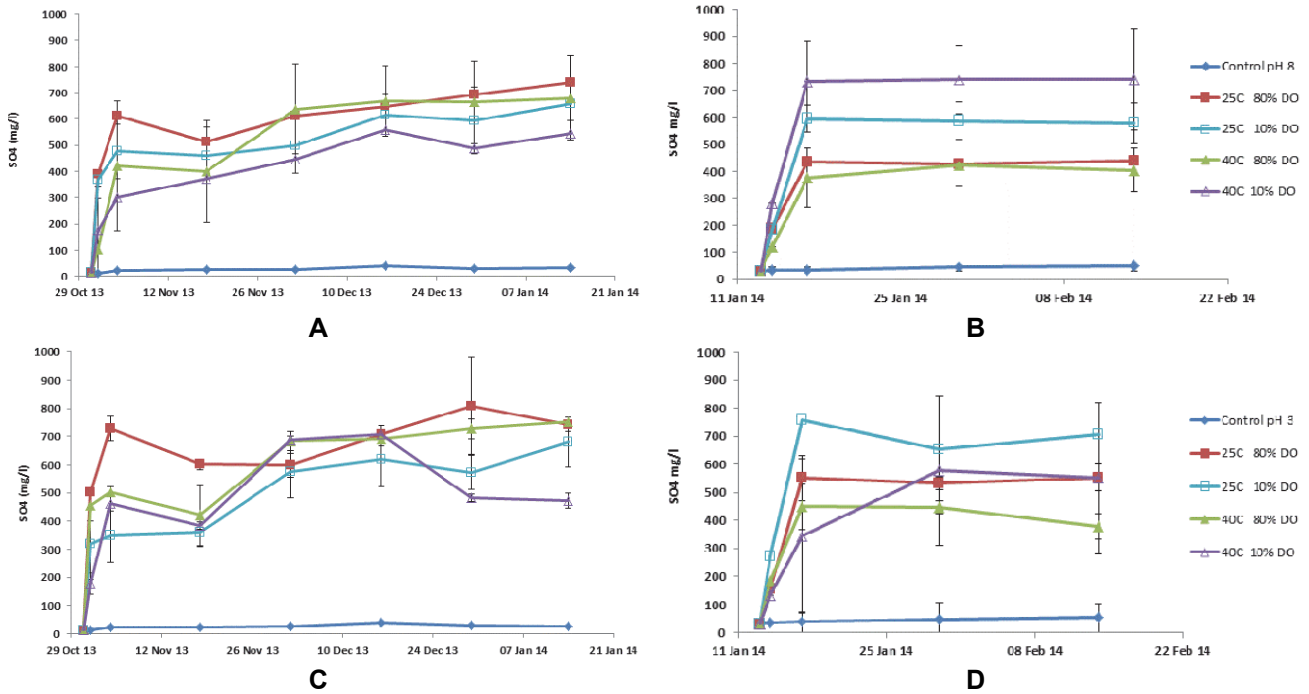


Figure 3.1. SO_4 production in all treatments at pH 8 (top panels, A first incubation, and B, second incubation) and pH 3 (bottom panels, C, first incubation and D, second incubation). Error bars are standard deviations. In all treatments, a majority of SO_4 formation occurred, and relative equilibrium concentrations were reached within in the first 3 days.

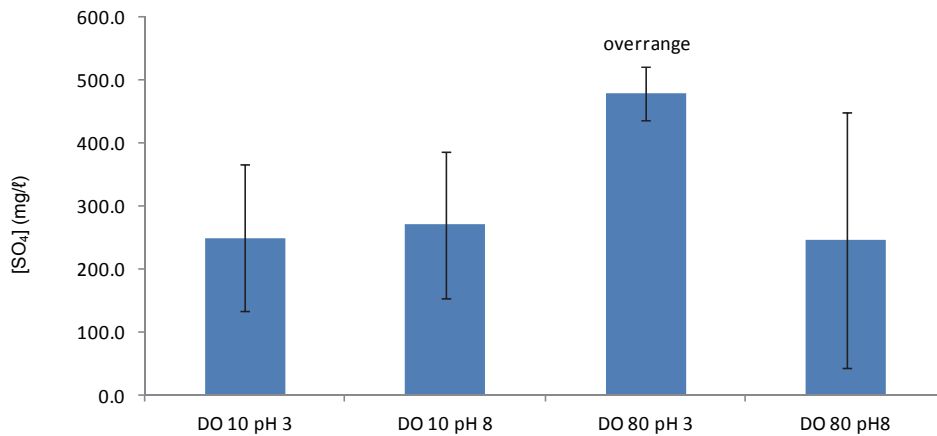


Figure 3.2. Mean SO_4 concentrations in mg/l at ~5 hours in the first incubation. The high DO/low pH treatment produced at least double the concentration of SO_4 than the other treatments ($P = 0.03$) over this short time. Four of the six samples in the high DO/low pH category were over-range, and values shown (510 mg/l) are underestimates. Samples for SO_4 analysis were drawn prior to placement in incubators, so replicates are not separated by temperature, and $n = 6$ for each treatment.

Table 3.1. Sulphate formation during the first incubation – progressing quickly in the initial hours and days and reaching relative equilibrium by ~31 days.

Treatment			SO ₄ concentrations (mg/l) ± SD				Equilibrium concentration days 28 - 56
Temp	pH	DO	Initial	5 hours	3 days	28 days	
40	3	10	< 15	178 (37.5)	461 (27.0)	687 (15.8)	587 (22.3)
40	8	10		174 (24.5)	300 (104.4)	446 (108)	510 (95.4)
40	8	80		103 (49.7)	421 (34.8)	638 (20.9)	663 (19.1)
40	3	80		454 (52.5)	504 (18.4)	683 (33.7)	713 (24.2)
25	3	10		320 (128.4)	349 (96.5)	575 (92.0)	612 (83.8)
25	8	10		366 (69.2)	477 (131.5)	499 (32.6)	592 (31.2)
25	8	80		391 (194.0)	611 (248.5)	610 (170.5)	673 (155.1)
25	3	80		> 500	729 (43.9)	599 (41.8)	714 (67.4)

Table 3.2. Sulphate formation during the second incubation progressed quickly and reached equilibrium by about day 3. Due to time limitations only one replicate per treatment was measured after 3-5 hours, and error estimates are not available.

Treatment			SO ₄ concentrations (mg/l) ± SD			
Temp	pH	DO	Initial	5 hours	3 days	Equilibrium concentration days 14-28
40	3	10	< 10	135	343 (38.1)	564 (57.6)
40	8	10		281	733 (25.5)	741 (10.1)
40	8	80		121	377 (51.7)	414 (65.3)
40	3	80		182	449 (151.2)	411 (149.6)
25	3	10		273	759 (25.73)	681 (35.7)
25	8	10		183	597 (82.1)	584 (32.4)
25	8	80		187	436 (35.2)	433 (103.2)
25	3	80		154	551 (111.1)	543 (71.6)

Production of SO₄ was marginally slower in the first few hours of second incubation (paired T-test, one-tailed P = 0.03), but by day 3, SO₄ production in the two incubations was statistically equal. Thus there is no evidence that oxidized sulphur based salts on the surface of the waste rock were being depleted.

Our ability to measure DO was compromised by high SO₄ concentrations through most of the study (high sulphate concentrations damage the DO probe), but we were able to measure DO on the first two and last two sampling dates (Table 3.4). DO clearly increased in the control treatments (from ~1.0 mg/l to 1.6 mg/l) in the first 3 days of incubation, suggesting that air was either leaking into the treatment containers, or had entered during measurement and sample collection despite efforts to limit exposure to the atmosphere. All low-oxygen treatments were sealed with parafilm and metal lids, and the change in DO is difficult to explain. Average DO in the high-oxygen controls decreased from 3.2 mg/l to 2.3 mg/l over the same period. DO concentrations in controls at day 17 and 31 of the second incubation also suggest contamination (Table 3.3). Low-DO waste rock treatments, however, contained much lower DO concentrations than controls. This suggests that leakage into the incubation containers was slow enough that the chemical reactions with waste rock consumed a majority of the leaked O₂. The data also suggest that this process occurs more quickly at higher temperature (Table 3.4). The SO₄ concentrations were not statistically different in almost all treatments on any given sampling day suggesting that SO₄ production was not limited by the *initial* availability of dissolved O₂.

Table 3.3. Dissolved oxygen concentrations in treatments on days 17 and 31 of the second incubation.

Treatment	Incubation temp (C)	DO (mg/l)	
		Day 17	Day 31
Low DO waste rock	40°	0.43	0.23
	22°	1.57	1.86
High DO waste rock	40°	4.14	3.79
	22°	3.47	2.33
Low DO Control	40°	3.17	3.50
	22°	3.27	4.15
High DO Control	40°	4.17	3.95
	22°	3.73	4.02

Total production of SO₄ by waste rock, summed over both incubations (105 days), was statistically equal in all treatments (Table 3.4). Additionally, the rapid increase in SO₄ concentration (within the first 3 days) in both incubations suggests that the waste rock examined here had a capacity for production of AMD that far beyond the measurements made in this study.

Table 3.4. Mean SO₄ production in 3ℓ of incubation water from 400 g waste rock over 105 days. Standard deviations were estimated from the average coefficient of variation in the two incubations. There were no significant differences in total SO₄ production between treatments.

Treatment			SO ₄ formation per treatment (mg)			
Temp	pH	DO	Incubation 1	Incubation 2	Total for both incubations (102 days)	Estimated SD
40	3	10	881	846	1727	120
40	8	10	765	1112	1877	158
40	8	80	995	621	1616	127
40	3	80	1070	617	1686	261
25	3	10	918	1022	1940	179
25	8	10	888	876	1764	95
25	8	80	1010	650	1659	387
25	3	80	1071	815	1886	209

The second incubation was run, in part, to determine whether rates of AMD production would decrease, i.e. if S was becoming depleted from the waste rock surface area. Although average SO₄ concentrations in all treatments were 592 mg/ℓ after the 31 days in the first incubation and 544 mg/ℓ after 31 days in the second incubation, the difference was not statistically significant (paired T-test, $P = 0.14$), providing no evidence that the rate of SO₄ formation had slowed.

3.4 DISCUSSION

We observed no statistically significant effects of initial oxygen availability, pH or incubation temperature on the production of SO₄ from coal mine waste rock. In particular, decreased availability of O₂ in incubation water did not inhibit production of SO₄. We note that dissolved oxygen in many of the low DO treatment replicates increased over the experiment, even though the incubation vessels were sealed, suggesting contamination.

Biologically driven changes in the rate of AMD formation are strongly linked to pH (see Akcil and Koldas 2006). At pH 4 and lower the activity of acidophilic iron-oxidising bacteria contribute strongly to the production of AMD. Microorganisms are potentially very important contributors to AMD formation, but were not assessed in this study.

We were not able to reproduce all of the relevant conditions for groundwater at 2000 m here. Also, high pressure cannot be easily manipulated in incubations (and was not included here). The rock used in our experiments was coal mine waste rock, and had already been fractured and exposed to the atmosphere and rainfall. Thus it is likely that oxidation had already occurred on the surface of the waste rock due to reaction with atmospheric O₂. A limitation of the study is that rock from unmined areas was not available. Thus our results likely apply more realistically to AMD formation in mine waste dumps and to the exposed/fractured rock within the mine void. Finally, this experiment was ~105 days in duration, and groundwater movement is a much slower process. Despite these limitations, the data presented here suggest that AMD forms rapidly under hypoxic conditions at a similar rate to high-oxygen conditions, irrespective of pH and temperature.

CHAPTER 4: COLUMN EXPERIMENTS

4.1 INTRODUCTION

Our primary hypothesis has been presented earlier; however it is useful to repeat it here as this experiment is the principal test of it:

We hypothesise that as the mining void fills, there is an abundance of sulphide, water and oxygen. Thus the void generates acid as the groundwater recharges. If pumping occurs from the ECL, it occurs at the zone with the highest acid-generating ability; i.e. the sulphide bearing minerals at the ECL will be in contact with water and with oxygen. If the ground were pumped from much deeper; for example 2000 m below grade, there is unlikely to be any oxygen present in the groundwater. Thus, the initial groundwater pumped will be as acidic as the rest of the void, however, with time, this portion (where the water is being pumped from) of the subsurface will recharge with non-acidic water due to the absence of oxygen at this depth, provided direct short-circuiting of surface water to this depth is avoided. Thus, we hypothesize that the water being pumped to the surface will be of continually improving quality with higher pH and lower sulphate content due to continual flushing of the water body. We have shown in Chapter 2 of this report that in theory it should be feasible to pump from depth, to maintain water at the ECL. This hypothesis can be conceptualised as a perched layer of acid at the ECL beneath which we see a water body of improving quality.

In this Chapter we present our test of this hypothesis.

The overall objective of the set of experiments was to determine if the simulation of anoxic conditions would lead to an increase in pH and a decrease in iron and sulphate content in water which has interacted with a bed of coal waste rock containing pyrite. In order to achieve the objective, three PVC columns were installed each operating under different conditions. The first column accepted oxygenated potable water from a single inlet at the top of the column. The second and third columns attempted to simulate anoxic conditions present underground. The second column accepted de-oxygenated water from a single inlet at the top of the column. The third column accepted de-oxygenated water from multiple feed points down the column in order to simulate ingress of ground water into aquifers from different depths underground. The water drawn from the bottom of each column was tested for pH, dissolved oxygen content, iron, sulphate and electrical conductivity.

If results of the experiment indicated that it was possible to remediate AMD through the use of anoxic conditions, the subsequent alteration of existing pumping facilities could be introduced to provide a long-term solution to AMD remediation.

In order to achieve the abovementioned objective, the following questions were to be answered through the use of the experiments:

- Does the removal of dissolved oxygen from feed water result in an increase in pH and a decrease in sulphate and iron content of water being drawn from the bottom of the column?
- Does the introduction of multiple feed points for de-oxygenated water into the column result in further increases in pH and a decrease in sulphate and iron content than for a single feed point at the top of the column?
- If the pH of the water increases and the iron and sulphate content decreases, is it a result of the iron pyrite initially being totally depleted which leaves no further pyrite to react to form acid?
- If the pyrite is not initially depleted, the improvement in the water quality may have been due to either insufficient time for AMD to be generated inside the column or due to a lack of oxygen present inside the system. How long does it take for AMD to be generated within the system upon the addition of oxygen?
- What is the mean residence time of the water inside the column? If the mean residence time is longer than the time it takes for AMD to be generated, then the improvement in water quality is a result of a suppression of oxygen levels. If the mean residence time is shorter than the time required for AMD generation then the improvement in water quality may be a result of the water passing through the pyrite bed at a rate higher than that of AMD generation.

- If the AMD reactions occur inside the column, do mixing and dispersion effects play a significant role in the process? In other words, can the column be considered as a plug flow reactor, continuous stirred tank reactor or a combination of both? Such information can be used to conduct further detailed studies involving reaction kinetics of the AMD process.

This Chapter is in large part based on the 4th year laboratory project report of Mr Ricky Bonner and Ms Nabeela Saber. This report is presented as Appendix

4.2 METHODS AND MATERIALS

4.2.1 Experimental Design

4.2.1.1 Proposed Method for Remediation in the Witwatersrand Basins

The proposed solution involves the utilization of the current pumping equipment and altering the suction point to 2 km underground where anoxic conditions exist. De-oxygenated water should continually ingress into the aquifers resulting in a continual source of water at such depths. According to theory, an absence of oxygen in the water should effectively immobilize the production of acid and thus the water drawn from such depths should be free of acid. The water could then be consumed by downstream users without the need for an expensive pre-treatment process.

Rainfall will still cause the ingress of oxygenated water which could lead to the generation of AMD near the surface. However, by properly sealing the existing mineshafts the water would not be able to interact with pyrite and form AMD. By balancing the rate at which water is pumped from underground with the rate of ingress of water near the surface, the water level should be able to be maintained at the ECL without any further generation of AMD, effectively leaving a layer of perched acid at the ECL.

4.2.1.2 Reactor Theory

A system in which the generation of AMD occurs can be considered as a type of reactor. It is thus of interest to the engineer studying the system to analyse and characterise its reactor behaviour as it can assist in developing further comprehensive modelling. AMD-generating systems are heterogeneous in nature and consequently can be considered as forms of packed bed reactors. In many cases water does not flow uniformly through the pyrite-containing ore and therefore each element of water interacts with the ore for different lengths of time.

4.2.1.3 Residence-Time Distribution (RTD) Function

The RTD function attempts to account for the non-uniform distribution of the length of time each element of water spends inside the reacting system. The RTD function can be determined by injecting an impulse of an inert chemical, which is formally called a tracer, into the reactor and measuring the tracer concentration at the outlet of the system as a function of time (Fogler, 2012). A basic overview of the set-up of such an experiment is presented in Figure 4.1.

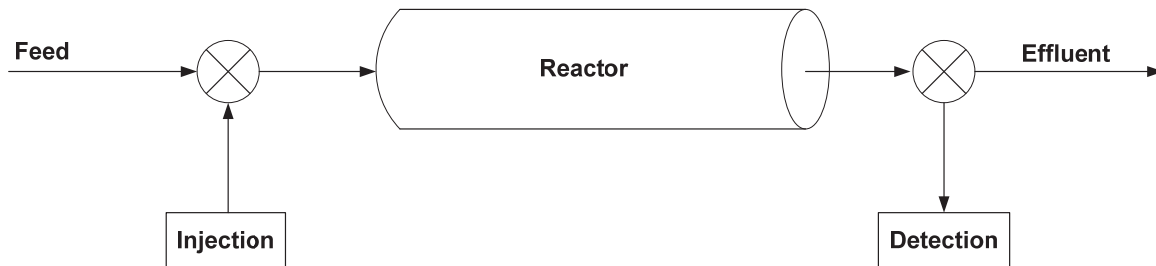


Figure 4.1: Schematic of RTD experiment

The RTD function, referred to as $E(t)$, can be calculated using Equation 4.1:

$$E(t) = \frac{C(t)}{\int_0^{\infty} C(t)dt} \quad 4.1$$

The RTD function describes quantitatively how much time different fluid elements have spent inside the reactor and the quantity $E(t)dt$ represents the fraction of fluid that has spent between time t and $t + \Delta t$ inside the reacting system. Consequently, it follows that:

$$\int_0^{\infty} E(t)dt = 1 \quad 4.2$$

The denominator in Equation 10 represents the area under the $C(t)$ versus t curve and can be found using Simpson's five-point quadrature numerical integration formula, which is provided in Equation 4.3.

$$\int_{X_0}^{X_N} f(X)dX = \frac{h}{3}(f_0 + 4f_1 + 2f_2 + 4f_3 + 2f_4 + \dots + 4f_{N-1} + f_N) \quad 4.3$$

With N having to be an even number, resulting in the rule that an odd number of points need to be used since there are a total of $N + 1$ points in the formula above. The quantity h can be determined using the following expression:

$$h = \frac{X_N - X_0}{N} \quad 4.4$$

4.2.1.4 Mean Residence Time

Due to dispersion and mixing effects which occur in real reacting systems, the residence time of the fluid cannot be determined by simply dividing the reactor volume by the volumetric flow rate of fluid. Instead, a mean residence time must be determined which takes into account the deviations from non-ideality and is provided in Equation 4.5.

$$t_m = \int_0^{\infty} tE(t)dt \quad 4.5$$

The mean residence time is calculated by plotting a curve of $tE(t)$ versus t and determining the area under the curve using Simpson's aforementioned numerical integration rule.

4.2.1.5 Variance

The magnitude of the variance provides an indication of the spread of the distribution, with a large variance indicating a significant spread (Fogler, 2012). The variance can be calculated using Equation 4.6:

$$\sigma^2 = \int_0^{\infty} (t - t_m^2)E(t)dt = \int_0^{\infty} t^2E(t)dt - t_m^2 \quad 4.6$$

4.2.1.6 Skewness

The skewness measures the extent to which the distribution is skewed in a particular direction with reference to the mean residence time (Fogler, 2012). It can be calculated using Equation 4.7.

$$s^3 = \frac{1}{\sigma^{3/2}} \int_0^{\infty} (t - t_m)^3 E(t)dt \quad 4.7$$

The skewness can then be used with the variance to determine a relative measure of the skewness of the distribution, indicated in Equation 4.8:

$$\beta = \frac{(s^3)^2}{(\sigma^2)^3} \quad 4.8$$

If the value of β approaches zero, it can be said that the data follows a Gaussian distribution (Torres and Oliveira, 1998).

4.2.1.7 Tanks-in-Series (T-I-S) Model

The variance can then be used to develop the tanks-in-series model, which essentially provides the number of ideal reactor tanks which need to be placed in series to give the same residence time distribution as the column (Fogler, 2012). The smaller the number of tanks in series required, the higher the degree of mixing inside the reactor while the larger the number of tanks in series required, the smaller the degree of mixing inside the reactor. The number of tanks in series is calculated using Equation 4.9, which was derived by Fogler (2012).

$$n = \frac{t_m^2}{\sigma^2} \quad 4.9$$

4.2.1.8 The Peclet Number and Dispersion Coefficient

The Peclet number is a dimensionless mathematical term which relates the rate of transport by convection to the rate of transport by diffusion or dispersion inside reactors, and is provided in Equation 4.10 for packed bed reactors (Fogler, 2012).

$$Pe_r = \frac{\text{Rate of transport by convection}}{\text{Rate of transport by diffusion or dispersion}} = \frac{UL}{\epsilon D_a} \quad 4.10$$

At higher Peclet numbers, the rate of transport by convection is far greater than the rate of transport by diffusion or dispersion while at lower Peclet numbers the rate of transport by diffusion or dispersion dominates. An alternative equation can be used to determine the Peclet number, which is related to the mean residence time and variance in Equation 4.11.

$$\frac{\sigma^2}{t_m^2} = \frac{2}{Pe_r} - \frac{2}{Pe_r^2} (1 - e^{-Pe_r}) \quad 4.11$$

Another way of presenting the Peclet number is through its inverse, called the dispersion number and is provided in Equation 4.12:

$$\delta = \frac{1}{Pe_r} = \frac{UL}{\epsilon D_a} \quad 4.12$$

According to Fogler (2012), as the dispersion number approaches zero the reactor tends to a plug flow behaviour while as the dispersion number approaches infinity the reactor tends to behave as a CSTR.

Once the mean residence time and reactor behaviour are determined, reactor design equations can be utilised to conduct further studies into the kinetics of the reacting system and parameters such as reaction rate constants and species conversion can be calculated.

4.2.2 Experimental Design

4.2.2.1 Proposed Experimental Program

The first phase of the experiments entailed pumping a continuous supply of water through each of the PVC columns loaded with coal waste rock containing pyrite. For column 1, unaltered tap water was pumped through a single feed point at the surface of the column. This experiment was designed to test what would happen if the only source of water were percolation and to mimic the generation of AMD at the surface. It was also designed to demonstrate potential remediation of AMD as recharge passes through the aquifer. For column 2, deoxygenated water was fed to the surface. This experiment was designed to indicate if AMD formed under anaerobic conditions. For column 3, deoxygenated water was fed 10 cm, 1 m, 2 m, 3 m, 4 m and 5 m from the surface. This experiment sought to reproduce ingress of deoxygenated water at different depths as would be expected in an aquifer.

The pH, conductivity, iron and sulphate levels of the discharge were then tested. If the AMD levels were high for the duration of the experiment, no remediation was occurring. If the AMD levels were initially high and

then decreased progressively with time, there would have been an improvement in the water quality. This improvement could be due to three different reasons:

- The pyrite was initially depleted, after which water was passed through the system without reaction, resulting in dilution effects.
- There was insufficient time for the water to react with the pyrite inside the column.
- There was limited oxygen availability inside the column, resulting in a suppression of the AMD reactions.

An attempt could then be made to regenerate acid to determine whether the pyrite reserves were depleted. If in this experiment acid was not generated, it would imply that pyrite reserves were depleted in the first phase of experimentation. If, however, the acid would be regenerated, it would mean that pyrite was not depleted. If this were to be the case, it would mean one of two things: either there would be no reaction due to oxygen limitation or there would be flushing of the AMD at a rate faster than it was produced. An impulse-response tracer experiment could then be conducted to determine which of these was occurring. If the mean residence time is less than the time taken for acid to be regenerated, then it would mean that flushing was occurring. However, if the mean residence time was significantly longer than the rate of acid regeneration, it would imply that the lowering of concentration would be as a result of prevention of acid formation.

The experimental logic diagram is provided in Figure 4.2.

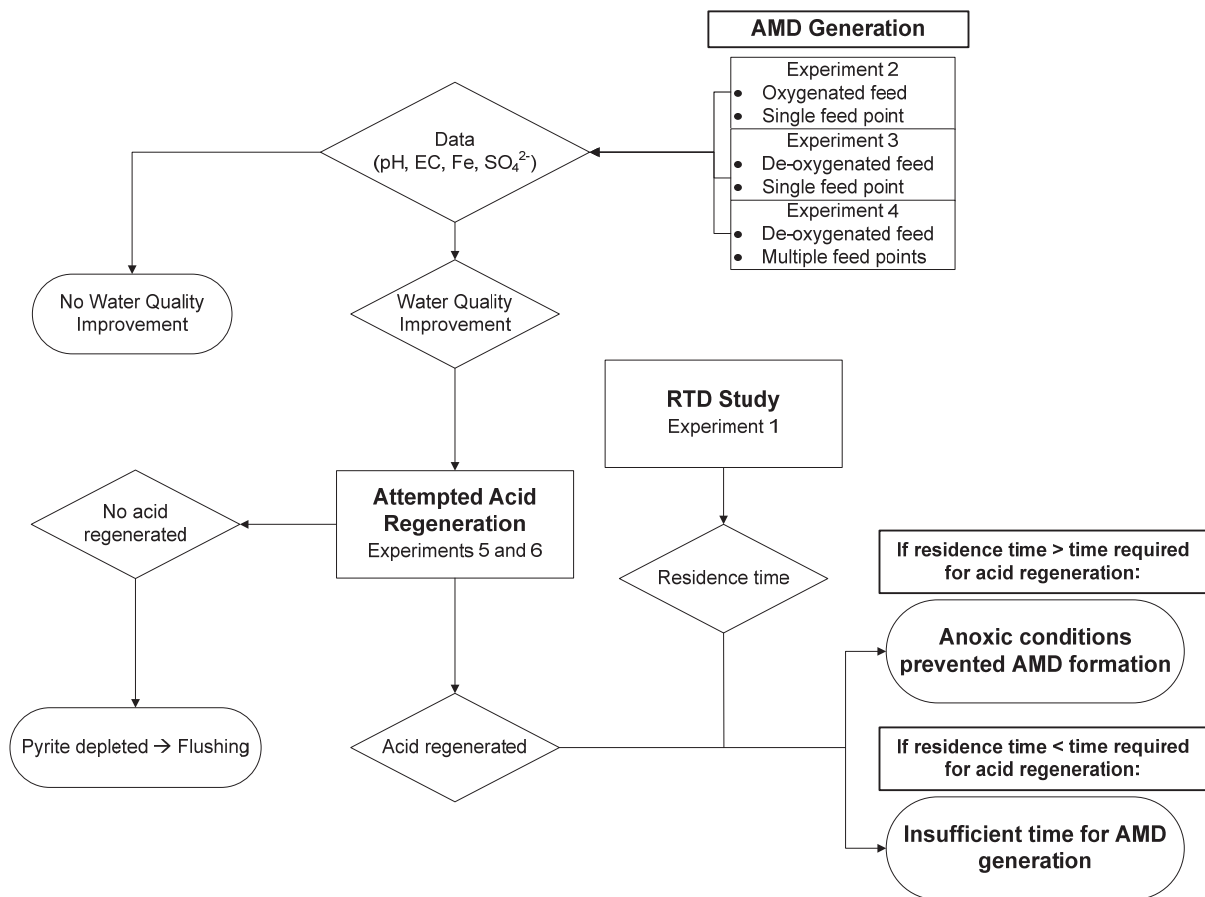


Figure 4.2: Experimental logic flow diagram

4.2.3 Experimental Set-up

Figure 4.3 provides a visual description of the experimental set-up used. Column 1 received potable water from feed tank 1 and the effluent from the column flowed into discharge tank 1. Column 2 and column 3 received de-oxygenated water from feed tank 2 and the effluent from both columns flowed into discharge tank 2. The dissolved oxygen in feed tank 1 was removed using a continuous supply of nitrogen gas via nitrogen gas cylinder 2. Column 3 accommodated multiple feed points along the length of the column in order to simulate the ingress of ground water underground. The transport of water to column 1 and the removal of AMD water from column 1 were performed using Pump 1A and Pump 1B respectively. The

transport of water to column 2 and the removal of AMD water from column 2 were performed using Pump 2A and Pump 2B respectively. The transport of water to column 3 and the removal of AMD water from column 3 were performed using Pump 3A and Pump 3B respectively. The letters 'A' and 'B' refer to the multiple heads on each respective peristaltic pump.

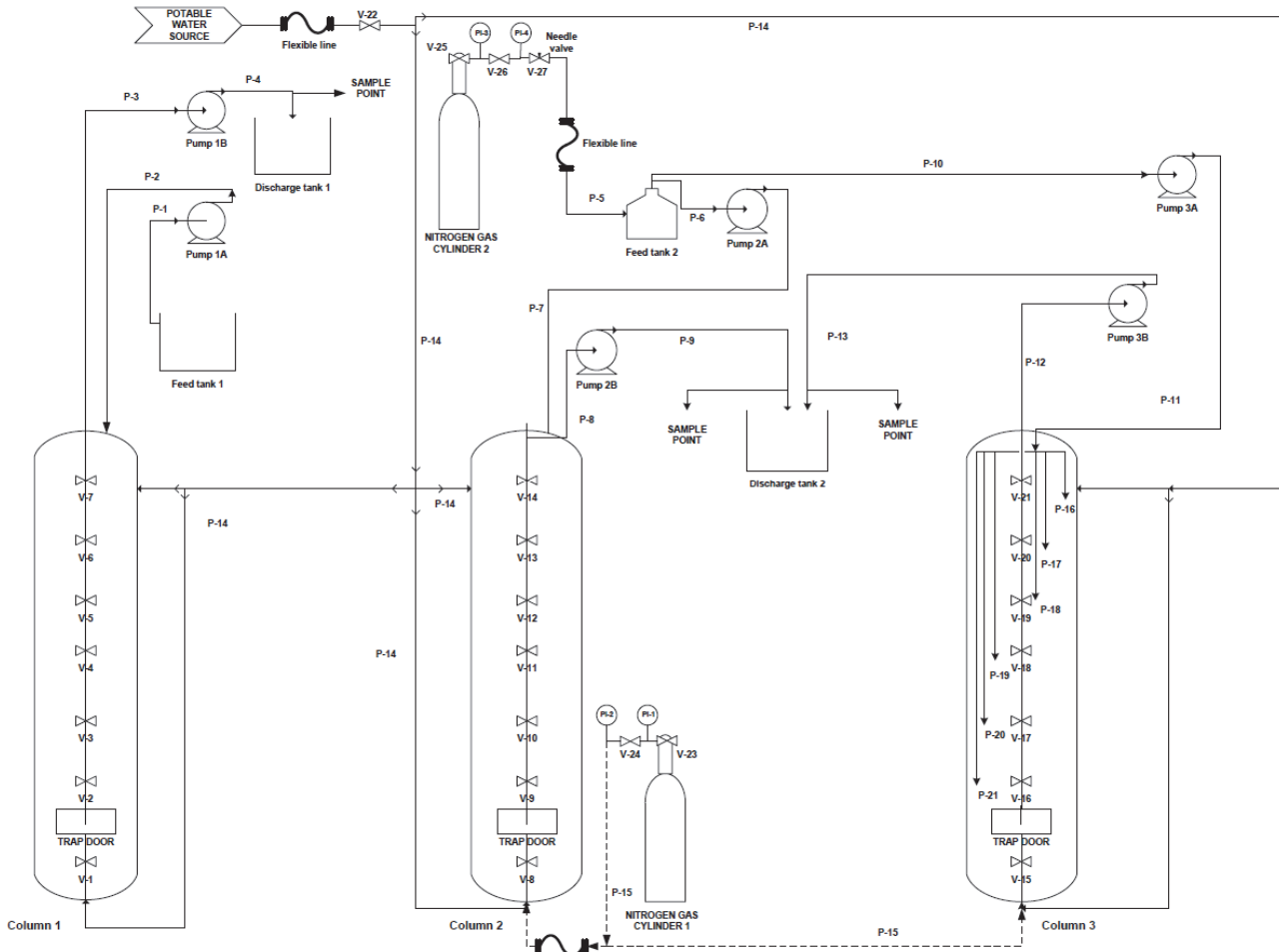


Figure 4.3: Experimental Set-up

4.2.4 Materials and Equipment required for Experimental Set-up

The following list provides information on the materials and equipment required for each phase of the experiments.

4.2.4.1 Experiment 1: Residence Time Distribution (RTD) Study

- Cylindrical plastic sampling vial of volume 25 mL
- 7 g iodated salt
- 1000 mL conical flask
- 250 mL measuring cylinder
- Funnel
- Potable water
- Hosepipe
- Flow meter
- Distilled water
- Roller towel
- Stopwatch
- PPE (Lab coat, safety glasses, closed shoes, plastic or rubber gloves)

Salt Calibration for Residence Time Distribution Study

- EC probe
- 75 ml measuring cylinder
- De-ionised salt
- Scale
- Spatula
- Potable water
- Distilled water
- Roller towel

Testing of Electrical Conductivity using Hannah Probe

- 250 ml measuring cylinder
- Standard solution having an EC of 14 uS/cm
- Distilled water
- Roller towel
- PPE (Lab coat, safety glasses, closed shoes, plastic or rubber gloves)

Calibration of Pumps

- 3 Identical multi-channel peristaltic pumps
- 500 ml Plastic water bottle with lid
- Potable water
- Stopwatch
- Electrical supply
- Multi-plug
- Two-pin adaptor

Start-up of Columns for Experiments 2, 3 and 4

- Coal waste rock
- Hosepipe
- Flow meter
- Potable water
- 2 polystyrene sheets
- Electric saw to cut the polystyrene sheeting
- 2 m Copper tubing for transportation of nitrogen gas in P-15
- Nitrogen gas cylinder with regulator
- Gas cylinder stand
- PPE (Lab coat, safety glasses, closed shoes, plastic or rubber gloves)

Preparation of Equipment used in Experiments 2, 3 and 4

- 3×25 L open-top buckets
- 1×25 L bucket which contains screw-able lid
- Tape measure
- 51 m silicon tubing with inner diameter of 3 mm to be used for transportation of water and AMD water throughout experiment
- 2 m additional silicon tubing with inner diameter of 10 mm to be used for transportation of nitrogen gas in P-5
- T-pieces for the silicon tubing
- Scissors
- Cable ties
- Masking tape
- Nitrogen gas cylinder with regulator and needle valve
- Gas cylinder stand
- Drill
- Tape measure
- Gas bubble stone to be placed on the end of P-5

Sample Collection during Experiments 2, 3 and 4

- Cylindrical plastic sampling vials of volume 25 mL
- Distilled water

- Labels
- Marker
- Freezer
- PPE (Lab coat, safety glasses, closed shoes, plastic or rubber gloves)

Testing of pH, Dissolved Oxygen Content and Electrical Conductivity using Consort Handheld Probe during Experiments 2, 3 and 4

- Standard solution having a pH of 7
- Standard solution having a pH of 4
- 250 mL conical flask
- 3×Syringes
- Polystyrene with dimensions: 60cm×10cm×1cm
- Drill
- Nitrogen gas
- PPE (Lab coat, safety glasses, closed shoes, plastic or rubber gloves)

pH Calibration of Multiprobe for Experiments 2, 3 and 4

- Standard solution having a pH of 7
- Standard solution having a pH of 4
- Laptop
- Multi-probe cabling
- Moxa connection cable used to connect Multi-probe cabling to USB port in laptop
- Distilled water

Testing of pH, Electrical Conductivity and Temperature using Hydrolab Multiprobe during Experiments 2, 3 and 4

- 14 m nylon string
- Laptop
- Multi-probe cabling
- Moxa connection cable

Testing of Iron and Sulphate Content using the Merck Pharo 300

- Merck spectroquant pharo 300
- Merck Iron (Fe) test kit 1.14761.0002
- Merck Sulphate (SO₄²⁻) test kit 1.14791.0001
- Filter paper
- Distilled water
- 3 × 250 mL measuring cylinders
- 10 mL pipette
- Test tubes
- Roller towel
- Waste disposal bucket
- PPE (Lab coat, safety glasses, closed shoes, plastic or rubber gloves)

Testing of Sulphate Content using the Barium Chloride Test

- Merck spectroquant pharo 300
- 6 x 100 mL glass stoppered conical flasks
- 1 x 250 mL conical flask
- 1000 mL measuring cylinder
- Funnel
- Scale
- Beaker
- Spatula
- Filter paper

- Distilled water
- 10 ml pipette
- PPE (Lab coat, safety glasses, closed shoes, plastic or rubber gloves)
- Roller towel

Chemicals Required

- Isopropyl Alcohol
- Glycerol
- Concentrated Hydrochloric acid
- Sodium Chloride
- Barium Chloride
- Sodium Sulphate
- Distilled water

4.2.4.2 Experiment 5: Attempted Acid Regeneration using Column 3

- Potable water
- Hosepipe
- PPE (Lab coat, safety glasses, closed shoes, plastic or rubber gloves)

Sample Collection during Experiment

- Cylindrical plastic sampling vials of volume 25 mL
- Stepladder
- PPE (Lab coat, safety glasses, closed shoes, plastic or rubber gloves)

4.2.4.3 Experiment 6: Attempted Acid Regeneration using Column 1

- Compressed air line
- Regulator
- Potable water
- Hosepipe
- PPE (Lab coat, safety glasses, closed shoes, plastic or rubber gloves)
- The materials and equipment required for sample collection during experiment, testing of iron content and testing of sulphate content using the BaCl test were required for this experiment.

4.2.5 Methodology

4.2.5.1 Experiment 1: Residence Time Distribution (RTD) Study

Preparation of RTD Study

Prior to conducting the RTD study, column 2 first required to be drained of the water used in the previous experiment. One end of P-14 was attached to V-8 while the other end was placed over the drain inside the laboratory. V-8 was opened and the column was allowed to drain.

Once the column was drained, V-8 was closed and P-14 was disconnected from V-8. The column was then filled with water by connecting one end of P-14 to V-22 and placing the other end over the top of the bed of coal. V-22 was opened and the water level was allowed to increase until it reached the same height as that of the top of the bed of coal. P-14 was then placed over the centre-pipe of the column and this piping supplied a continuous flow of water into the column via the centre-pipe. Additional hose pipe was connected to V-14 with the open end of the piping being allowed to rest in a 25 l bucket on the ground floor of the laboratory. This particular line of piping withdrew water from the column near the top of the bed of coal rock, thus allowing for continuous removal of water from the vessel and ultimately resulting in steady-state operation as a result of continuous input and removal of water.

V-22 was then opened, resulting in a flow of water down the centre-pipe of the column. V-14 was also opened such that water could be removed from the column. V-14 was then adjusted carefully until the water inside the centre-pipe reached a constant level which indicated that steady-state operation had been achieved. The conductivity of the solution was then measured every hour until it reached a constant value, indicating that residual undissolved metal salts from the previous experiment had been successfully removed. Once the conductivity of the solution stabilised, a sample of the solution was taken which was used to construct a calibration curve of conductivity versus concentration of the iodated table salt to be used as a tracer in the study. The curve allowed for the conductivity measurements taken during the experiment to be correlated back to a concentration of salt. Since the conductivity meter operated within certain conductivity limits and could not read conductivities in excess of 3999 $\mu\text{S}/\text{cm}$, careful consideration needed to be given to the amount of salt to be used as a tracer in the study. Therefore it was decided to construct the calibration curve just before the tracer study commenced.

Calibration Procedure for RTD Study

The total volume of sample collected was determined to be 12.2 mL. Without any salt addition, the conductivity of the solution was first determined. Iodated table salt was then added in increments and the corresponding conductivity of the solution was measured. Based on the calibration curve and the total volume of the column in which the study was to be conducted, it was decided that an iodated table salt solution of 7.04 g dissolved in 1 ℓ of tap water would be a sufficient amount of tracer to be used as an impulse. The mass of impulse would be sufficiently high such that the conductivity spike resulting from the tracer passing through the column would be easily distinguishable but at the same time the mass would not be too excessive to cause the conductivity readings to be in excess of 3999 $\mu\text{S}/\text{cm}$.

Operation of RTD Study

Once the system reached a steady-state operation point and the conductivity had stabilised, the tracer was added through the centre-pipe of the column. A conductivity reading at the outlet pipe was taken and was defined to be at time zero. Conductivity readings were then taken at the outlet pipe every 10 minutes until the conductivity readings started to increase drastically, at which point the readings were taken every 5 minutes. The volumetric flow rate was also measured every 30 minutes by measuring the time taken for the outlet line to fill a 250 mL beaker. The flow rate measurements ensured that the flow rate was being kept constant throughout the experiment and also allowed for a prediction of the expected residence time of the tracer impulse inside the column, which was estimated to be between 3 and 4 hours. Once the conductivity readings reached a maximum and were starting to decrease, conductivity readings were then taken every 10 minutes until the conductivity reached the initial base conductivity just prior to the addition of the tracer to the column. V-22 was then fully closed and the outlet hose pipe was placed over the drain which allowed for the water inside the column to be removed.

Calibration of Pumps

Figure 4.4 depicts the Watson Marlow double head peristaltic pump used in the experiments.



Figure 4.4: Watson Marlow double head peristaltic pump

Calibration of the three pumps was required in order to determine the pump speed setting which would provide the required flow rate of water entering and exiting the columns. A 10 ℓ bucket was first filled with

potable water and the suction tube from the pump was placed inside the bucket. The outlet tube from the pump was then placed inside a 50 ml beaker to serve as the collection reservoir. The pump was then switched on and a speed of 50 rpm was selected in order for water to be drawn through the piping. A speed of 2 rpm was then selected and the pump was allowed to run for 120 s. Once the 120 s had elapsed, the volume of water which filled the bucket was measured. This was repeated twice more at a speed of 2 rpm to obtain an averaged flow rate reading. The procedure was repeated at pump speeds of 5 rpm, 10 rpm, 15 rpm and 20 rpm. A calibration curve of volumetric flow rate versus pump speed was then constructed to determine the required flow rate for the experiments.

4.2.5.2 Upon Start-up of Columns for Experiments 2, 3 and 4

A photograph of the three columns used during the experiments is shown in Figure 4.5.

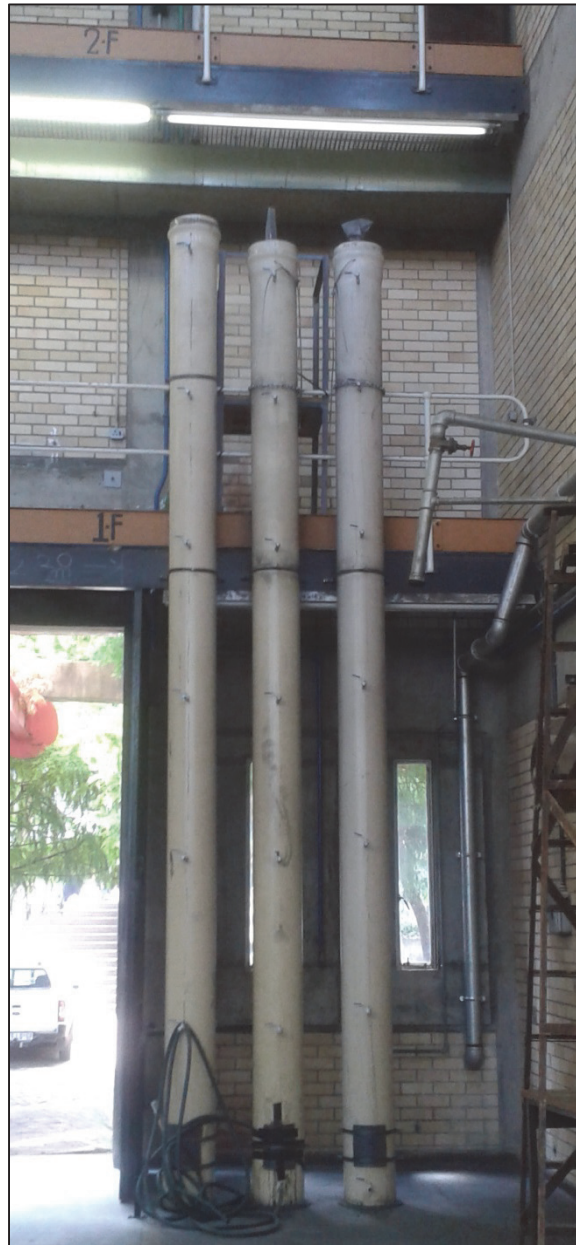


Figure 4.5: The three PVC columns loaded with coal waste rock containing pyrite

Experiment 2: Column 1- Oxygenated Feed Water Column

Prior to filling the column with coal, the trap door at the bottom of the column was required to be tested for any potential leakages. This was accomplished by connecting the hose pipe, indicated by P-14 in Figure 3, to V-1 at the bottom of the column. V-1 and V-22 were then opened to allow the column to be filled with

water until the water level reached approximately 0.5 m in height. Once the trap door was certified to contain no leakage points, the column was drained of the water by disconnecting P-14 from V-22 and placing the outlet into the demarcated drain inside the laboratory. Once the column was drained, it was filled with coal to within 10 cm of the top of the column. P-14 was then disconnected from V-1. One end of P-14 was connected to V-22 and the other end was placed over the top of the bed of coal inside the column to commence filling with water. A Gardena flow meter was then fitted onto the outlet of P-14. V-22 was then opened and water filled the voids inside the column. The flow rate was noted every 5 minutes and the total time taken to fill was also recorded as this would assist in indicating the volume occupied by water inside the column. The volume occupied by water, together with the required residence time of between 2.5 and 3 weeks, allowed for the correct flow rate of water entering and exiting the column to be calculated. Once the water level exceeded that of the coal, V-22 was closed and the outlet of P-14 was removed from the top of the column. A circular polystyrene sheet, with cut-outs to allow for the feed and exit pipes from the column, was then placed over the top of the column. The sheet would assist in limiting the amount of water lost to the atmosphere during the experiments due to evaporation.

Experiments 3 and 4: Column 2 and 3 (De-oxygenated Feed Water Columns)

Column 2, which contained a single feed point, as well as column 3 which contained multiple feed points as indicated in Figure 3 were both tested for leakage points at their trap doors in the same way described for the trap door of column 1. Coal was then also filled to within 10 cm of the top of each column. However, since anoxic conditions were desired to be achieved within both columns, it was decided to bubble nitrogen gas through each of the columns when being filled with water. For column 2, P-15 was connected to V-8 at the bottom of the column. The nitrogen gas supply was opened by slightly opening V-23 situated on nitrogen gas cylinder 1. V-24, situated on the nitrogen gas regulator, was then opened until a pressure of 200 kPa was observed on PI-2. Once V-22 was opened and the column started filling with water, V-8 was slightly opened to allow nitrogen gas to bubble through the column. In order to prevent water from flowing through P-15 towards the nitrogen gas regulator, it was ensured that the pressure of the nitrogen gas entering through V-8 was always higher than the pressure head exerted by the level of water inside the column. To accomplish this, V-23 was opened further every 5 minutes to account for the additional pressure head exerted by the increasing level of water inside the column. Once the level of water exceeded that of the level of coal, V-22 was closed and a circular sheet of polystyrene, with the same configuration as that for column 1, was placed over the top of the column. The nitrogen gas supply was shut-off by closing V-8 as well as V-23 and V-24. The procedure was repeated for column 3, with the nitrogen gas being supplied to the column via V-15. Another identical circular polystyrene sheet was also placed over the top of column 3.

4.2.5.3 Preparation of Equipment to be used in Experiments 2, 3 and 4

Equipment for Column 1

Two plastic buckets each with a volumetric capacity of 25 ℓ were placed approximately 1 m from column 1 on the first floor of the laboratory. One of the buckets served as feed tank 1 while the other bucket served as discharge tank 1. Silicon tubing of the required length was cut and inserted into Pump 1A, which served as the feed line into the column. One of the ends of the tubing was placed into feed tank 1 and the other end was secured to the rim of the top of the column. Additional silicon tubing was then cut to serve as the discharge line from the column. The tubing was fed down the centre-pipe of the column until the end reached the bottom of the column. The tubing was then inserted into Pump 1B and the other end of tubing was placed into discharge tank 1.

Equipment for Columns 2 and 3

Since columns 2 and 3 required a feed of deoxygenated water, both columns drew water from feed tank 2 which had a capacity of 25 ℓ. In order to ensure that the water drawn from feed tank 2 was deoxygenated, nitrogen gas cylinder 2 was secured in a stand against the wall adjacent to feed tank 2. Three holes were drilled into the lid of feed tank 2; one of the holes accommodated the nitrogen gas feed line indicated by P-5 while the other two holes accommodated the feed lines for columns 2 and 3 indicated by P-6 and P-10 respectively. The three holes thereby allowed for nitrogen gas to enter and water to be drawn from the feed tank while still ensuring that the tank was effectively sealed hence preventing entry of oxygen into the vessel

during the experiments. The required length of silicon tubing was then cut for the feed lines of both columns. For column 2, the tubing was placed in feed tank 2, inserted into Pump 2A and then secured to the rim of the top of the column. For column 3, the tubing was placed into feed tank 2 and then inserted into Pump 3A. Since column 3 required multiple feed points for the deoxygenated water, a distribution network for the feed was constructed. 10 pieces of silicon tubing each 10 cm in length were cut and were connected to the green T-pieces such that 6 discharges were available from the single inlet tube from Pump 3A indicated by P-11. The 6 discharges were placed into the 6 available Perspex tubes indicated by P-16 to P-21 in Figure 3. The required length of silicon tubing for the discharge lines from columns 2 and 3 were then cut and fed down the centre-pipes of each column. Once the tubing reached the bottom of the column, the tubing was inserted into Pump 2B and Pump 3B for columns 2 and 3 respectively. Both discharge lines were then placed into discharge tank 2.

4.2.5.4 Commencement of Experiments 2, 3 and 4

Feed tanks 1 and 2 were both filled with potable water. A bubble stone was inserted and secured onto the end of P-5. The bubble stone ensured effective distribution of nitrogen gas bubbles inside feed tank 2. In order to ensure the dissolved oxygen was removed from feed tank 2, the lid was removed from the feed bucket and V-25 on the nitrogen gas cylinder and V-26 on the nitrogen gas regulator were opened until a pressure of 100 kPa was read on PI-4. V-27 was then fully opened to allow the nitrogen gas to bubble through the water for 5 minutes. Once the 5 minute period had elapsed, the lid was then screwed back onto the feed bucket and V-26 was adjusted such that a pressure of 10 kPa was read on PI-4. V-27 was then adjusted so that a bubbling rate of 2 bubbles per second was achieved. Each of the pumps was then switched on to the required pump speed as determined through the pump calibration curves.

4.2.5.5 Upon Replacement of Feed Water for Columns 2 and 3

In order to ensure that the amount of dissolved oxygen entering the system from newly introduced feed water was minimised, nitrogen gas was required to bubble through the tank while the tank was being filled with fresh feed water. V-26 was opened until a pressure of 200 kPa was achieved and V-27 was fully opened. Once the bucket was completely filled with water, nitrogen gas was allowed to bubble through for a further 5 minutes. After the 5 minute period had elapsed, the lid was then tightly screwed back onto the bucket and V-26 was closed until a pressure of 10 kPa was read on PI-4. V-27 was closed until a bubbling rate of 2 bubbles per second was achieved. This particular procedure allowed for feed water to be replaced without the risk of introducing oxygen into the system and also allowed for the experiments to be continued during filling.

4.2.5.6 Sample Collection during Experiments 2, 3 and 4

The discharge lines from each of the three columns were removed from the discharge tanks and were placed into 10 ml plastic sample vials. Once the discharges filled three quarters of the plastic sample vials, the discharge lines were placed back in the discharge tanks and the sample vials were sealed and labelled clearly, indicating the column from which the water originated as well as the date and time of sampling. The vials were then placed in the freezer in the Biochemical Laboratory to prevent biological reactions from occurring prior to sample analysis.

4.2.5.7 Testing of Iron and Sulphate Content

Iron and sulphate tests were conducted using a Merck Spectroquant pharo 300, and reagent kits which are shown in Figure 4.6.



Figure 4.6: Merck iron and sulphate test kits

Fe-14761 Method for Testing of Iron Content

The spectroquant was switched on and the Fe-14761 method was selected. A blank sample was verified by placing a cuvette filled with distilled water into the placeholder. 1 ml of sample was pipetted into a beaker and distilled water was pipetted into the same beaker for the purpose of dilution, keeping note of the individual volumes pipetted. Since the spectroquant is limited to a range of 0.005-5 mg/l of iron, the sample needed to be diluted where the dilution ratio was calculated as follows:

$$\text{Dilution ratio} = \frac{V_{\text{sample}} + V_{\text{distilled water}}}{V_{\text{sample}}} \quad 4.13$$

An aliquot of 5 ml of diluted sample was pipetted into a test tube. Three drops of Reagent 1 from the Fe-14761 test kit was added to the test tube and the content of the test tube was allowed to stand for three minutes. Thereafter, the content of the test tube was pipetted into a cuvette and placed into the placeholder in the Spectroquant to record the indicated concentration and absorbance. The actual concentration of iron in the sample was calculated by multiplying the dilution ratio with the concentration recorded.

Calibration of Spectroquant for Fe-14761 Test

A calibration of the Spectroquant was required to be performed to relate the concentration measured with the actual concentration. This was accomplished through preparing known solutions of iron content and comparing its concentrations with those measured by the Spectroquant. The calibration was performed by pipetting 5 ml of four solutions of known iron concentrations between 0.005-5 mg/l into test tubes following the above mentioned method specified for the testing of iron.

SO₄²⁻14791 Method for Testing of Sulphate Content

The water bath was allowed to heat up to 40°C and the SO₄²⁻14791 91 method was selected on the spectroquant. A blank sample was verified by placing a cuvette filled with distilled water into the placeholder. 1 ml of sample was pipetted into a beaker and distilled water was pipetted into the same beaker, keeping note of the individual volumes pipetted. The spectroquant is limited to a range of 25-300 mg/l of SO₄²⁻ thus the sample needed to be diluted. The dilution ratio was calculated using the formula described for iron testing. Thereafter, 2.5 ml of diluted sample was pipetted into a test tube followed by the addition of two drops of Reagent 1 from the sulphate testing kit. The test tube was closed and the contents were shaken. One green microspoonfull of Reagent 2 was added to the test tube and the contents were shaken. The test tube was placed in the water bath for 5 minutes at 40°C. Thereafter, 2.5 ml of Reagent 3 was added to the test tube and the contents were shaken. The contents of the test tube were filtered into a second test tube. Four drops of Reagent 4 was added to the filtrate and the test tube was shaken. The test tube was placed into the water bath for 7 minutes at 40 °C.

Calibration of Spectroquant for SO₄²⁻-14791 Test

A calibration of the spectroquant was required to be performed to relate the concentration measured with the actual concentration. This was accomplished through preparing known solutions of sulphate content and

comparing their concentrations with those measured by the spectroquant. The calibration was performed by pipetting 2.5 ml of distilled water and five additional solutions of known concentration of sulphate between 25 and 300 mg/l into test tubes following the method specified for the testing of sulphate. Dilution was not applicable for the distilled water sample and the five additional solutions since the concentration was expected to lie within the range.

Barium Chloride Test for Sulphate

The barium chloride test for sulphate relies on the precipitation of barium sulphate in a colloidal form of uniform size which is enhanced in the presence of a sodium chloride, hydrochloric acid and glycerol solution. When barium chloride is added to the water sample containing the abovementioned solution, the following reaction occurs:



The absorbance of the barium sulphate formed was then measured using the Merck Spectroquant Pharo 300 at a wavelength of 420 nm and the subsequent sulphate concentration was then determined using a calibration curve of absorbance versus concentration of sulphate ion.

Conditioning Reagent

Glycerol (25 ml) was first poured into a 1000 ml beaker. 15 ml of concentrated hydrochloric acid were then added to the same beaker. 50 ml of isopropyl alcohol were then added to the beaker and the contents were thoroughly stirred.

Sodium chloride (37.5 g) was then dissolved in distilled water and the resulting solution was added to the 1000 ml beaker. All of the contents were then mixed and the final volume was made up to 250 ml using distilled water. The contents were then transferred to a 250 ml conical flask.

Standard Sulphate Solutions

Anhydrous sodium sulphate (1.479 g) was dissolved in distilled water. The resulting solution was then transferred to a 1000 ml flask and made up to 1000 ml using distilled water.

Six 100 ml glass stoppered flasks were then cleaned and prepared for usage. 10 ml of the standard sulphate solution was added to the first flask, 20 ml to the second flask, 30 ml to the third flask, 40 ml to the fourth flask and 50 ml to the fifth flask. The sixth flask was used for the blank and as such no sulphate solution was added.

A 5 ml aliquot of conditioning reagent was then added to each of the six flasks. Distilled water was then used for each of the flasks to make their respective volumes up to 100 mL. As a result of the dilutions, the first flask would contain a sulphate concentration of 100 mg/l, the second flask 200 mg/l, the third flask 300 mg/l, the fourth flask 400 mg/l, the fifth flask 500 mg/l and the sixth flask 0 mg/l since it was the blank.

Preparation of Samples for Spectroquant Analysis

A 3 ml aliquot of sample was then pipetted from the 100 ml flask and placed into a test tube. 0.1 g of barium chloride was then added to the test tube and the contents were then thoroughly mixed through vigorous shaking. The contents were then emptied into a 10 ml cuvette and immediately placed inside the Spectroquant for absorbance measurement. This procedure was repeated for each of the six standard solutions in a triplicate analysis.

Sulphate Test Set-up on Merck Spectroquant Pharo 300

The Spectroquant was first turned on at the main power supply. At the main menu, the absorbance method was selected and the wavelength set at 420 nm. A cuvette was filled with distilled water and inserted into the machine for a zero adjustment. Once the zero adjustment was made the sulphate analysis could commence.

Construction of Calibration Curve

Once the absorbance was measured for each of the standard sulphate solutions, a curve of absorbance versus sulphate concentration was constructed for use during the testing of samples collected from the experiments.

Sulphate Testing of Samples Collected

2 ml of sample were pipetted into a beaker and 10 ml of distilled were then added for the purpose of dilution. The contents were thoroughly mixed and 5 ml of the resulting solution was then pipetted into a 100 ml conical flask. 5 ml of conditioning reagent was then added to the flask and the volume was made up to 100 ml using distilled water. 3 ml of the solution was pipetted from the conical flask and into a test tube. 0.1 g of barium chloride was then added to the test tube and was mixed. The contents of the test tube were then emptied into a 10 ml cuvette and placed inside the Spectroquant for analysis.

Once the absorbance was measured for the sample, its concentration was calculated using the calibration curve which was constructed. The dilutions using distilled water prior to analysis ensured that the absorbance of the solution fell within the range of the calibration curve. Once the concentration was determined from the calibration curve, the dilution factors were then taken into account to calculate the actual sulphate concentration of the sample.

4.2.5.8 Testing of pH, dissolved oxygen content and electrical conductivity using Consort portable handheld probe

The testing of pH, dissolved oxygen content and electrical conductivity was performed once a week on a Wednesday. Prior to using the handheld probe for testing of samples, the pH meter was to be checked for accuracy purposes. This was performed by filling a conical flask with a standard solution having a pH of 7 and using the pH probe to determine the pH. This was repeated for a standard solution having a pH of 4.

Upon collection of samples from columns, a rectangular piece of polystyrene approximately 60 cm in length and 10 cm in width was constructed. Five holes were drilled in the polystyrene cut-out; the first of which accommodated the insertion of the nitrogen gas bubble stone, the second and third of which accommodated the insertion of syringes containing sample and the third and fourth of which accommodated insertion of pH, dissolved oxygen and electrical conductivity probes.

V-1 at the bottom of column 1 was opened and a syringe inserted into discharge to collect the sample. This was repeated for the filling of a second syringe. V-1 at the bottom of column 1 was closed. A conical flask was covered with the polystyrene sheet such that holes 1 and 2 were over the conical flask. P-5 was removed from feed tank 2 and inserted into the first hole. V-26 on the gas regulator and V-27 were adjusted until a steady pressure of 100 kPa was read on PI-4. Nitrogen was allowed to fill conical flask for 30 seconds which resulted in the removal of oxygen gas from the conical flask through the second hole. After 30 seconds, the second hole was covered with a syringe containing sample and the polystyrene sheet was shifted to the left such that only the second hole was over the entrance of the conical flask. P-5 was removed from the first hole and placed back in feed tank 2. V-26 and V-27 were adjusted so that the required bubbling rate of 2 seconds was again achieved in feed tank 2.

Using the syringe, sample was injected into the conical flask. The second syringe was placed over the third hole in the polystyrene sheet and the sheet was shifted to the left such that only the third hole was over the entrance of the flask. The empty syringe was removed from the second hole. Sample was injected into the flask through the third hole using the second syringe. Once the syringe was emptied, the sheet was shifted to the left such that no hole was over the entrance of the flask. The syringe was removed from the third hole. The Consort handheld meter was switched on and “%-Dissolved Oxygen” was selected. The “calibrate” button was pushed and then the meter was immediately turned off. The dissolved oxygen probe was inserted into the fourth hole of the polystyrene sheet and the sheet was shifted such that the fourth hole was directly above the entrance of the flask. The probe was inserted into the flask and swirled around. The meter was turned on and allowed to stabilise. The % dissolved oxygen and the temperature was recorded.

Thereafter, the “ppm-O2” setting was selected. The “calibrate” button was pushed and then the meter was immediately turned off. The meter was turned on and allowed to stabilise. The ppm-O2 and the temperature were recorded. The probe was removed from the flask and the sheet was shifted to the left until no hole was situated above the entrance of the flask.

The pH setting on the meter was selected. The “Calibrate” button was pushed and the meter was immediately turned off. The pH probe was inserted into the fifth hole and the sheet was shifted across until the fifth hole was directly above the flask. The probe was inserted into the flask and swirled around. The meter was turned on and allowed to stabilise. The pH and temperature was recorded. The pH probe was removed from the flask and the sheet was shifted to the right until no hole was above the entrance of the flask.

The electrical conductivity setting was selected on the meter. The “calibrate” button was pushed and the meter was immediately turned off. The electrical conductivity probe was inserted into the fourth hole and the sheet was shifted to the right until the probe was directly above the flask. The probe was inserted into the flask and swirled around. The meter was turned on and allowed to stabilise. The electrical conductivity and temperature was recorded. The meter was turned off and the polystyrene sheet was removed from the conical flask. The conical flask, pH probe, dissolved oxygen probe, electrical conductivity probe and syringes were cleaned with distilled water and the procedure was repeated for columns 2 and 3.

4.2.5.9 Usage of the Hydras Multiprobe for Experiments 2 and 4 (Columns 1 and 3)

The multiprobe was used to collect online data for pH, electrical conductivity and temperature at the bottom of the AMD columns. Figure 4.7 provides a visual of the Hydras Multiprobe.



Figure 4.7: Hydras Multiprobe used to collect online data

pH Calibration of Multiprobe

The Multiprobe was connected to a laptop and Hydras software was started. “Sonde” was operated. A known solution with a pH of 7 was prepared. The solution was poured into multiprobe sampling port and the multiprobe was calibrated using Hydras software. The sampling port was emptied and cleaned with distilled water. This was repeated for a known solution with a pH of 4. Once completed, multiprobe was disconnected from the laptop.

Calibration for electrical conductivity and temperature was not necessary as instructed by the user manual.

Deployment of Multiprobe

Prior to deploying the Multiprobe in one of the columns, the Multiprobe needed to be programmed to collect data. This was performed by connecting the Multiprobe to a laptop. Hydras software was started and "Sonde" operated. Ensure the time displayed on the software matches with the time displayed on the laptop. A new log file was created. The start and end time for sample collection was entered and the interval for sample collection. The settings were saved and the Multiprobe was enabled. The Multiprobe was disconnected from the laptop. Nylon string was tied onto the handle of the Multiprobe. The Multiprobe was deployed in the column by carefully lowering the Multiprobe using the nylon string. Once the Multi-probe reached the bottom of the column, nylon string was tied to the top of the column.

Collection of Data once Sample Collection Period was completed

The Multiprobe was connected to the laptop. Hydras software was started and "Sonde" operated. The relevant log file was downloaded. The Multiprobe was disconnected from the laptop.

4.2.5.10 Experiment 5: Attempted Acid Regeneration using Column 3

Column 3 was drained of any residual water from previous experiments and allowed to stand exposed to the atmosphere through the top of the column. Potable water was then used for filling of the column until the water level reached that of the top of the bed of coal. Samples were taken from each of the valves V-15 to V-21 once a week for a period of two weeks. The use of all valves along the length of the column provided the opportunity for a spatial representation of the potential AMD generation to be developed.

4.2.5.11 Experiment 6: Attempted Acid Regeneration Using Column 1

The column was first filled with potable water by attaching P-14 to V-22 with the other end of P-14 being placed over the top of the bed of coal. Once the water level reached that of the bed of coal, V-22 was closed. The compressed air line inside the laboratory was then opened for 30 minutes to allow accumulated condensates to be flushed out of the system after which the compressed air line was closed. One end of silicon tubing was attached to the compressed air source while the other end was attached to V-2. V-2 was then fully opened and the compressed air source was opened slightly so that the compressed air could flow through the column. Extensive care was taken to use a flow rate of air which was sufficient to prevent reverse flow of water back through the silicon supply tube owing to the pressure head exerted by the water. The air flow rate could also not be too high as it would cause significant entrainment and loss of water through the top of the column. A water sample was taken from V-3 once a week for two weeks after the commencement of the experiment.

Once the two week period had elapsed, the compressed air tap as well as V-2 were fully closed. The column was then drained by connecting one end of P-14 to V-1 and the other end being placed over the drain inside the laboratory.

4.3 SAFETY/ HAZOP CONSIDERATIONS

Safety was an important factor to consider during the course of the project. Hence, a detailed risk assessment identifying all the possible hazards, the cause of the hazard and the consequences was performed prior to commencement of the project. This assessment was performed for the Third Year Process Control Laboratory and for the Biochemical Laboratory. Preventative and reactive controls were put in place to eliminate hazards or reduce the likelihood of the hazard occurring, and to reduce the immediate impact of the hazard occurring.

4.4 RESULTS

4.4.1 Experiment 1: Residence Time Distribution Study

This section focuses on the results and discussion of the RTD study, as highlighted in Figure 4.8.

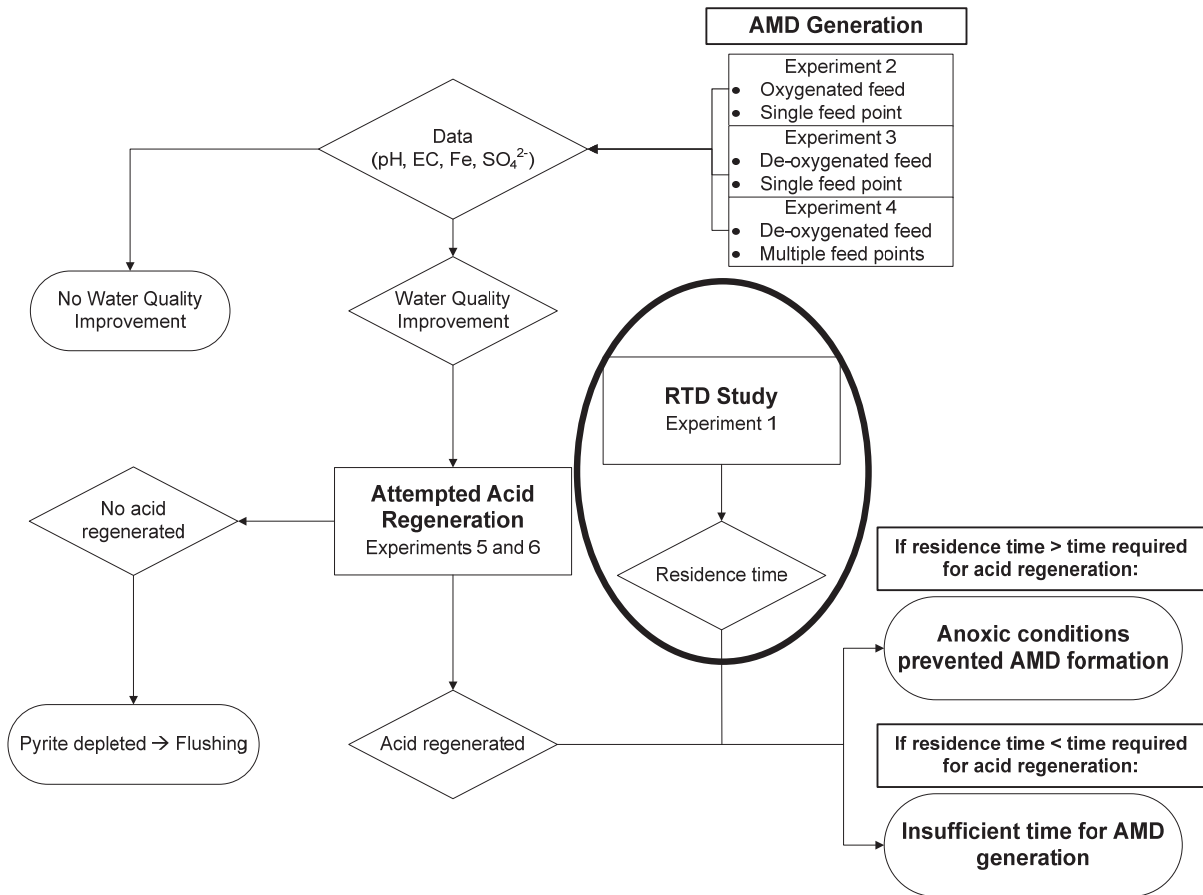


Figure 4.8: Results of RTD study in relation to the rest of the experimental work

The conductivity measurements taken at the outlet pipe from the column are provided in the student report appended to this report. A summary of the key parameters used in the RTD study are provided in Table 4.1.

Table 4.1: Summary of physical parameters for RTD study

Amount of tracer used in impulse	7.04 g dissolved in 1 ℓ of potable water
Average flow rate of water (ml/s)	5.39
Total volume of column (ℓ)	220
Void fraction	0.36
$\tau = \frac{V}{Q}$ (min)	244.9

A visual of the variation in concentration of tracer at the exit pipe with time is presented in Figure 4.9. Using Equation 4.10 and Simpson's numerical integration formula provided in Equation 4.11, the RTD function was determined and is provided in Figure 4.10.

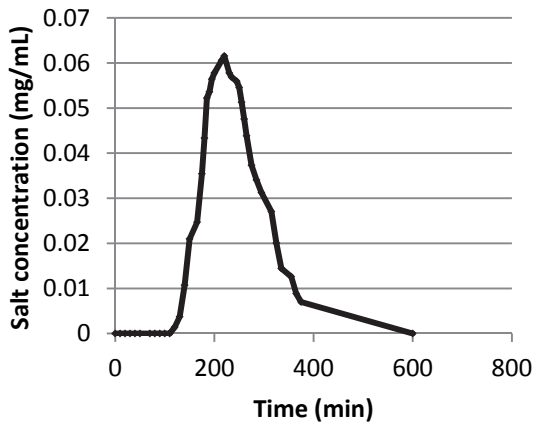


Figure 4.9: Concentration of tracer at exit pipe versus time

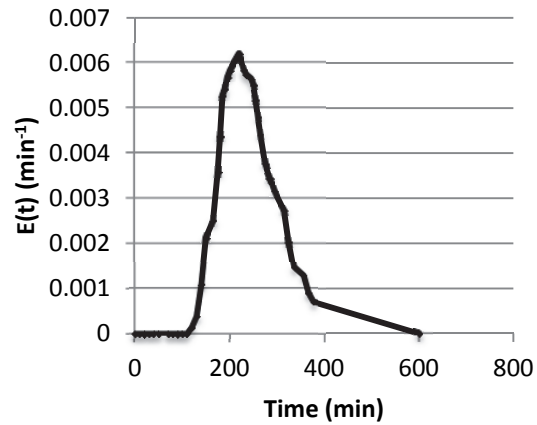


Figure 4.10: Residence-time distribution function

The RTD curve in Figure 4.10 was then discretised into a series of elements. The area under each of these elements was determined to provide Figure 4.11, in which an exact breakdown of the residence time distribution is made.

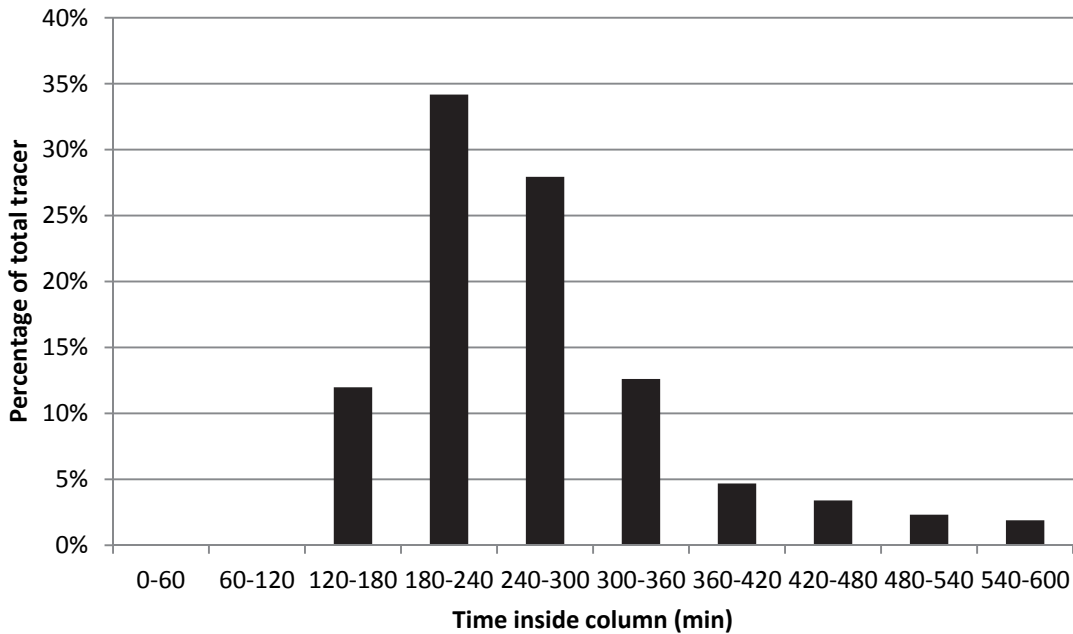


Figure 4.11: Distribution of residence times

Through the use of Figure 4.11, it becomes clear that the majority of the tracer spends between 180 and 300 minutes inside the reactor and it would thus be expected that the mean residence time of the tracer inside the column would fall within the range of 180 and 300 minutes.

4.4.1.1 Mean Residence Time

Using Equation 4.12, the mean residence time was determined to be 256.2 minutes. In an attempt to determine how the column behaves as a reactor when compared to an ideal reactor, the mean residence time was compared to the residence time if the column behaved ideally. The results of the comparison of the residence times are thus provided in Table 4.2.

Table 4.2: Comparison between mean residence time determined experimentally and the ideal residence time determined analytically

Mean residence time (min)	256.2
Ideal residence time (min)	244.9
Relative difference	4 %

The relative difference of 4% indicates that the residence times are similar in magnitude. The difference between the values, however, can largely be attributed to dispersion effects occurring inside the column which the ideal residence time calculation does not factor into account. A visual explanation for the reason why the experimentally determined mean residence time is greater than the ideal residence time is provided upon comparison between Figures 4.12 and 4.13.

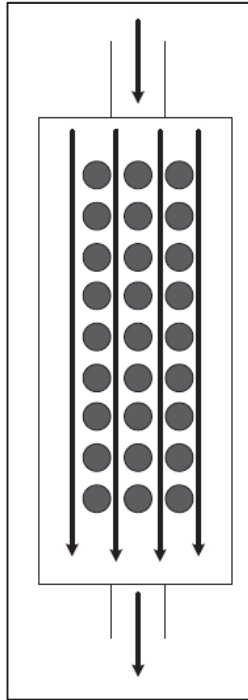


Figure 4.12: Ideal flow of water through packed ore

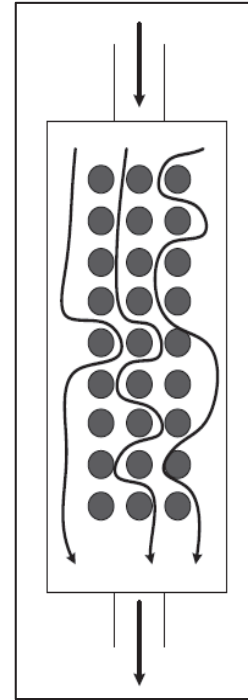


Figure 4.13: Flow of water through packed ore with dispersion effects

With no dispersion effects, the water flows via a straight path through the packed ore while as can be seen in Figure 4.13, the flow path of water through the bed is longer since the water winds around the packed coal rock particles ultimately resulting in a longer residence time.

4.4.1.2 Variance and Skewness

The values for the variance, skewness and relative skewness are provided in Table 4.3.

Table 4.3: Summary of parameters calculated from the RTD function and mean residence time

Parameter	Value
Variance (min^2)	4617.84
Skewness (min^3)	230.93
Relative skewness (β)	$5.4 \times 10^{-7} \approx 0$

Since the relative measure of the skewness is approximately zero, the RTD data follow a Gaussian distribution. This result was expected since the data presented in Figure 4.9 through to Figure 4.11 appears to be symmetrical about a central axis with little bias to the left or right.

4.4.1.3 Tanks-in-Series Model

The variance as well as the mean residence time was used to determine the required number of tanks in series. Using Equation 4.16, the number of tanks in series was determined to be 14.2, which was then rounded up to 15 tanks. Figure 4.14 was used to interpret the result of the calculation.

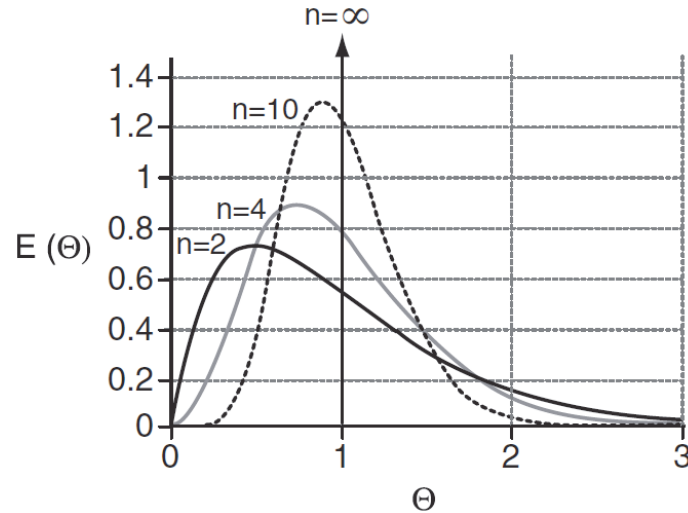


Figure 4.14: Residence time distribution function for different numbers of tanks in series, from Fogler, 2012

As the number of tanks in series approaches zero, a reactor behaves more as a CSTR while as the number of tanks in series increases a reactor behaves more as a plug flow. Through the use of Figure 4.14 and the result obtained of 15 tanks in series for the column, it can be remarked that the column behaves much more as a plug flow reactor than as a CSTR. However, the event of slight dispersion and mixing cannot be ruled out since the number of tanks in series does not tend to infinity.

4.4.1.4 The Peclet number, Dispersion Coefficient and Dispersion Number

Microsoft Excel was used to calculate the Peclet number which was found to be 27.37 and the dispersion number obtained was 0.0365. In Figure 4.15 a graphical interpretation of the dispersion number is provided.

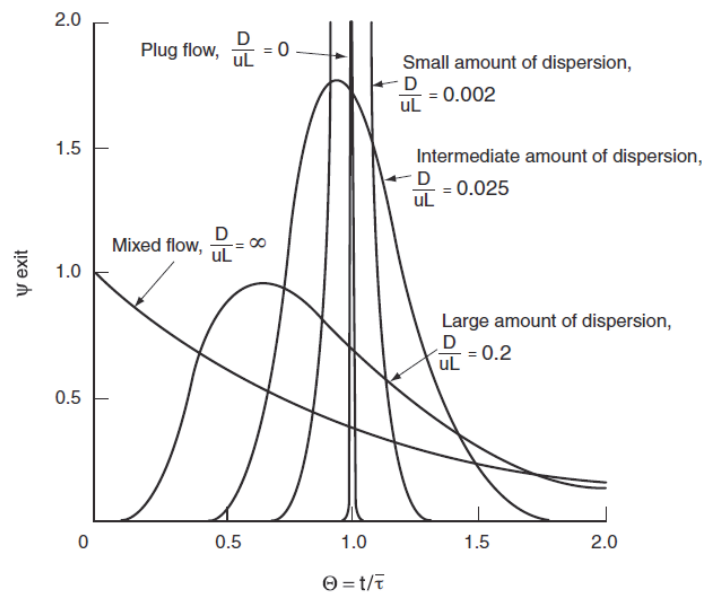


Figure 4.15: Graphical interpretation of the magnitude of the dispersion number, from Fogler, 2012

As the dispersion number increases, the behaviour inside a reactor tends to mixed flow and hence a CSTR, while as the dispersion number tends to zero the reactor tends to behave as a plug flow. The dispersion

number for the column is closest in magnitude to an intermediate amount of dispersion. Therefore, in similar fashion to the T-I-S model, it can be said that the column behaves more as a plug flow than a CSTR, but with noticeable dispersion and mixing.

The T-I-S model, skewness calculation as well as the dispersion number resulting from the RTD study all point towards the column's behaviour being characterised more as a plug-flow reactor than a CSTR, with slight dispersion and mixing occurring. The slight dispersion and mixing can be attributed to the nature of packed bed reactors and the fact that the fluid inside the column was required to traverse through the packing with multiple routes on offer to ultimately reach the exit of the reactor.

4.4.1.5 Scaling of Residence Time obtained in RTD Study to Residence Time used in Experiments 2-4

Equation 4.13 can be used to establish the flow regime inside packed beds (Richardson & Harker, 2002):

$$Re^* = \frac{\rho U d_p}{\mu(1-\varepsilon)} \quad 4.15$$

The parameters used in the calculation, as well as the result, are provided in tab 4.4.

Table 4.4: Summary of parameters used in Reynolds number calculation as well as result of calculation

Parameter	Value
Density of water, ρ (kg/m ³)	998
Superficial velocity of water, U (m/s)	0.000147
Average particle diameter of coal in column, d_p (m)	0.02
Viscosity of water (Pa.s)	8.9×10^{-4}
Re	5.15

The value of the packed bed Reynolds number and its corresponding flow regime are provided in tab 4.5.

Table 4.5: Typical packed bed Reynolds number boundaries

Region	Value
Laminar	$Re^* < 10$
Transitional	$10 \leq Re^* \leq 2000$
Turbulent	$2000 < Re^*$

Since the calculated Reynolds number was less than 10, the flow regime used in the RTD study could be regarded as laminar. It was thus possible to scale the mean residence time used in the RTD study to the mean residence time used in experiments 2-4. By noting the following three relations:

$$V_{RTD} = t_{m,RTD} \times Q_{RTD}$$

$$V_{experiment} = t_{m,experiment} \times Q_{experiment}$$

$$V_{RTD} = V_{experiment}$$

We can surmise:

$$t_{m,experiment} = t_{m,RTD} \times \left(\frac{Q_{RTD}}{Q_{experiment}} \right) \quad 4.16$$

By substituting the relevant values into Equation 4.16:

$$t_{m,experiment} = (256.2 \text{ min}) \times \frac{(5.39 \text{ mL/s})}{(0.0487 \text{ mL/s})} = 28\,325.67 \text{ min} = 2.81 \text{ weeks} \quad 4.17$$

With the actual experimental residence time known and the column being characterised similar to a plug-flow reactor, it would be possible in future experimentation to determine further key parameters in the column

through the use of reactor design equations. This could include detailed kinetic studies involving the evaluation of reaction rates and rate constants.

4.4.2 Experiments 2, 3 and 4

This section focuses on the results and discussion of experiments 2 to 4, with its relevance highlighted in the figure which follows.

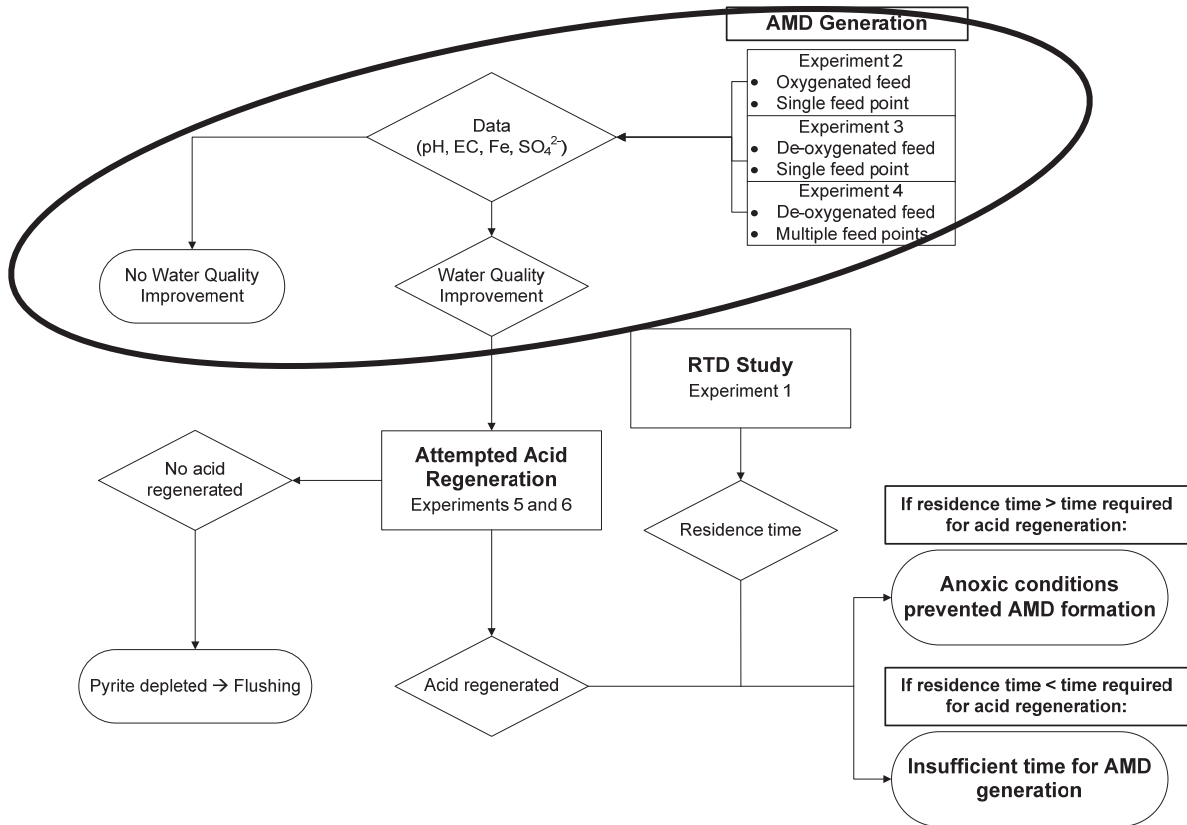


Figure 4.16: Results of Experiments 2-4 in relation to the rest of the experimental work

Since construction, Column 2 had a slow leak and as such had only become active in this experiment on 21st May 2014. Partially this was the result of the pressure at the base of the columns which would be 6 bar gauge when filled. Column 3 was started on 11th March 2014; a week earlier than column 1 since its construction was completed a week earlier. All findings relating to the columns are presented.

4.4.2.1 Summary of experimental parameters

A residence time of between 2.5 and 3 weeks was chosen because it provided sufficient time for the possibility of a reaction occurring. When filling each of the columns a void space of 80 ℓ was determined relative to the total volume of the column of 220 ℓ. This translated into a void fraction of 36 % and a flow rate between 160 mL/hr and 190 mL/hr. A pump speed of 5 rpm satisfied the flow rate. Day 0 on the graphs to follow represents the base case of the potable water fed to all three columns for the experiments. The following table is a summary of the parameters:

Table 4.6: Base case parameters of potable water feed

Base case parameters	
pH	7.12
EC (uS/cm)	216
Iron concentration (mg/ℓ)	0.0325
Sulphate concentration (mg/ℓ)	202

4.4.2.2 Comparison of Column 1 (oxygenated feed water), Column 2 (low deoxygenated feed water) and Column 3 (low deoxygenated feed water with multiple feed points)

pH

The change in pH of the water removed from the base of the columns is shown in Figure 4.17. For all three columns, the pH was initially low after day 1 relative to the base case on day 0 and gradually rose thereafter. However, a slight deviation from a rise in pH initially can be seen for Column 2. The low deoxygenated water feed with multiple feed points (Column 3) had a slightly higher pH than Column 1 and Column 2 after 30 days and 16 days, respectively.

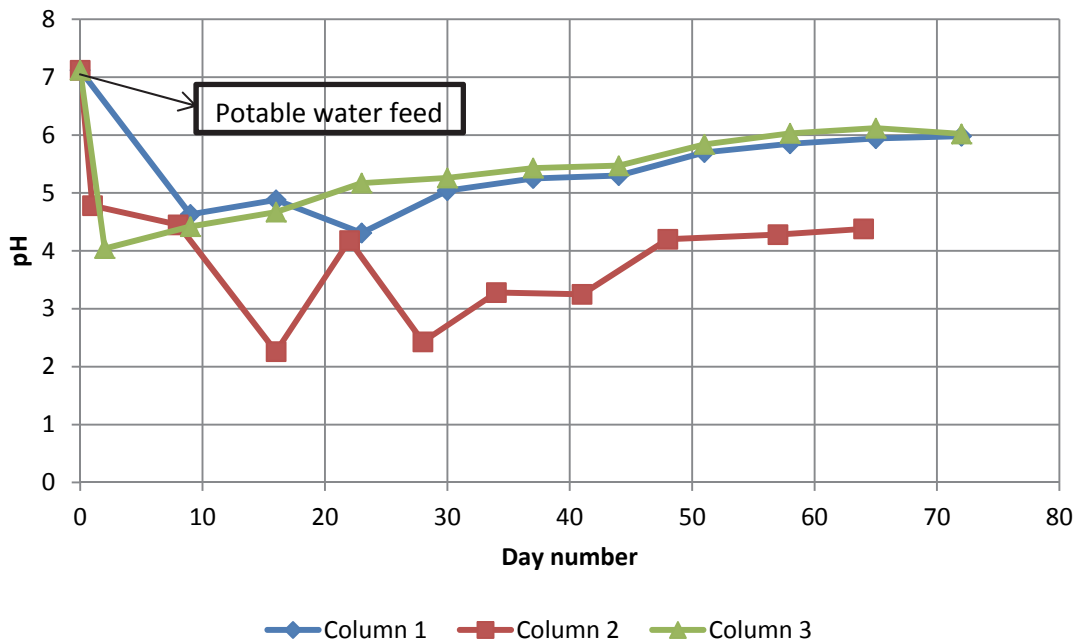


Figure 4.17: pH in Column 1, Column 2 and Column 3 with increasing time as assessed at the end of each week

According to Figure 4.13, in comparison to the pH of the potable water feed of 7.12, the pH for all three columns in the initial phase of the experiments was initially low decreasing to a pH of between 4 and 5 which indicates rapid acid generation. Thereafter, the pH steadily increased with time with an overall increase of 2 units. This indicated that by pumping from the base of the columns water quality improved. Improvement of the water quality occurred regardless of the oxygen content of the feed since a gradual increase in pH was observed for Column 1 (oxygenated feed), which was very similar to that of Column 3 (low deoxygenated feed with multiple feed points) from day 30 onwards, and higher than that of Column 2 (low deoxygenated feed) from day 22 onwards.

There seemed to be greater improvements resulting from Column 3 compared to Column 1 and Column 2, since the pH was slightly higher than Column 1 from day 30 onwards, and much higher than Column 2 from day 16 onwards. In addition, for Column 3, the overall increase in pH was 2.08 units after 65 days, whilst for columns 1 and 2 the overall increase was 1.31 and 1.95 units, respectively. This was possibly observed because the low deoxygenated water fed towards the base of the column through the multiple feed points short-circuits a large portion of coal above the feed point. Anaerobic conditions exist lower down within the column since oxygen penetration through the coal waste rock containing pyrite is limited. These conditions may have precluded the possibility of acid formation at deeper levels within the column thus resulting in a greater improvement in water quality.

Although it seemed that the setup of Column 3 (low deoxygenated feed with multiple feed points) lead to a greater improvement in water quality, it was not reliable to read into this as a definite conclusion since the results obtained for Column 2 fluctuated substantially in the initial phase of approximately 4 weeks, and the pH for Column 2, being fed with a low deoxygenated water feed remained below that of Column 1

(oxygenated feed). It appeared that the unstable behaviour of Column 2 may have been a result of continuous leaking experienced and subsequent draining of the column which interrupted the start-up of the experiment for well over 2 months. Therefore, the positioning of the feed namely, through a single feed point (Column 1 and 2) or multiple feed points (Column 3) did not play a significant role in how the water quality developed over the course of the experiments since Column 1 and 3 achieved the same pH of 6.02 after 72 days, and it is not reliable to compare Column 2 and 3 due to the leakage problems experienced.

Electrical Conductivity (EC)

The change in electrical conductivity (EC) of the water removed from the base of the columns is presented in Figure 4.18. For all three columns the electrical conductivity was initially high relative to the base case on day 0 and gradually decreased thereafter. However, a slight deviation from a decrease in electrical conductivity can be seen for Column 2.

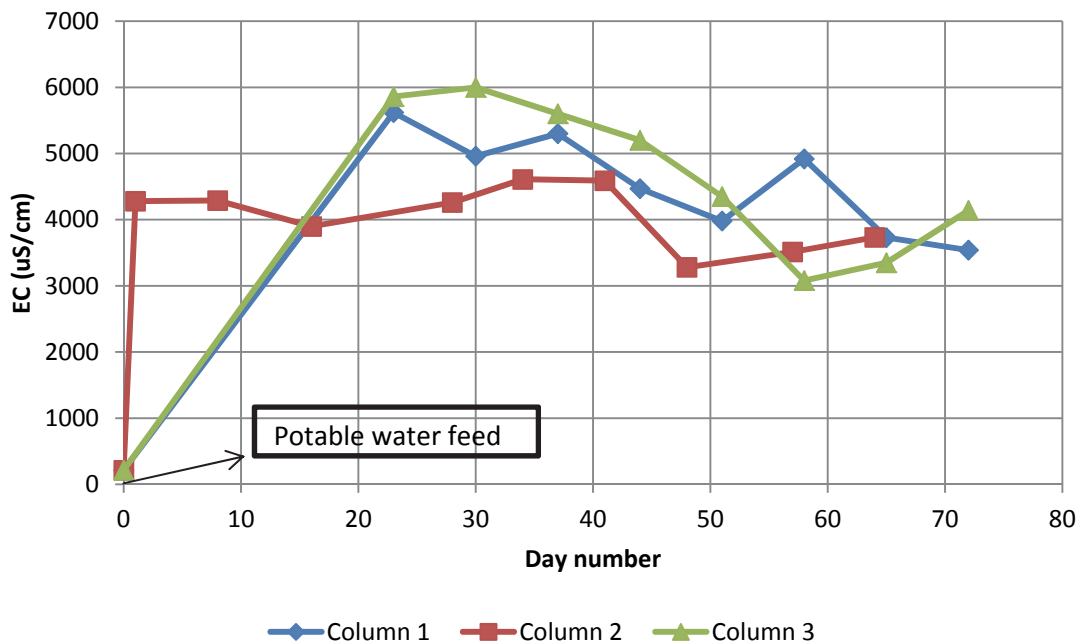


Figure 4.18: Electrical conductivity in Column 1, Column 2 and Column 3 with increasing time as assessed at the end of each week

The EC of the samples taken from each of the columns was affected by the heavy metal ions released into the water by the formation of acid through the acid generation process. The EC obtained for all of the columns over the course of the experiment indicated that by pumping from the base of the columns, water quality improved since the EC for all three columns was initially high compared to the base case of 216 uS/cm, and gradually decreased thereafter.

There is no observable trend between the columns in Figure 4.14 in order to compare the water quality since the EC of Columns 2 and 3 began to increase again from day 48 and day 58, respectively. The sudden increase in the EC of Columns 2 and 3, as well as other noticeable deviations in Figure 4.18 was explained by Figure 4.28, Figure 4.29 and Figure 4.30 which follow, which depict the relationship between EC and temperature of the water.

Iron Concentration

The change in iron concentration for Column 1, Column 2 and Column 3 is presented in figure 4.19. For Column 1 and Column 3 the iron concentration rose rapidly and then decreased significantly. The iron concentration for Column 2 rose slightly and then fluctuated substantially throughout the experiment showing a slight decrease.

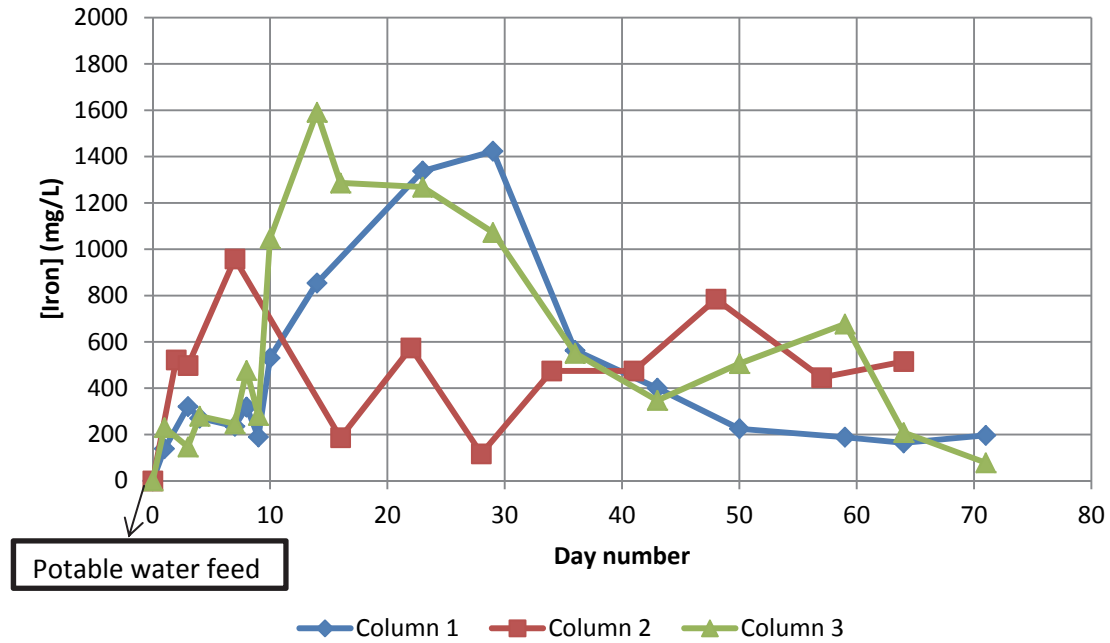


Figure 4.19: Iron concentration in Column 1, Column 2 and Column 3 with increasing time as assessed at the end of each week

The iron concentrations obtained over a period of time for Column 1 and Column 3 indicated that by pumping from the base of the column, water quality improved since the iron concentration was initially high and significantly decreased thereafter. Improvement of water quality occurred regardless of the oxygen content of the feed since a significant decrease in iron concentration was observed for Column 1 (oxygenated water feed).

The simulation of anoxic conditions by the recharge of low deoxygenated water feed with multiple feed points, Column 3 resulted in a slightly greater improvement of water quality than Column 1 from day 14 since the iron concentration for column 1 only began to gradually decrease from day 29 and the overall decrease from the corresponding peaks until after day 71 for Column 3 was 1513 mg/l, whereas the overall decrease for Column 1 was 1226 mg/l.

Due to the unstable behaviour of the iron concentration for Column 2, a conclusive comparison with Column 1 and Column 3 could not be made and hence, the improvement in the water quality observed could not be attributed to the position of the feed water to the columns.

Sulphate Concentration

The change in sulphate concentration for Column 1, Column 2 and Column 3 is presented in Figure 4.20. The sulphate concentration for all three columns rose rapidly and then proceeded to decrease. The values fluctuated substantially throughout the experiment for Column 1 and Column 3 whereas a decreasing trend can be seen for Column 2. It is believed that this is a result of the type of analysis used for Column 1 and Column 3 namely, the Merck SO_4^{2-} -14791 Test. The Barium Chloride (BaCl) test for sulphate was used for Column 2 which gave significantly more precise results. It was not possible to reanalyse for Column 1 and Column 3 using the Barium Chloride test for sulphate since once the sample was defrosted it may not be refrozen. The samples were frozen immediately after being taken from the column for the purpose of halting any further biological activity.

The sulphate concentration obtained over a period of time for all three columns indicated that by pumping from the base of the column, water quality improved since the sulphate concentrations for all three columns rose rapidly and proceeded to decrease thereafter. Improvement of water quality occurred regardless of the

oxygen content of the feed since a decrease in sulphate concentration was observed for Column 1 (oxygenated water feed).

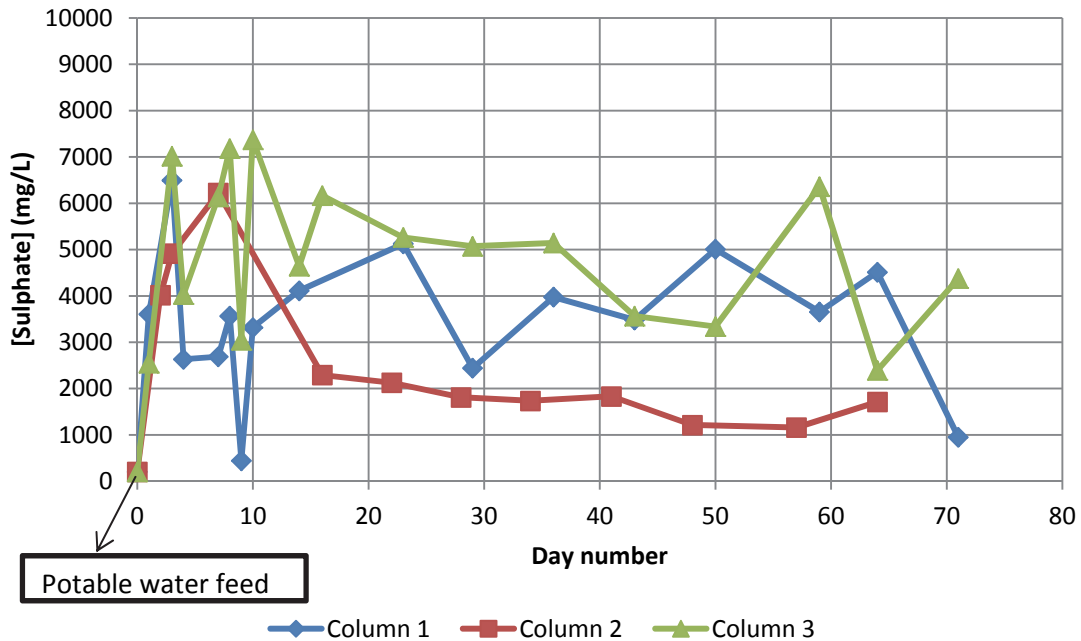


Figure 4.201: Sulphate concentration in Column 1, Column 2 and Column 3 with increasing time as assessed at the end of each week

Due to the different types of sulphate tests used for Column 1 and 3 namely, the Merck SO_4^{2-} -14791 Test and Column 2, the Barium Chloride (BaCl) test for sulphate, the trends between Column 1 and 3 and Column 2 cannot be compared and hence, the improvement in the water quality observed could not be attributed to the position of the feed water to the columns.

Having investigated the pH, EC, iron and sulphate concentrations in all three cases where oxygenated water was fed to Column 1 and low deoxygenated water was fed from a single feed point to Column 2 and from multiple feed points to Column 3, the result was improved water quality with time when pumping water from the base of the columns. This could have been observed due to the depletion of the iron pyrite in the coal waste rock within the columns and subsequent dilution effects; or the inability of oxygen to penetrate through the solid packing thus precluding acid formation under such anoxic conditions.

4.4.2.3 Comparison of Column 1 (oxygenated feed water) and Column 3 (low de-oxygenated feed water with multiple feed points) using the Multiprobe

The Hydrolab MS5 automated multiprobe, able to measure and record pH, EC and temperature was initially placed in Column 3 from 28 March 2014 to 16 April 2014 and then transferred to Column 1 from 16 April 2014 to 23 April 2014. Whilst the probe did not record the beginning of the experiment in Column 1, the data recorded clearly showed an increase in pH, and a decrease in EC as indicated in Figure 4.17. This has also been shown in Figure 4.18 presenting the data recorded for Column 3.

The results obtained from the use of the Hydrolab multiprobe clearly indicated that by pumping from the bottom of the column water quality improved since the pH for Column 1 and Column 3 increased, and the EC decreased. Improvement of the water quality occurred regardless of the oxygen content of the feed as depicted by Figure 4.21, Column 1. There seems to be greater improvements resulting from recharge with low deoxygenated water feed (Column 3) although there was more time for the experiment.

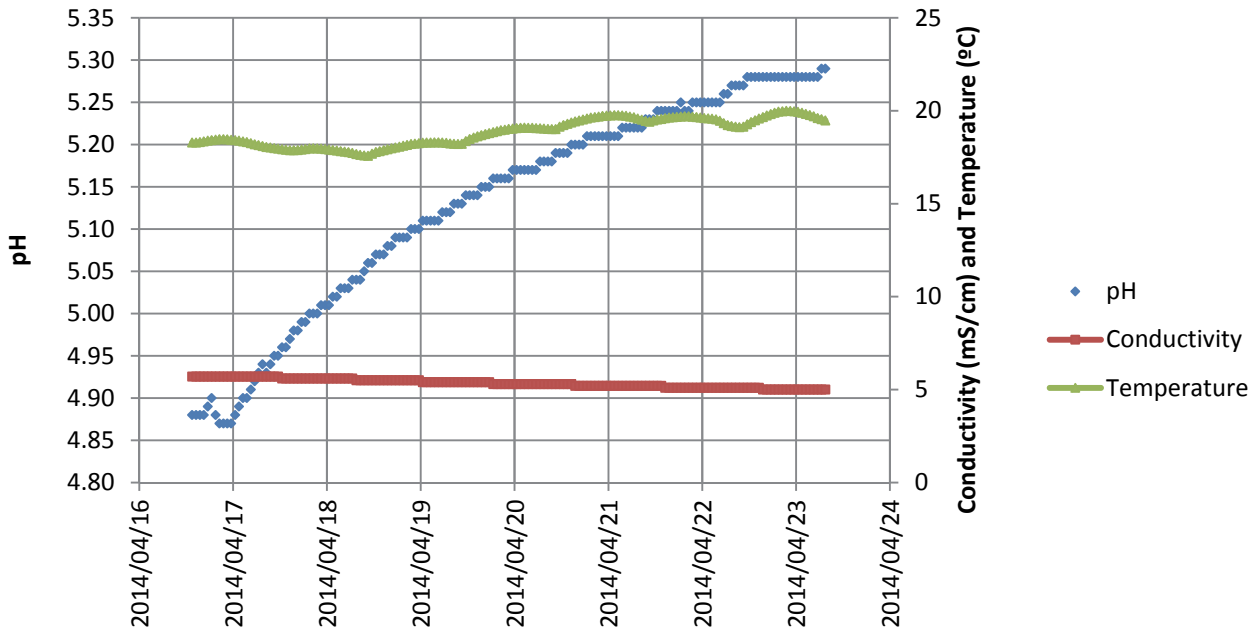


Figure 4.21: pH, EC and temperature profiles within Column 1

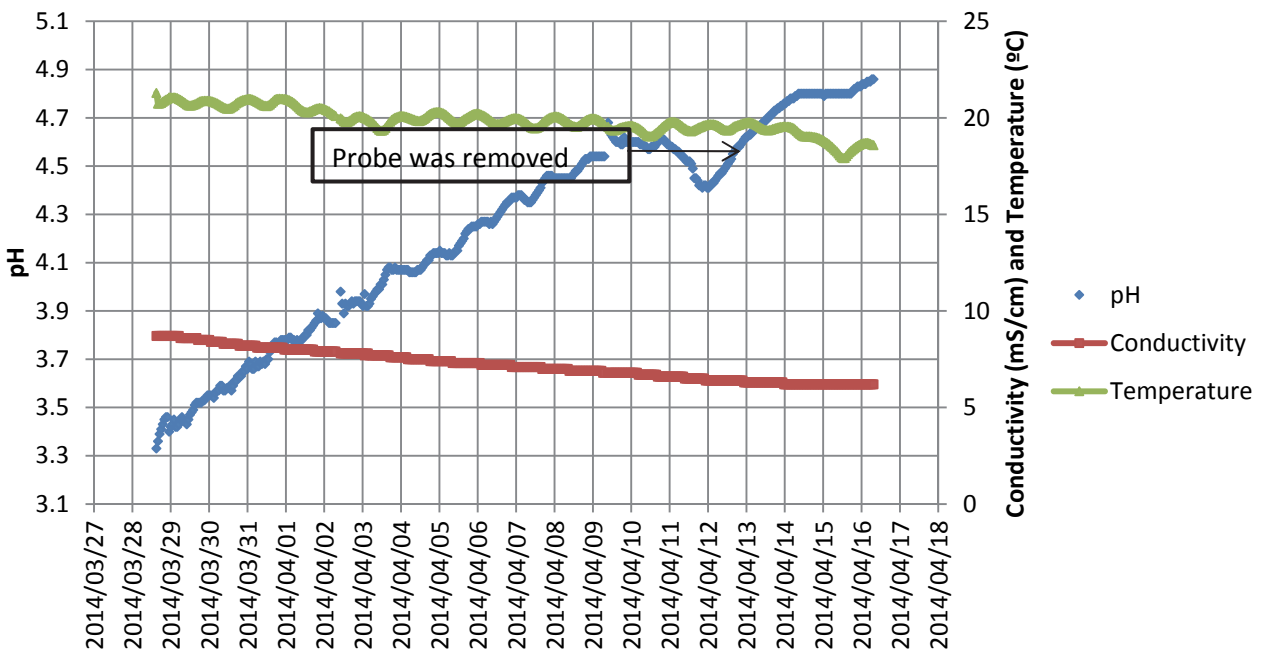


Figure 4.22: pH, EC and temperature profiles within Column 3

4.4.2.4 Comparison of pH with Iron and Sulphate Concentration and Electrical Conductivity (EC) for Column 1, Column 2 and Column 3

Comparison of pH with Iron Concentration

The pH and iron concentration for all three columns as a function of time is presented in Figure 4.19, Figure 4.20 and Figure 4.21 for the respective columns. The iron concentration for both Column 1 and Column 3 decreased with an increase in pH. The iron concentration and pH for Column 2 fluctuated substantially throughout the experiment.

Pumping scheme to eliminate AMD

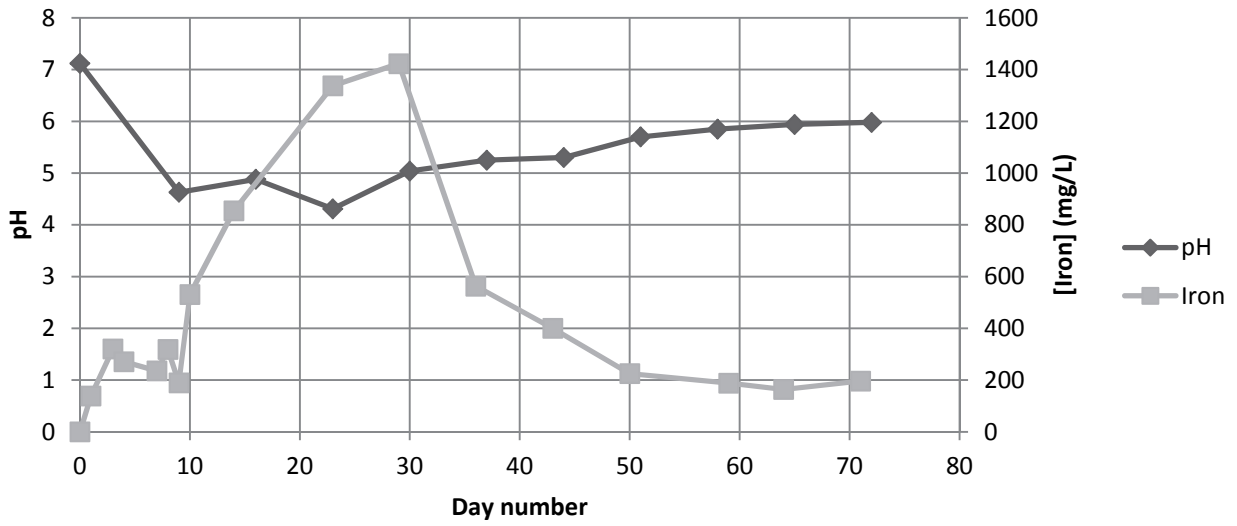


Figure 4.23: pH and iron concentration profiles within Column 1

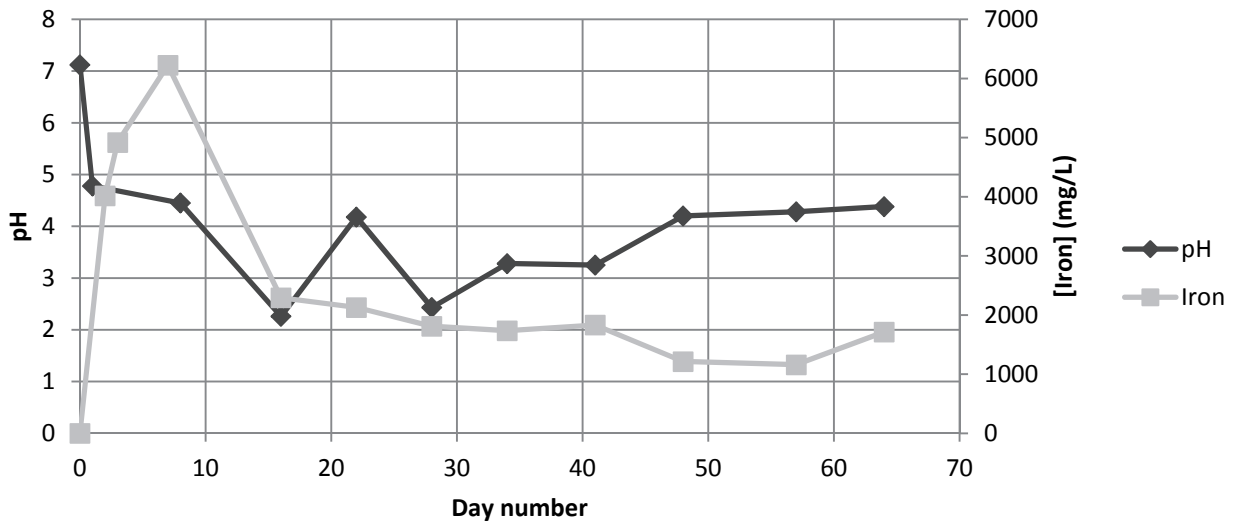


Figure 4.24: pH and iron concentration profiles within Column 2

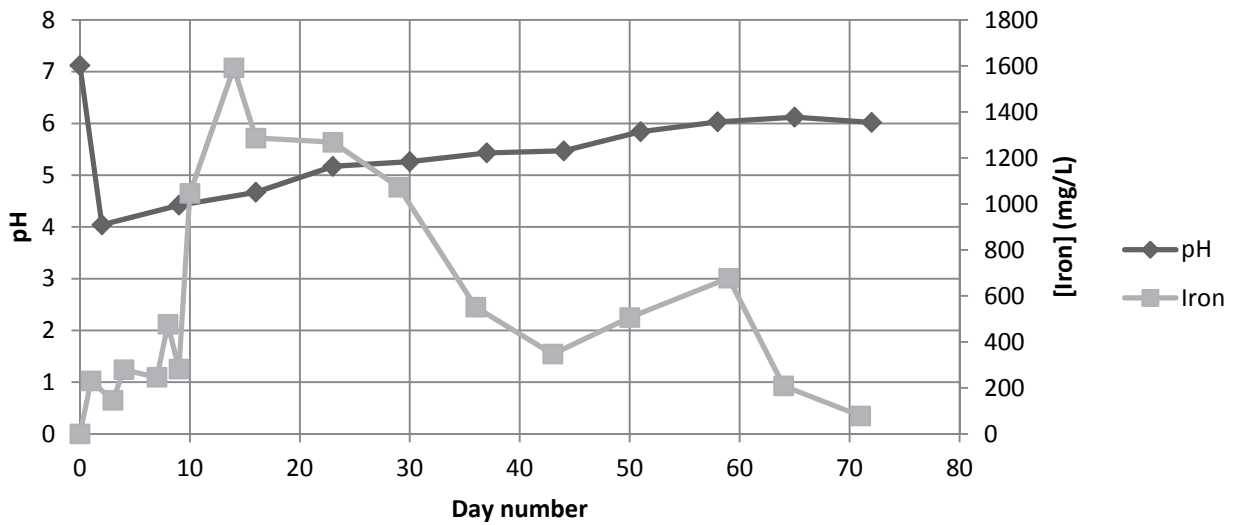


Figure 4.25: pH and iron concentration profiles within Column 3

The decrease in iron concentration as the pH increased for Column 1 and Column 3 indicated an improvement in the water quality by pumping from the base of the column. This was observed since according to the mechanism of acid generation, an increase in pH indicated a decrease in acid formation. This resulted in the iron concentration of the water decreasing due to precipitation of the iron, since at higher pH values metals, specifically iron tends to precipitate out (Metzger, 2005).

Due to the unstable behaviour of the iron concentration for Column 2, a conclusive comparison with the pH could not be made.

Comparison of pH with Sulphate Concentration

The pH and sulphate concentration for all three columns as a function of time is presented in Figure 4.26, Figure 4.27 and Figure 4.28 for the respective columns. The sulphate concentrations for all three columns rose rapidly and then proceeded to decrease as the pH increased. The sulphate concentration for Column 1 and Column 3 fluctuated rapidly throughout the experiment whereas a decreasing trend can be seen for Column 2.

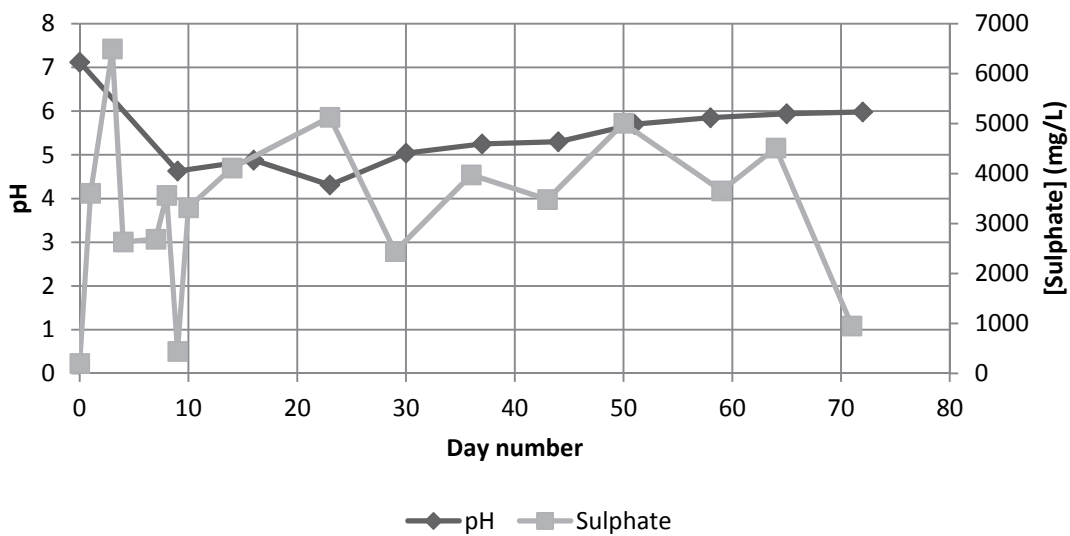


Figure 4.26: pH and sulphate concentration profiles within Column 1

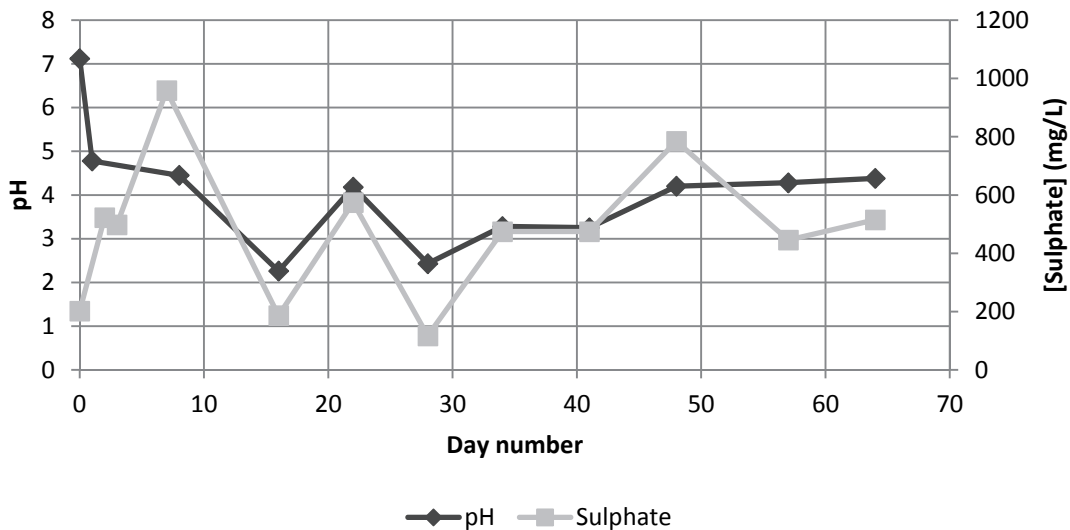


Figure 4.27: pH and sulphate concentration profiles within Column 2

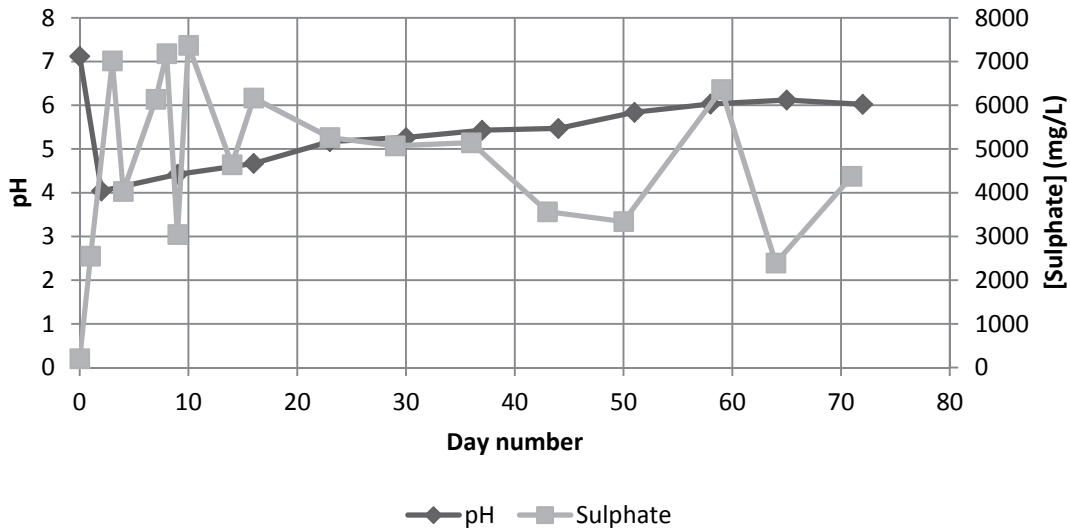


Figure 4.28: pH and sulphate concentration profiles within Column 3

The sulphate concentration after day 9 for Column 1, Figure 4.26 is significantly lower than the days that follow. The reason for this sudden deviation was unknown, however it was likely due to the type of sulphate test used which also resulted in fluctuating data over the course of the experiment.

Overall, the gradual decrease in sulphate concentration as the pH increased for all three columns indicated an improvement in the water quality by pumping from the base of the column. This was observed since according to the mechanism of acid generation, an increase in pH indicated a decrease in acid formation which led to a subsequent decrease in sulphate concentration.

Comparison of pH with Electrical Conductivity

The pH and EC for all three columns as a function of time is presented in Figure 4.29, Figure 4.30 and Figure 4.31 for the respective columns. The EC for Column 1 and Column 3 decreased as the pH increased however this behaviour is more evident in Figure 4.17 and Figure 4.18 which depicts the data recorded from the Hydrolab multiprobe. The EC and pH for Column 2 fluctuated substantially throughout the experiment.

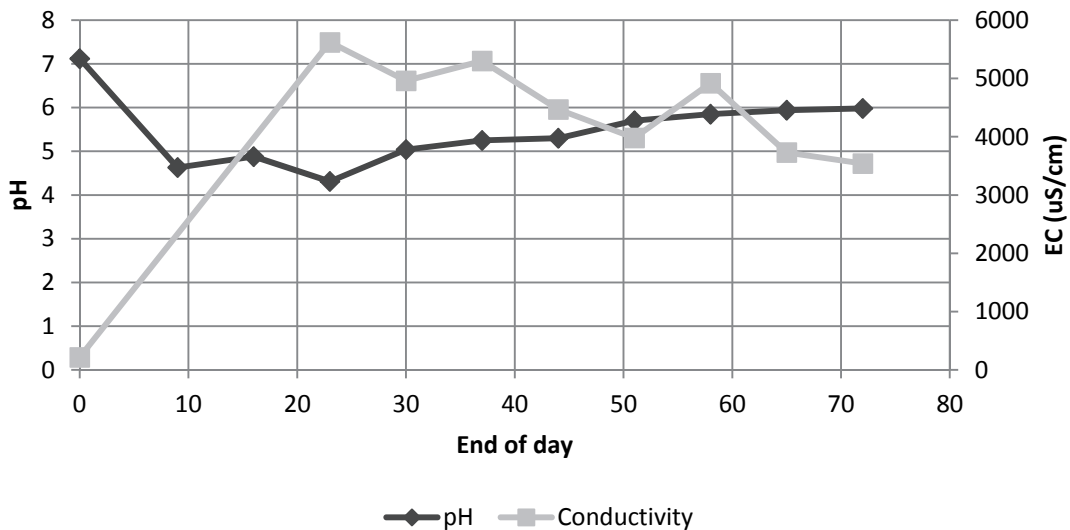


Figure 4.29: pH and electrical conductivity profiles within Column 1

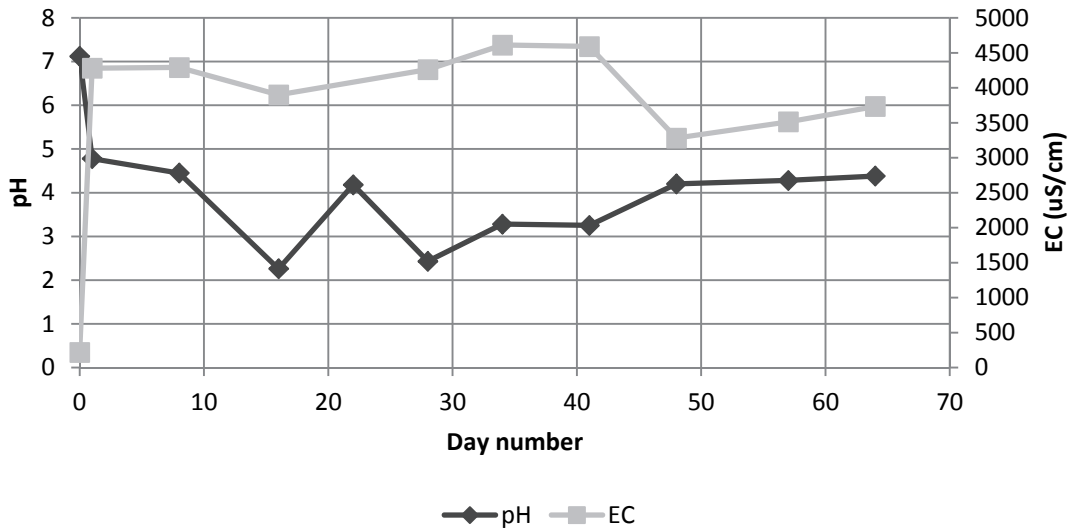


Figure 4.30: pH and electrical conductivity profiles within Column 2

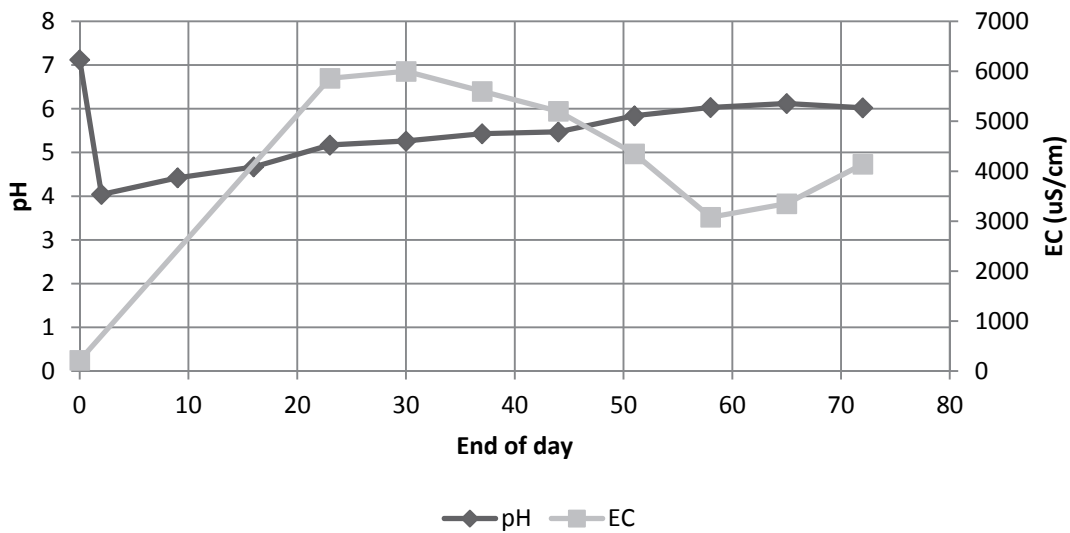


Figure 4.31: pH and electrical conductivity profiles within Column 3

The gradual increase in pH and decrease in EC for Columns 1, 2 and 3 depicted by Figures 4.29, 4.30, and 4.31, respectively, indicated that by pumping from the base of the column, water quality improved regardless of the oxygen content of the feed. However this trend between the pH and the EC was not very apparent since it was established in preceding comparisons that the temperature of the water plays an influential role on the EC.

An overall decrease in acid formation led to an overall increase in pH and decrease in EC. As EC decreased there were fewer heavy metals ions such as iron, and sulphate present in the water. Therefore an increase in pH indicated a decrease in iron and sulphate concentration of the water pumped from the base of the column. This trend has been observed for Column 1 and Column 3 in Figures 4.23 and 4.25, respectively, and for Columns 1, 2 and 3 in Figures 4.26, 4.27 and 4.28, respectively, and is explained by the mechanism of acid generation.

The principal process involved occurs when pyrite-containing rocks are contacted by oxygenated water, where the overall reaction occurs. The reactions occur in multiple stages, and the primary oxidant is ferric iron instead of molecular oxygen. The attack of the ferric iron on the pyrite mineral occurs first, and then the resulting ferrous iron is converted back to ferric iron by re-oxidation using oxygen dissolved in the mine water. In addition to pyrite being present, other metal sulphides also exist. In the presence of oxygen, these metal sulphides dissolve and release metal ions into solution. Oxygenated water is therefore essential for

continuation of the cycle that produces acidity. Thus, the observation of improved water quality may have implied that pumping from the base of the columns possibly induced anoxic conditions that precluded the generation of AMD since the pH increased and the EC, iron and sulphate concentrations decreased in all three columns. However, it is also possible that the depletion of the iron pyrite in the coal waste rock and subsequent dilution effects lead to the improvement in water quality, or there was insufficient time for the water to react with the pyrite inside the column thus resulting in flushing of the AMD at a rate faster than it was produced.

4.4.2.5 Comparison of Electrical Conductivity with Temperature for Column 1 (oxygenated feed water), Column 2 (low deoxygenated feed water) and Column 3 (low deoxygenated feed water with multiple feed points)

The change in electrical conductivity of the water removed from the base of the column appeared to decrease with a decrease in temperature of the water over the duration of the experiment. This trend and vice versa, has been observed for Columns 2 and 3 depicted by Figure 4.32 and Figure 4.33 respectively.

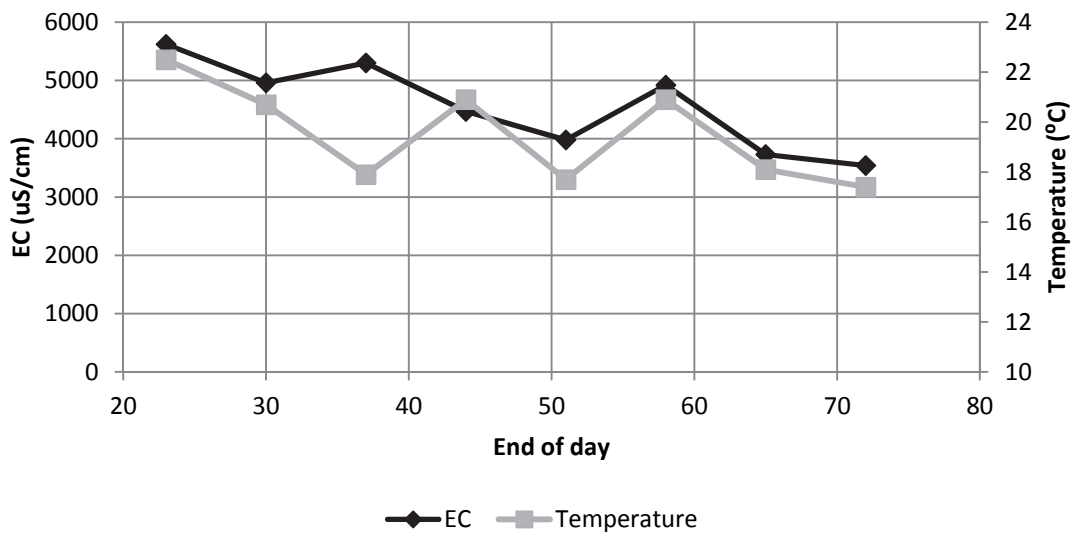


Figure 4.32: EC and temperature profiles within Column 1

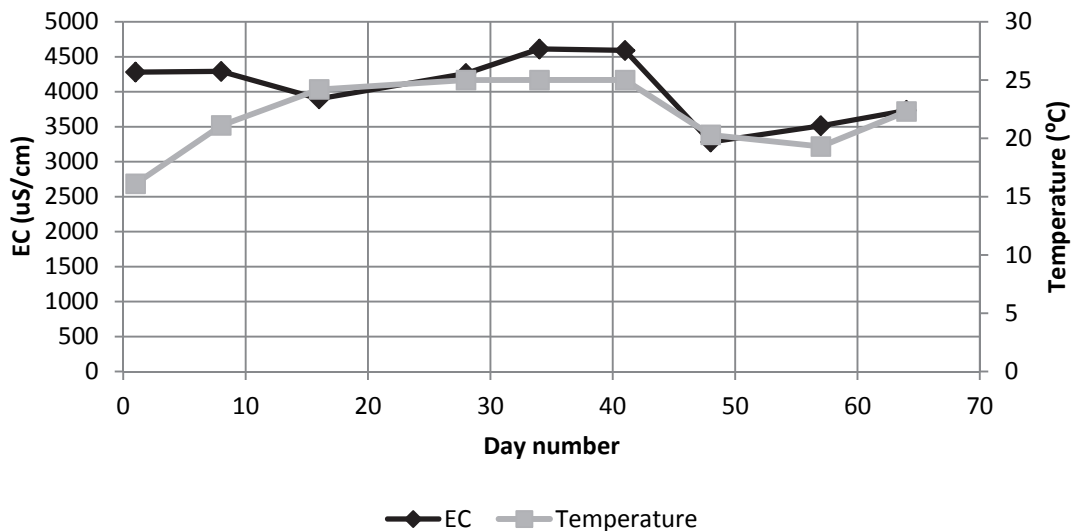


Figure 4.33: EC and temperature profiles within Column 2

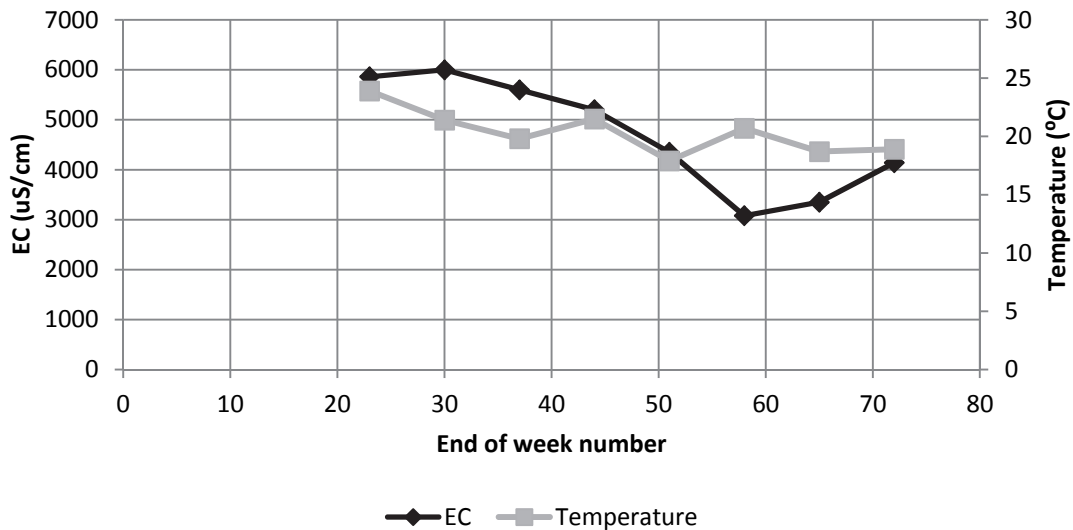


Figure 4.34: EC and temperature profiles within Column 3

The measurements of EC of the water drawn from the base of the column obtained over the course of the experiment for Columns 1, 2 and 3 were related to the temperature of the water. For all three columns, the EC decreased as temperature decreased, and vice versa. Due to the apparent dependency of EC on the temperature of the water for Columns 1, 2 and 3, it was not possible to deduce a comparison between the columns in terms of the improvement in water quality. Figure 4.15 which depicts the change in iron concentration, and Figure 4.16 in sulphate concentration further revealed that temperature may have been a more dominant parameter in the trend observed for the EC for all three columns rather than the iron and sulphate concentration of the water since they did not follow the same trend as the EC as closely as the temperature does. However, the trends observed in Figure 4.32, Figure 4.33 and Figure 4.34 with temperature showing a more dominant relation with EC compared to iron and sulphate in Figure 4.19 and Figure 4.21 may have been coincidental. EC is usually affected by the presence of heavy metal ions in the water, and temperature may have decreased due to solubility effects and the fact that the winter months were approaching. Hence, it cannot be concluded with confidence that temperature is the causal factor of the trend observed for the change in EC over the course of the experiment.

It has been shown in experiments 2-4 that acid is rapidly generated by the coal waste rock containing pyrite and that with time, all water quality parameters (pH, EC, iron and sulphate concentration) improved significantly by pumping water from the base of the columns where AMD was unable to form. However, conclusive evidence has not been shown whether this improvement in water quality was a result of dilution effects following depletion of the pyrite in the coal waste rock, or if AMD was no longer being generated due to the establishment of anaerobic conditions, or if a residence time of 2.81 weeks was insufficient time for acid to be generated within the columns. Therefore, in light of the above mentioned, further experiments were conducted in an attempt to regenerate the formation of acid.

4.4.3 Experiment 5: Attempted Acid Regeneration using Column 3

The following figure highlights the relevance of this section as well as the results and discussion section for experiment 6.

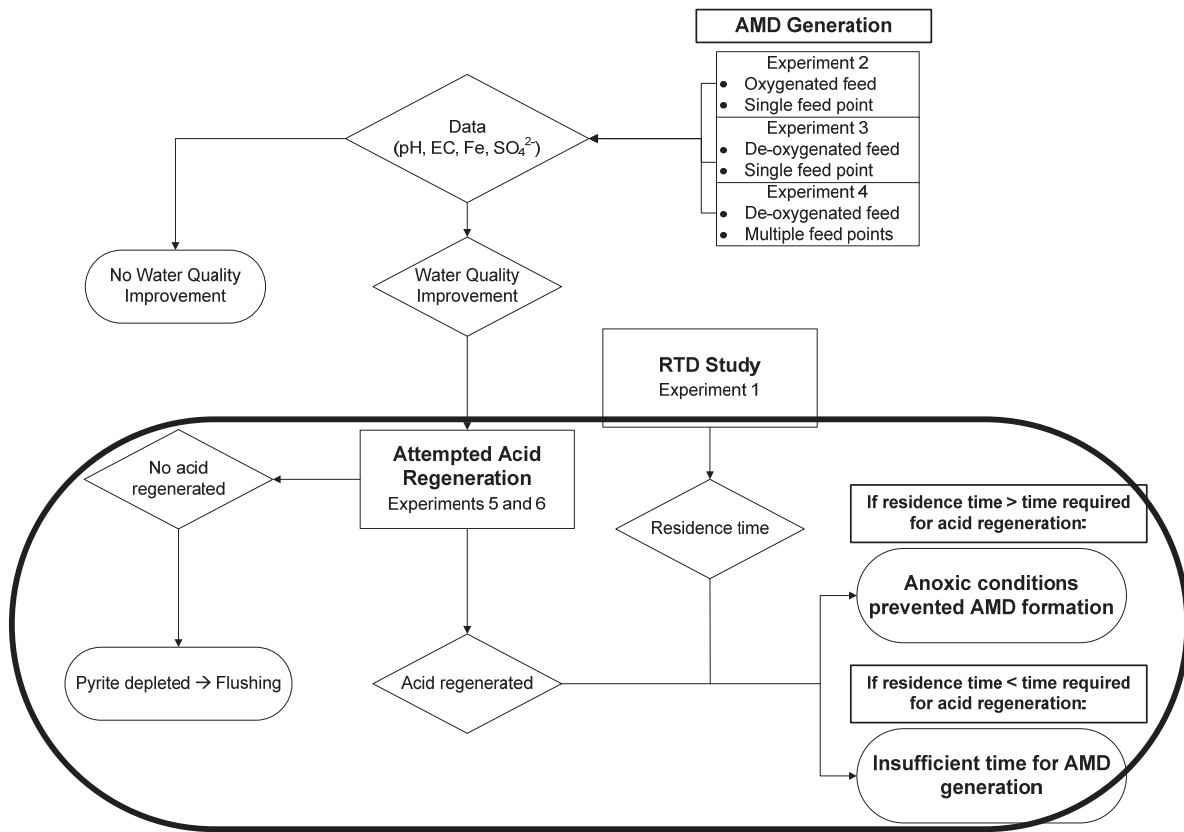


Figure 4.35: Results and discussion of attempted acid regeneration experiments in relation to the rest of the experimental work

The improvement in water quality resulting from column 3 during previous experimentation could have been a result of depletion in pyrite reserves due to reaction with the water and oxygen and subsequent dilution effects, insufficient time for the pyrite to react with the water since the water may have been removed from the column at a rate higher than that of AMD generation, or a deprivation of oxygen as a key reactant in the AMD-generating reactions. In order to determine which of these factors were responsible for the improvement in the water quality with time, the column was exposed to air for a duration of two weeks. If the results indicated that significant amounts of acid were generated in this short period of time, it could be said that the improvement in water quality observed previously could not have been a result of depletion in pyrite and subsequent dilution effects. Samples of water were taken from V-21 down to V-15, corresponding to depths of 0 to 6 m.

It can be seen from Figure 4.36 that at the end of week 1 (8 September 2014), the pH was lowest at the surface of the column and between 1-6 m the pH was constant at 7.1. During week 2 the pH decreased throughout the column since the pH at each point in the column was lower at the end of week 2 when compared to the end of week 1.

The variation of the conductivity of the water with column depth on both 8 September and 15 September 2014 is depicted in Figure 4.37. On both dates a general decrease in conductivity can be seen as the column depth increases. When the black and grey curves are compared to each other, it can be seen from a depth of 0 m to a depth of 2 m that the conductivity decreases with time while from a depth of 3 m to 6 m the conductivity increases with time.

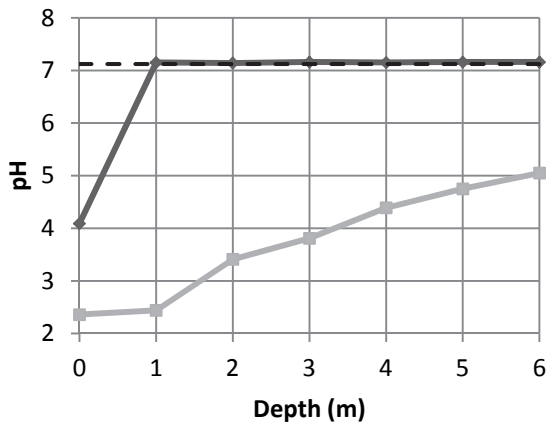


Figure 4.36: Variation of pH with depth inside column 3. Black line indicates 8 September and grey line indicates 15 September. The dashed line indicates the pH of tap water

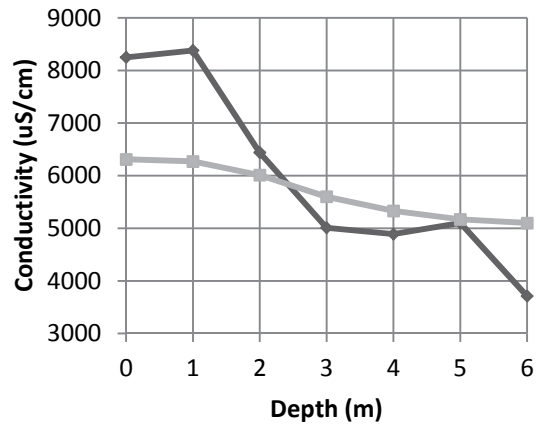


Figure 4.37: Variation of conductivity of water with depth inside column 3. Black line indicates 8 September and grey line indicates 15 September

The pH of the tap water has been displayed in Figure 4.36 to emphasise the noticeable decrease in pH as time proceeded by considering the fact that the column was originally filled with tap water from the same source. The decrease in pH with time provides clear evidence that acid was being generated inside the column. Another observation is the rate at which the acid was being generated. Within a timespan of two weeks, significant quantities of acid were being generated throughout the column as indicated by the drop in pH across all column depths. The notably high rate of acid generation not only rules out the possibility of depletion in pyrite reserves in the column, but supports the notion that an abundance of pyrite remained inside the bed of coal rock. During week 1, the pH decreased only at the surface of the column meaning that acid was only generated at the surface in week 1. It was only during week 2 that acid started to generate further down the column. Another observation can be made upon comparison of the black, grey and dashed curves: the largest decrease in pH during week 1 occurred at the surface of the column while the largest decrease in pH during week 2 occurred 1 m from the surface of the column. The top of the column was exposed to the atmosphere and hence a vast quantity of oxygen. It could thus be said that a significant amount of acid was generated at the surface during week 1 because of the abundance of oxygen available to initiate the AMD reactions. In Figure 4.37, the conductivity of the water inside the column decreases with column depth during week 1 and week 2. Since conductivity is a measure of the amount of cations and anions in solution, it could be said that there is a greater quantity of iron and sulphate in the upper layers of the column than at lower column depths. This could be an indication of more AMD being generated at or near the surface of the column where more oxygen is available for reaction.

From Figures 4.36 and 4.37, a common trend is observed when the black and grey curves are compared. The grey curves in each of the figures appear to be a rotated product of the black curves, which indicate a more even distribution of pH and conductivity throughout the column at the end of week 2. In Figure 4.36, the grey curve crosses over the black curve and the difference in conductivity of water between the top and very bottom of the column is much smaller after week 2 than after week 1. The trend in each of the figures can be explained using Figure 4.37.

The high availability of oxygen at the surface of the column during week 1 led to the formation of an acidic layer high in iron and sulphate content between a depth of 0-1 m. Due to limited levels of oxygen available at depths lower than 1 m, it then follows that acid generation was suppressed. The subsequent growth of the AMD layer during week 2 could have been a result of some downward diffusion of AMD from the highly concentrated surface layer, but mainly due to oxygen penetration further down the column resulting in the reaction between the water, oxygen and pyrite to form AMD at these lower depths. It is predicted that eventually there would be AMD at the bottom of the column because oxygen would penetrate to these depths and initiate reaction and there would also be some diffusion of AMD from upper layers.

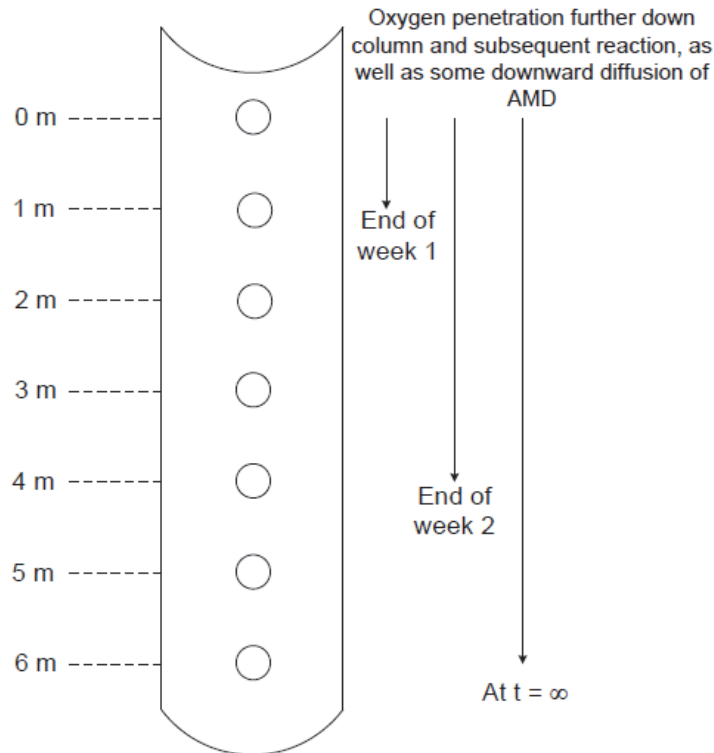


Figure 4.38: Extent of oxygen penetration and subsequent AMD formation

The variation in iron and sulphate content with column depth is shown in Figure 4.39 and Figure 4.40 respectively.

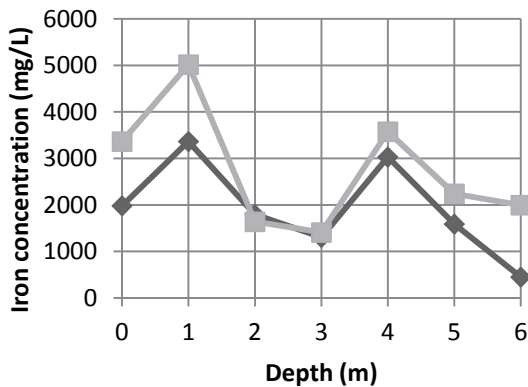


Figure 4.39: Variation of iron concentration with column depth. Black line indicates 8 September and grey line indicates 15 September

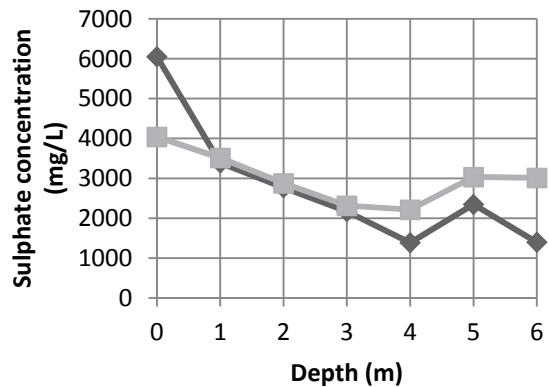


Figure 4.40: Variation of sulphate concentration with column depth. Black line indicates 8 September and grey line indicates 15 September

In Figure 4.39, the iron concentration peaks at a column depth of 1 m on both 8 September 2014 and 15 September 2014, followed by a sharp decrease in the concentration until a column depth of 3 m. The concentration then increases at a depth of 4 m and further down the column it decreases again. On comparison of the black and grey curves, there is a clear increase in iron concentration throughout the column from week 1 to week 2, except between a depth of 2 and 3 m where the iron concentration did not vary. Another observation can be made with regards to the actual concentration of the iron in the water: the concentration of iron is significantly greater than when compared to the concentration of iron in the column in experiment 4.

In Figure 4.40, the sulphate concentration is highest near the surface at the end of week 1 and at the end of week 2. There is a general trend of a decrease in sulphate concentration up until a depth of 4 m, after which

the sulphate concentration picks up slightly and levels off. The sulphate concentration is notably higher than the concentration of normal tap water which is approximately 200 mg/l.

The elevated iron and sulphate concentrations inside the column clearly suggest that the AMD-generating reactions occurred to a large extent during the two weeks of the experiment. The sharpest increase in iron concentration during week 2 occurred at a depth of 1 m, which is not surprising as it correlates with a sharp decrease in the pH during week 2 as shown in Figure 4.36.

It can thus be said that AMD was generated at a significantly high rate and two weeks was more than a sufficient amount of time for the process to occur. Since the reactions require pyrite to be present as a key reactant in the process, it can be said with confidence that the pyrite was most certainly not depleted during the previous experiment with column 3.

4.4.4 Experiment 6: Attempted Acid Regeneration Using Column 1

In similar fashion to column 3, the quality of water improved with time during the previous experiment involving column 1 (experiment 2). The column was filled with tap water and a supply of continuous compressed air was bubbled through the column for two weeks. The upward pressure exerted on the water from the compressed air in effect caused a fluidised behaviour, with extensive movement and mixing of the water body. The vigorous supply of oxygen was meant to solve the question pertaining to the factor responsible for the improvement of water quality during the previous experiment. If AMD were to be generated during the two weeks then the improvement in quality could not be attributed to a depletion of pyrite inside the column and subsequent dilution effects. Due to the excessive mixing of the water and the abundance of oxygen available throughout the column, it was deemed necessary only to sample the water from one location and this was done at a depth of 4 m.

The change in the pH of the water with time and the change in sulphate concentration in the water with time are described in Figure 4.41 and Figure 4.42 respectively.

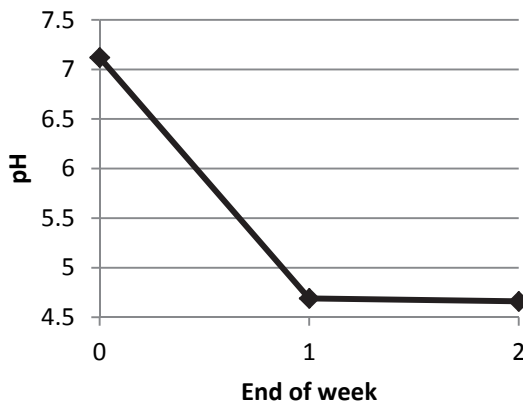


Figure 4.41: Variation of pH of water with time. The initial pH value was taken as the pH of the tap water used to fill the column

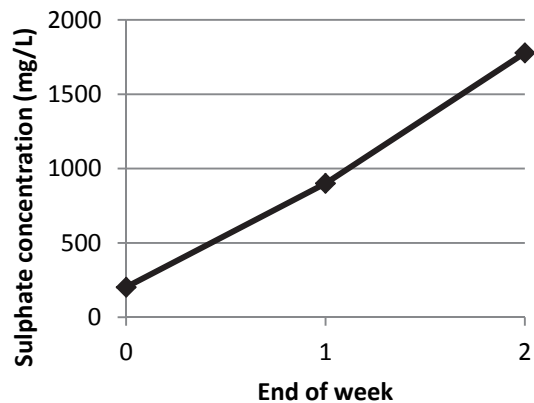


Figure 4.42: Variation of sulphate concentration in the water with time. The initial sulphate concentration was taken as the sulphate concentration of the tap water used to fill the column

As shown in Figure 4.41, there is a sharp decrease in the pH of the water during week 1 followed by a slight decrease in the pH in week 2. The sulphate concentration increases significantly during weeks 1 and 2. The most noticeable and immediate observation made upon examination of Figure 4.41 and Figure 4.42 are the rapid changes in pH and sulphate concentration which occurred during the experiment. These changes translate into noticeable quantities of AMD being generated within two weeks.

In both experiments 5 and 6, high levels of AMD were generated within 2 weeks. After the initial phase of the previous experiments involving columns 1 and 3, the water reached a steady pH of around 6 with a

residence time of 2.81 weeks. This change in pH is in stark contrast to the sharp decrease in the pH observed during experiments 5 and 6 which suggests three important points:

- The pyrite was not depleted and thus depletion in its reserves inside the column was not the cause for the steady improvement in the water quality.
- Acid was regenerated within 2 weeks in experiments 5 and 6, indicating that a residence time of 2.81 weeks was adequate for acid to be generated in the first phase of experiments (experiments 2-4). Insufficient time for the water to react with the pyrite to form AMD could thus be ruled out as a reason for the improvement in water quality.

The improvement in water quality was a result of induced anoxic conditions.

4.5 CHAPTER CONCLUSIONS

The generation of AMD in the Witwatersrand basins has had a detrimental effect on water resources. It has been well documented that oxygen is a necessary reactant in the AMD generation process and the continuous withdrawal of water from 2 km underground could be a potential solution to the problem since there is a low availability of oxygen at such depths and the extent of acid generation could be limited. The proposed idea was tested by conducting a series of experiments in which water was continuously fed and withdrawn from the bottom of 6 m tall columns packed with coal waste rock containing pyrite.

Based on the parameters pH, iron and sulphate content as well as electrical conductivity, results from experiments 2-4 indicated that water quality in all three columns improved with time. Acid was rapidly generated in the initial phases for all three columns but the pH steadily increased with time thereafter and an overall increase in pH of 2 units was observed. Iron as well as sulphate content notably decreased for all three columns after the initial acid generation phase. This suggests that the oxygen content in the feed as well as the positioning of the feed played no significant role in how the water quality developed over the course of the experiment.

The results from experiments 2-4 could not, however, assist in identifying whether the improvement in water quality was due to the depletion of iron pyrite and subsequent dilution effects, insufficient time for AMD to be generated, or the lack of oxygen present inside the column at lower depths because of its inability to penetrate through the solid packing.

Acid was regenerated in experiments 5 and 6 by inducing aerobic conditions to determine if the iron pyrite was depleted. The results from the experiments showed that the pH decreased and the iron and sulphate content increased indicating rapid acid generation in the space of two weeks. This suggested that the pyrite reserves were not depleted and the rates of reaction were rapid.

The results from the RTD study indicated that convective transport of water down the length of the column was much more significant than dispersion and mixing effects since a Peclet number of 27.4 was determined which is relatively large in magnitude. Results from the number of tanks in series model showed that the column could be modelled as 15 tanks in series. Both these sets of results pointed to the conclusion that the column behaved more as a plug flow reactor than as a CSTR over the course of experiments 2-4.

The RTD study also enabled the mean residence time to be determined which was used in experiments 2-4. It was found to be 2.81 weeks and by considering the fact that it took only 2 weeks for acid to be regenerated in experiments 5 and 6, it could be said that there was ample time for AMD to form in experiments 2-4 and the improvement in water quality was a result of induced anoxic conditions. These experiments provided evidence that the hypothesis of an improvement in water quality resulting from pumping water from 2 km underground has not been disproved.

CHAPTER 5: THE WAY FORWARD

We have shown in this project that the pumping requirements are not substantially different to the current set-up proposed by the IMC if pumps are to be deeply submerged. We have also shown that acid is rapidly generated by the rock. We have very clearly shown that with time, all water quality parameters improve significantly by pumping water from the base of the columns. Additional experiments have shown that this improvement in quality is not a result of pyrite depletion or of flushing of the aquifer as the acid generating reactions are much faster than the residence time of the columns. We have therefore been unable to disprove our hypothesis in this project. It has been suggested that we repeat the experiment with gold bearing ore/waste rock which will be conducted as part of a future study.

We believe that the project needs to be extended to field conditions, with the installation of deep wells into the aquifer to abstract water. We believe that we should install a 2 km deep abstraction well adjacent to the HDSP plant with an extraction capacity of between 500 000 L/day and 1 000 000 L/day. This water would need to be continuously monitored for EC, Redox potential and pH. Weekly composite samples could be taken and assayed for parameters such as sulphate, iron, conductivity, redox potential, etc. The depth of 2 km can be justified on the basis of aquifer recharge: If the aquifer naturally rises at a rate of 15 m/day, a depth of 2 km would allow surface water a period of at least 1000 days before entering the well suction point. Concurrently to this, a full geohydrological study would need to be conducted to understand where the aquifer recharge originated and to fully understand the movement of groundwater within the Central Wits Basin.

CHAPTER 6: REFERENCES

- AKCIL, A and KOLDAS, S (2006) Acid Mine Drainage (AMD): causes, treatment and case studies. *J Clean Prod*, **14** 1139-45.
- BACKHURST, JR, COULSON, JM, HARKER, JH and RICHARDSON, JF (1999) *Coulson and Richardson's Chemical Engineering*. Vol 1. 6th ed. Oxford: Butterworth-Heinemann.
- CUKROWSKA, E, MCCARTHY, TS and TUTU, H (2008) The chemical characteristics of acid mine drainage with particular reference to sources, distribution and remediation: The Witwatersrand Basin, South Africa as a case study. *Appl Geochem*, **23**, 3666-84.
- DEPARTMENT OF WATER AFFAIRS (2012) Feasibility Study for a Long-Term Solution to address the Acid Mine Drainage associated with the East, Central and West Rand Underground Mining Basins in the Gauteng Province – Information Document. Department of Water Affairs – South Africa, May 2012.
- DIZ, HR (1997) Chemical and biological treatment of acid mine drainage for the removal of heavy metals and acidity, Ph.D. thesis, Virginia Polytechnic Institute and State University, USA.
- DURAND, JF (2012) The impact of gold mining on the Witwatersrand on the rivers and karst system. *J Afr Earth Sci*, **68**, 24-43.
- EXPERT TEAM OF THE INTER-MINISTERIAL COMMITTEE (2010) Mine Water Management in the Witwatersrand Gold Fields with Special Emphasis on Acid Mine Drainage. Available at: <https://www.dwaf.gov.za/Documents/ACIDReport.pdf> [Accessed 24 December 2014].
- HAALAND, SE (1983) Simple and explicit formulas for the friction factor in turbulent pipe flow. *J Fluid Eng-T ASME*, **105**(1), 89-90.
- HALLBERG, KB and JOHNSON, DB (2005) Acid mine drainage remediation options: a review. *Sci Total Environ*, **338**, 3-14.
- JANET, J.P., C.M. SHERIDAN, D.C. DRAKE, K. RUMBOLD, and K.G. HARDING. 201x. Increasing Pumping Depth as a Solution in the Long-Term Management of Acid Mine Drainage, *Water SA*, xx, xx-xx (submitted for review).
- JOSIPOVIC M., H.J. ANNEGARN, M.A. KNEEN, J.J. PIENAAR, and S.J. PIKETH. Atmospheric dry and wet deposition of sulphur and nitrogen species and assessment of critical loads of acidic deposition exceedance in South Africa. *S Afr J Sci*. 2011; **107**(3/4), Art. #478, 10 pages. DOI: 10.4102/sajs.v107i3/4.478
- KOLVER, L. 2013. Shift from 'blame seeking' will aid efforts to tackle SA's acid mine drainage challenge. *Mining Weekly* August 16 Issue.
- MCCARTHY, TS (2011) The impact of acid mine drainage in South Africa. *S Afr J Sci*, **107**(5/6), 1-7.
- ODENDAAL, N (2013) *Group Five starts work on TCTA AMD contract*. [Online] *Mining Weekly*, Available at: <http://www.engineeringnews.co.za/article/group-five-starts-work-on-tcta-amd-contract-a-02-22> [Accessed 3 June 2013].
- OWENS, B (2013) *Mining: Extreme prospects*. [Online] Nature Publishing Group, Available at: http://www.nature.com/nature/journal/v495/n7440_supp/full/495S4a.html [Accessed 29 May 2013].
- RORRER, GL, WETLY, JR, WICKS, CE and WILSON, RE (2008) *Fundamentals of Momentum, Heat and Mass Transfer*. 5th ed. Hoboken, New Jersey: John Wiley and Sons.
- ROSE, S, and W.C. ELLIOT. 2000. The effects of pH regulation upon the release of sulphate from ferric precipitates formed in acid mine drainage. *Applied Geochemistry*. **15**: 27-34
- SEBESTOVA, E., MACHOVIC, V., PAVLIKOVA, H., LELAK, J. and MINARIK, L. 1996. Environmental-impact of brown coal mining in Sokolovo Basin with especially trace metal mobility. *Journal of Environment Science and Health, Part A: Environmental Science & Engineering & Toxic and Hazardous Substance Control* **31**: 2453-2463.
- SHERIDAN, C. (2013). "Paying the price." *TCE The Chemical Engineer* (867): 30-32.
- SINNOTT, RK (2005) *Coulson and Richardson's Chemical Engineering*. Vol 6 – Chemical Engineering Design (4th Ed.). Elsevier.

APPENDICES: Pumping Calculations

Appendix A: Current Scenario

Table A1: Calculation data for low estimate parameters, current scenario

Flow rate [m ³ /day]	Linear Velocity [m/s]	Re []	Friction Factor []	Head Loss to Friction [m]	Elevation Head [m]	Pump Head [m]	Pump Energy [kW]
2000	0.241	8.42E+03	0.00810	0.14	300	300	68
4000	0.481	1.68E+04	0.00673	0.45	300	300	136
6000	0.722	2.53E+04	0.00608	0.92	300	301	205
8000	0.962	3.37E+04	0.00568	1.53	300	302	274
10000	1.203	4.21E+04	0.00540	2.27	300	302	343
12000	1.444	5.05E+04	0.00518	3.14	300	303	413
14000	1.684	5.89E+04	0.00500	4.14	300	304	483
16000	1.925	6.74E+04	0.00486	5.25	300	305	554
18000	2.165	7.58E+04	0.00474	6.48	300	306	626
20000	2.406	8.42E+04	0.00464	7.82	300	308	699
22000	2.647	9.26E+04	0.00455	9.28	300	309	772
24000	2.887	1.01E+05	0.00447	10.84	300	311	847
26000	3.128	1.09E+05	0.00439	12.52	300	313	922

Table A2: Calculation data for midrange estimate parameters, current scenario

Flow rate [m ³ /day]	Linear Velocity [m/s]	Re []	Friction Factor []	Head Loss to Friction [m]	Elevation Head [m]	Pump Head [m]	Pump Energy [kW]
2000	0.327	1.03E+04	0.00767	0.24	300	300	68
4000	0.655	2.06E+04	0.00641	0.80	300	301	137
6000	0.982	3.09E+04	0.00581	1.63	300	302	205
8000	1.310	4.13E+04	0.00544	2.72	300	303	275
10000	1.637	5.16E+04	0.00518	4.04	300	304	345
12000	1.965	6.19E+04	0.00498	5.60	300	306	416
14000	2.292	7.22E+04	0.00482	7.37	300	307	488
16000	2.620	8.25E+04	0.00469	9.37	300	309	562
18000	2.947	9.28E+04	0.00458	11.58	300	312	637
20000	3.275	1.03E+05	0.00448	14.00	300	314	713
22000	3.602	1.13E+05	0.00440	16.62	300	317	791
24000	3.930	1.24E+05	0.00432	19.45	300	319	870
26000	4.257	1.34E+05	0.00426	22.48	300	322	952

Table A3: Calculation data for high estimate parameters, current scenario

Flowrate [m ³ /day]	Linear Velocity [m/s]	Re [.]	Friction Factor [.]	Head Loss to Friction [m]	Elevation Head [m]	Pump Head [m]	Pump Energy [kW]
2000	0.472	1.30E+04	0.00722	0.47	300	300	68
4000	0.943	2.59E+04	0.00607	1.57	300	302	137
6000	1.415	3.89E+04	0.00553	3.22	300	303	207
8000	1.886	5.19E+04	0.00519	5.38	300	305	277
10000	2.358	6.48E+04	0.00495	8.02	300	308	350
12000	2.829	7.78E+04	0.00477	11.13	300	311	424
14000	3.301	9.08E+04	0.00463	14.69	300	315	500
16000	3.773	1.04E+05	0.00451	18.70	300	319	579
18000	4.244	1.17E+05	0.00441	23.15	300	323	660
20000	4.716	1.30E+05	0.00433	28.02	300	328	745
22000	5.187	1.43E+05	0.00425	33.33	300	333	832
24000	5.659	1.56E+05	0.00419	39.05	300	339	924
26000	6.130	1.69E+05	0.00413	45.20	300	345	1019

Appendix B: Proposed Scenario

Table B1: Calculation data for low estimate parameters, proposed scenario

Flowrate [m ³ /day]	Linear Velocity [m/s]	Re [.]	Friction Factor [.]	Head Loss to Friction [m]	Elevation Head [m]	Pump Head [m]	Pump Energy [kW]
2000	0.241	8.42E+03	0.00810	0.68	300.00	301	68
4000	0.481	1.68E+04	0.00673	2.27	300.00	302	137
6000	0.722	2.53E+04	0.00608	4.62	300.00	305	207
8000	0.962	3.37E+04	0.00568	7.66	300.00	308	279
10000	1.203	4.21E+04	0.00540	11.37	300.00	311	353
12000	1.444	5.05E+04	0.00518	15.72	300.00	316	430
14000	1.684	5.89E+04	0.00500	20.68	300.00	321	510
16000	1.925	6.74E+04	0.00486	26.24	300.00	326	592
18000	2.165	7.58E+04	0.00474	32.39	300.00	332	679
20000	2.406	8.42E+04	0.00464	39.10	300.00	339	770
22000	2.647	9.26E+04	0.00455	46.39	300.00	346	865
24000	2.887	1.01E+05	0.00447	54.22	300.00	354	965
26000	3.128	1.09E+05	0.00439	62.61	300.00	363	1070

Table B2: Calculation data for midrange estimate parameters, proposed scenario

Flowrate [m ³ /day]	Linear Velocity [m/s]	Re []	Friction Factor []	Head Loss to Friction [m]	Elevation Head [m]	Pump Head [m]	Pump Energy [kW]
2000	0.327	1.03E+04	0.00767	1.20	300	301	68
4000	0.655	2.06E+04	0.00641	4.00	300	304	138
6000	0.982	3.09E+04	0.00581	8.17	300	308	210
8000	1.310	4.13E+04	0.00544	13.59	300	314	285
10000	1.637	5.16E+04	0.00518	20.21	300	320	363
12000	1.965	6.19E+04	0.00498	27.98	300	328	447
14000	2.292	7.22E+04	0.00482	36.87	300	337	535
16000	2.620	8.25E+04	0.00469	46.85	300	347	630
18000	2.947	9.28E+04	0.00458	57.89	300	358	731
20000	3.275	1.03E+05	0.00448	69.99	300	370	840
22000	3.602	1.13E+05	0.00440	83.12	300	383	957
24000	3.930	1.24E+05	0.00432	97.26	300	397	1082
26000	4.257	1.34E+05	0.00426	112.42	300	412	1217

Table B3: Calculation data for high estimate parameters, proposed scenario

Flowrate [m ³ /day]	Linear Velocity [m/s]	Re []	Friction Factor []	Head Loss to Friction [m]	Elevation Head [m]	Pump Head [m]	Pump Energy [kW]
2000	0.472	1.30E+04	0.00722	2.34	300	302	69
4000	0.943	2.59E+04	0.00607	7.87	300	308	140
6000	1.415	3.89E+04	0.00553	16.12	300	316	215
8000	1.886	5.19E+04	0.00519	26.91	300	327	297
10000	2.358	6.48E+04	0.00495	40.11	300	340	386
12000	2.829	7.78E+04	0.00477	55.65	300	356	484
14000	3.301	9.08E+04	0.00463	73.46	300	373	593
16000	3.773	1.04E+05	0.00451	93.50	300	394	715
18000	4.244	1.17E+05	0.00441	115.73	300	416	849
20000	4.716	1.30E+05	0.00433	140.12	300	440	999
22000	5.187	1.43E+05	0.00425	166.64	300	467	1165
24000	5.659	1.56E+05	0.00419	195.27	300	495	1349
26000	6.130	1.69E+05	0.00413	225.99	300	526	1552